Politecnico di Milano
Facoltà di Ingegneria Industriale
Corso di Laurea Magistrale in Ingegneria Aeronautica

Turbulent skin-friction drag reduction described with AGKE and triple decomposition

Relatore: Prof. Maurizio QUADRIO
Correlatore: Ing. Alessandro CHIARINI

Tesi di Laurea di:
Federica GATTERE
Matr. 905572

Anno Accademico 2019-2020

Contents

Abstract

A fully developed channel flow, subjected to oscillatory spanwise wall motion, is studied with a focus on the interaction between the coherent velocity profile introduced by the control, i.e. the *Stokes layer*, and the near-wall cycle. Two Direct Numerical Simulations have been performed for the controlled and uncontrolled flows at constant power input (CPI), such that at statistical equilibrium both simulations have the same power input. Our study relies upon the Anisotropic Generalised Kolmogorov Equations (AGKE), the exact budget equations for the second-order structure function tensor $\langle \delta u_i \delta u_j \rangle$. The AGKE highlight the production, transport, redistribution and dissipative processes of each component of the Reynolds stresses considering simultaneously the physical space and the space of scales.

In the present work, we have derived and used the AGKE written for a triple decomposition of the velocity which takes into account the presence of mean, coherent and stochastic contributions. The effect of the control on the terms of the AGKE has been described and linked to changes in the near-wall cycle dynamics. The decreased intensity of the normal components $\langle \delta u_i \delta u_i \rangle$ and the shift of their largest values towards smaller scales indicate an overall weakening of the near-wall structures and a shrinking of their sections. The *Stokes layer* transfers its energy to the stochastic turbulent fluctuations directly interacting with $\langle \delta w \delta w \rangle$ only. This process occurs at precise wall distances and scales — naturally highlighted by the AGKE — that further elucidate the dynamics of the near-wall structures and their interaction with the *Stokes layer* when the control is applied. The spatial and scale fluxes show that the transport processes weaken in the controlled case but qualitatively remain almost unchanged with the excess of $\langle \delta u_i \delta u_i \rangle$ in the buffer layer transferred at all wall distances and in a wide range of scales. For $\langle \delta u \delta u \rangle$ the fluxes feature a slight shift towards larger wall distances, in agreement with the thickening of the viscous sublayer. However, the same

does not hold true for $\langle \delta v \delta v \rangle$ and $\langle \delta w \delta w \rangle$ indicating that the thickening of the viscous sublayer mainly influences the dynamics of $\langle \delta u \delta u \rangle$. The effect of the control on the AGKE term for $\langle -\delta u \delta v \rangle$ is not trivial. In the controlled case the production of $\langle -\delta u \delta v \rangle$ increases and its largest values shift towards larger wall distances and smaller scales. On the other hand, the pressure strain becomes more negative and its largest values shift towards the wall. This leads to an increase of the negative sink of $\langle -\delta u \delta v \rangle$ in the buffer layer accompanied by the increase of positive source of $\langle -\delta u \delta v \rangle$ at slightly larger wall distances and smaller scales. Interestingly, in the control case, a new region of positive source arises in the viscous sublayer.

Sommario

Il seguente lavoro descrive una corrente turbolenta confinata tra due pareti, modificata da un controllo volto alla riduzione d'attrito. Nello specifico, l'analisi è focalizzata sull'interazione tra il profilo di velocità coerente, introdotto dalla tecnica della parete oscillante (*Stokes layer*), e il ciclo di parete. Sono state eseguite due simulazioni numeriche dirette (DNS) per una corrente senza forzamento e una corrente controllata, mantenendo la potenza per il pompaggio costante (CPI) in modo tale che all'equilibrio statistico esse abbiano la stessa potenza di pompaggio. Questo studio si basa sulle Anisotropic Generalised Kolmogorov Equations (AGKE), le equazioni di bilancio del tensore delle funzioni di struttura del secondo ordine $\langle \delta u_i \delta u_j \rangle$. Le AGKE descrivono i processi di produzione, trasporto, redistribuzione e dissipazione di ogni componente degli sforzi di Reynolds considerando simultaneamente lo spazio delle scale e lo spazio fisico.

In questo lavoro sono state derivate le AGKE scritte per una tripla decomposizione della velocità in contributo medio, coerente e fluttuante. L'effetto del controllo in termini di AGKE è stato descritto e associato ai cambiamenti che esso impone alla dinamica del ciclo di parete. La diminuzione dell'intensità delle componenti normali $\langle \delta u_i \delta u_i \rangle$ e lo spostamento dei loro valori massimi verso scale più piccole indica un indebolimento delle strutture vicino a parete e una diminuzione della loro sezione. Lo *Stokes layer* trasferisce energia alle fluttuazioni turbolente interagendo direttamente solo con $\langle \delta w \delta w \rangle$. Questo processo avviene a una precisa distanza dalla parete e a precise scale – naturalmente descritte dalle AGKE – che chiariscono ulteriormente la dinamica delle strutture del ciclo di parete e della loro interazione con lo *Stokes layer*. I flussi spaziali e di scala mostrano che i processi di trasporto sono indeboliti dall'imposizione del controllo, sebbene qualitativamente rimangano invariati, con l'eccesso di $\langle \delta u_i \delta u_i \rangle$ che viene trasferito dal *buffer layer* verso diverse distanze da parete e diverse scale. Le linee di campo dei flussi di

$\langle \delta u \delta u \rangle$ vengono traslate a una maggiore distanza da parete, in accordo con l'ispessimento del substrato viscoso. Lo stesso spostamento non avviene per i flussi di $\langle \delta v \delta v \rangle$ e $\langle \delta w \delta w \rangle$, indicando che l'ispessimento del substrato viscoso influenza prevalentemente la dinamica delle strisce ad alta e bassa velocità del ciclo di parete. L'effetto del controllo su $\langle -\delta u \delta v \rangle$ mostra che la produzione di questo termine aumenta e il suo valore massimo si sposta a distanze maggiori dalla parete. Al contrario, il termine di interazione tra pressione e velocità diventa maggiormente negativo e il suo massimo valore si sposta più vicino a parete. Questo spostamento relativo tra produzione e *pressure strain* porta all'incremento nel *buffer layer* dell'intensità sia del pozzo negativo di $\langle -\delta u \delta v \rangle$, sia della sua sorgente positiva. Inoltre, una nuova zona di sorgente positiva viene creata nel substrato viscoso, quando il controllo è attivo.

Chapter 1

Introduction

One of the characteristic features of turbulence is its ability to transport and mix mass and momentum of the fluid more effectively than laminar flows do. For wall-bounded turbulent flows, it is reflected in an enhancement of the wall shear stress and hence drag (Fukagata *et al.*, 2002), compared to a comparable laminar flows. Flow control for drag-reduction aims to suppress or mitigate the negative effects of turbulence near the wall, in order to cut energy consumption and boost cost-effectiveness and environmental efficiency.

Considering their energy expenditure and control nature, drag reduction strategies can be classified into two categories, namely passive and active. The former usually need a deformation of the surface of the wall, such as riblets (Bechert *et al.*, 1997) without the need for energy supply. Among passive technologies, riblets are the closest to be implemented in practical applications. Laboratory tests showed that they can reduce drag up to 8%, but they have the main drawback of needing continuous maintenance. The latter reach their goal by performing some sort of actuation on the fluid flow, needing external energy to work. Among active strategies, the ones concerning the motion of the walls seem promising. In this regard it is worth mentioning spanwise wall oscillation (Jung *et al.*, 1992), streamwise travelling waves of spanwise velocity (Quadrio *et al.*, 2009), spanwise travelling waves (Du & Karniadakis, 2000; Du *et al.*, 2002) and streamwise travelling waves of wall deformation (Nakanishi *et al.*, 2012). They share the property of being predetermined strategies, meaning control parameters are decided *a priori*, but they differ on the direction of the forcing created by the actuation. The first three introduce a perturbation in the direction parallel to the

wall, whereas the last introduce a perturbation in the perpendicular direction through deformation of the wall. The in-plane actuation strategies impose an unsteady transverse shear which continuously changes the inclination of the near-wall structures in wall-parallel planes, destabilising the regeneration mechanism of the near-wall cycle (Schoppa & Hussain, 2002). If actuation parameters are properly tuned, this process can lead to the suppression of turbulence. Quadrio & Ricco (2004) and Gatti & Quadrio (2013) carried out a comprehensive parameter study to identify the optimal actuation scenarios. Even though streamwise travelling waves are observed to attain a larger drag-reduction rate (up to 48%), the present work focuses on harmonic spanwise wall motion. The latter identifies the best trade-off between the simplicity of the actuation law and the maximum achievable drag-reduction. It needs only two control parameters, namely the amplitude and the period of the oscillation, yet it can reach a gross drag-reduction rate of 45%. If the balance between the benefits and costs of the control is analysed, it is found that the maximum saving is about 7%. These margins are reached around the so-called 'optimal' actuation period $T^+ \equiv Tu_\tau^2/\nu = 100 - 125$.

The imposed harmonic spanwise oscillation induces a transverse flow near the wall, which agrees well with the exact laminar solution of the Stokes second problem (Quadrio & Sibilla, 2000; Choi, 2002). The superposition of the *Stokes layer* influences the low-speed streaks and the quasi-streamwise vortices that have been identified to be part of the self-sustaining mechanism of wall-turbulence, i.e. the wall cycle (Jeong *et al.*, 1997). It has been repeatedly observed that the spanwise shear periodically changes the tilting angle of the near-wall structures. However, whether this mechanism should be studied with a focus on streaks or the quasi-streamwise vortices is still open to question. On one hand, some works (e.g. Baron & Quadrio, 1996; Howard & Sandham, 2000; Choi & Clayton, 2001; Karniadakis & Choi, 2003; Yakeno *et al.*, 2014) reported a weakening in the quasi-streamwise vortices intensity when the control is active. Yakeno *et al.* (2014) proved that, when the spanwise shear is in the same direction of the vortical motion, associated sweep events are enhanced, while a half period later spanwise shear counteracts the vortical motion and events of the fourth quadrant are drastically suppressed (Wallace *et al.*, 1972). Conversely, ejections are always damped regardless of the phase. On the other hand, many authors (e.g. Laadhari *et al.*, 1994; Di Cicca *et al.*, 2002; Touber & Leschziner, 2012; Blesbois *et al.*, 2013) focused on the effect of spanwise oscillation on the streaky structures rather than vortices. Blesbois *et al.* (2013), analysing the linearised Navier-Stokes

equations, found out that the optimal perturbation to achieve drag reduction agrees well with the characteristic time of the low-speed streaks observed by DNS studies. Di Cicca *et al.* (2002) and Laadhari *et al.* (1994) associated the observed larger decrease in streamwise Reynolds stresses with the control, damping primarily streaks rather than vortices. Touber & Leschziner (2012) showed that when the spanwise shear changes rapidly across phases, streaks do not have sufficient time to re-orientate properly, thus they are weak and not well-established. This phenomenon interferes with the regeneration mechanism of the near-wall cycle. Instead, if control frequency is far from the optimum, there are phases for which the shear vector changes little in time and streaks are allowed to re-organise themselves. In the latter scenario, owing to the interaction of the fluctuating field with the *Stokes layer*, a new production of turbulent spanwise stress arises, reducing the drag-reduction margin.

To investigate how the *Stokes layer* communicates with the turbulent structures, it can be useful to compare the behaviour of natural to drag-reduced flows. Traditionally, the differences between the two cases have been studied either through spectral analysis or single-point statistics. The former has been applied by Choi (2002), Choi *et al.* (2002), Touber & Leschziner (2012) in the frequency domain. Knowing the convective velocities of the structures, their characteristic time scales can be associated with the correspondent characteristic lengths. Spectra have been inspected by Touber & Leschziner (2012), Agostini & Leschziner (2017) and Agostini & Leschziner (2018) almost uniquely to address the problem of the footprinting of the large scale motion on the small-scale fluctuations. When the near-wall structures are strongly damped by the control, the trace in the wall region of the outer-layer structures is enhanced. In the context of spanwise oscillating walls, single-point statistics has been employed by Baron & Quadrio (1996) and Howard & Sandham (2000) to compare the budget of the turbulent kinetic energy along the wall-normal direction between natural and controlled flows. Touber & Leschziner (2012) described the budgets of the entire set of Reynolds stresses formed with the stochastic component of the velocity, after performing a triple decomposition of the velocity field in mean, coherent and fluctuating contributions. They identify the important interactions within the various contributions of each budget and among budgets for different stresses. The same decomposition strategy has been adopted by Agostini *et al.* (2014) to analyse the phase-by-phase budgets of the fluctuating stresses.

A first step in the direction of unifying the dual vision, which counter-

poses scale and physical spaces, has been done by means of the Generalised Kolmogorov Equation (Hill, 2001). GKE is the exact budget equation for the second-order structure function $\langle \delta u_i \delta u_i \rangle$, i.e. the scale energy, that describes the amount of energy carried by certain scales at a certain location in the space. Moreover, GKE, unlike spectra, properly defines the concept of scale in the inhomogeneous wall-normal direction. This tool has been extensively applied to several problems of different complexity, e.g. turbulent channel flow (see for istance Marati *et al.*, 2004; Cimarelli *et al.*, 2016), Rayleigh–Bénard convection (Rincon, 2006), turbulent wakes (Portela *et al.*, 2017, 2020). Portela *et al.* (2020) also applied a triple decomposition of the velocity to the GKE to study quasi-periodic vortex shedding in the turbulent wake of a square prism. However, GKE has been only marginally applied to drag-reduced flows. Gatti *et al.* (2017) studied differences among uncontrolled, opposition-controlled (Choi *et al.*, 1994) and by spanwise wall-oscillation controlled flows.

However, GKE can not properly account for the anisotropy of the flow, thus it is unsuitable to highlight all the features of a flow under control. To overcome this issue, Gatti *et al.* (2020) introduced an extension of the GKE, namely the Anisotropic Generalised Kolmogorov equations (AGKE). AGKE are the exact budget equations for each component of the second-order structure function tensor of the fluctuating velocity $\langle \delta u_i \delta u_j \rangle$. They study the production, transport, redistribution and dissipative processes of every Reynolds stress tensor component considering the space of scales and the physical space simultaneously. Unlike the GKE, AGKE allows the scale and space investigation of the pressure strain term and feature the budget equation for the off-diagonal component $\langle -\delta u \delta v \rangle$, which is responsible for the turbulent drag enhancement (Fukagata *et al.*, 2002). A first and non-complete analysis of a channel flow subjected to oscillatory spanwise wall motion via AGKE has been carried out by Chiarini *et al.* (2019).

The present investigates a turbulent channel flow subjected to oscillatory spanwise wall motion, focusing on the interaction between the coherent motion introduced by the control (i.e. the *Stokes layer*) and the velocity turbulent fluctuations. For this purpose, AGKE are written for a triple decomposition of the velocity, which takes into account the presence of mean, coherent and stochastic contributions. Thus, the fluctuations of the natural and controlled flow can be properly compared, and the interplay between the coherent and fluctuating stresses can be revealed. Data used to carry out this analysis result from two Direct Numerical Simulation (DNS) of a

fully-developed turbulent channel flow for the controlled and uncontrolled cases. The DNS has been performed under CPI condition to keep the power input of both simulations unchanged.

The work is structured as follows. First, the AGKE written by means of the triple decomposition are presented in § 2 and numerical datasets used to perform the present analysis are described in § 2.2. In § 3 the main differences between uncontrolled and controlled flows in the diagonal (§ 3.1) and off-diagonal (§ 3.2) components of the terms involved in the budget equations are highlighted. Lastly, results are briefly discuss in chapter § 4. Additional material is included in the appendices. Appendix A reports the complete derivation of the budget equations of the structure function tensor of both the coherent and fluctuating velocities; appendix B describes the solver specifically developed to carry out the present analysis and appendix C the residuals computed to assess the statistical convergence of the code. Appendix D reports the single-point statistics.

Chapter 2

Method

2.1 Anisotropic Generalised Kolmogorov Equations using triple decomposition

When a turbulent flow exhibits a coherent periodic features (e.g. a periodic wall oscillation in a controlled channel flow), it is useful to follow Hussain & Reynolds (1970) and decompose the velocity field in its mean, coherent and purely stochastic parts. According to this approach, the velocity u_i has been decomposed into the mean U_i, the periodic $\tilde{u}_i$ and the chaotic u_i'' contributions:

$$u_i = U_i + \tilde{u}_i + u_i''. \tag{2.1}$$

The mean value U_i represents the time average of the velocity field, namely:

$$U_i(\boldsymbol{x}) = \langle u_i(\boldsymbol{x}, t) \rangle = \lim_{\tau \to +\infty} \frac{1}{\tau} \int_0^\tau u_i(\boldsymbol{x}, t) dt. \tag{2.2}$$

The term $\tilde{u}_i$ represents the coherent part of the velocity u_i and it is defined as:

$$\tilde{u}_i(\boldsymbol{x}, \phi) = \overline{u_i(\boldsymbol{x}, t)} - U_i(\boldsymbol{x}) \tag{2.3}$$

where $\bar{\cdot}$ denotes the phase averaging. The latter is defined as:

$$\overline{u_i(\boldsymbol{x},t)} = \lim_{N\to+\infty} \frac{1}{N}\sum_{n=0}^{N} u_i(\boldsymbol{x}, t+nT) \tag{2.4}$$

where T is the period of the coherent motion and the correspondent phase is defined as $\phi = 2\pi t/T$. The same decomposition applies to the pressure. Therefore, velocity and pressure fields can be re-cast in two new sets of equations:

$$\begin{cases} \boldsymbol{u} = \boldsymbol{U} + \boldsymbol{u'} \\ \boldsymbol{u'} = \tilde{\boldsymbol{u}} + \boldsymbol{u''} \end{cases} \tag{2.5}$$

$$\begin{cases} p = P + p' \\ p' = \tilde{p} + p'' \end{cases} \tag{2.6}$$

In this work we write the Anisotropic Generalised Kolmogorov Equations (AGKE), derived by Gatti *et al.* (2020), for the triple decomposition. As shown in Gatti *et al.* (2020), the AGKE are the exact budget equations for each component of the second-order structure function tensor $\left\langle \delta u_i' \delta u_j' \right\rangle$ where $\delta u_i'$ is the difference of the ith fluctuating velocity component between two points $\boldsymbol{x}$ and $\boldsymbol{x_0}$ identified by their midpoint $\boldsymbol{X} = (\boldsymbol{x} + \boldsymbol{x_0})/2$ and separation $\boldsymbol{r} = \boldsymbol{x_0} - \boldsymbol{x}$. Here the AGKE are derived for both the the coherent and stochastic parts, i.e. $\langle \delta\tilde{u}_i \delta\tilde{u}_j \rangle$ and $\left\langle \delta u_i'' \delta u_j'' \right\rangle$. The AGKE for $\left\langle \delta u_i' \delta u_j' \right\rangle$ are recovered by summing the AGKE for the coherent and stochastic contributions.

The AGKE for $\langle \delta\tilde{u}_i \delta\tilde{u}_j \rangle$ and $\left\langle \delta u_i'' \delta u_j'' \right\rangle$ can be compactly written as:

$$\frac{\partial \tilde{\phi}_{ij,k}}{\partial r_k} + \frac{\partial \tilde{\psi}_{ij,k}}{\partial X_k} = \tilde{\xi}_{ij}, \tag{2.7}$$

$$\frac{\partial \phi_{ij,k}}{\partial r_k} + \frac{\partial \psi_{ij,k}}{\partial X_k} = \xi_{ij}; \tag{2.8}$$

here repeated indices imply summation. $\tilde{\phi}_{ij,k}$ and $\phi_{ij,k}$ denote the fluxes of $\langle \delta\tilde{u}_i \delta\tilde{u}_j \rangle$ and $\left\langle \delta u_i'' \delta u_j'' \right\rangle$ respectively, in the space of scale r_k:

$$\tilde{\phi}_{ij,k} = \underbrace{\langle \delta U_k \delta \tilde{u}_i \delta \tilde{u}_j \rangle}_{\text{Mean Transport}} + \underbrace{\langle \delta \tilde{u}_k \delta \tilde{u}_i \delta \tilde{u}_j \rangle}_{\text{Coherent Transport}} + \underbrace{\langle \overline{\delta u_k'' \delta u_i''} \delta \tilde{u}_j \rangle}_{\text{Turbulent transport}}$$
$$+ \underbrace{\langle \overline{\delta u_k'' \delta u_j''} \delta \tilde{u}_i \rangle}_{\text{Turbulent transport}} \underbrace{-2\nu \frac{\partial \langle \delta \tilde{u}_i \delta \tilde{u}_j \rangle}{\partial r_k}}_{\text{Viscous transport}} \quad k = 1, 2, 3 \tag{2.9}$$

$$\phi_{ij,k} = \underbrace{\langle \delta U_k \delta u_i'' \delta u_j'' \rangle}_{\text{Mean transport}} + \underbrace{\langle \delta \tilde{u}_k \overline{\delta u_i'' \delta u_j''} \rangle}_{\text{Coherent transport}}$$
$$+ \underbrace{\langle \delta u_k'' \delta u_i'' \delta u_j'' \rangle}_{\text{Turbulent transport}} \underbrace{-2\nu \frac{\partial \langle \delta u_i'' \delta u_j'' \rangle}{\partial r_k}}_{\text{Viscous transport}} \quad k = 1, 2, 3 \tag{2.10}$$

$\tilde{\psi}_{ij,k}$ and ψ_{ij} denote the fluxes in the physical space X_k:

$$\tilde{\psi}_{ij,k} = \underbrace{\langle U_k^* \delta \tilde{u}_i \delta \tilde{u}_j \rangle}_{\text{Mean transport}} + \underbrace{\langle \tilde{u}_k^* \delta \tilde{u}_i \delta \tilde{u}_j \rangle}_{\text{Coherent transport}} + \underbrace{\langle \overline{u_k''^* \delta u_i''} \delta \tilde{u}_j \rangle}_{\text{Turbulent transport}} + \underbrace{\langle \overline{u_k''^* \delta u_j''} \delta \tilde{u}_i \rangle}_{\text{Turbulent transport}}$$
$$+ \underbrace{\frac{1}{\rho} \langle \delta \tilde{p} \delta \tilde{u}_i \rangle \delta_{kj}}_{\text{Pressure transport}} + \underbrace{\frac{1}{\rho} \langle \delta \tilde{p} \delta \tilde{u}_j \rangle \delta_{ki}}_{\text{Pressure transport}} \underbrace{-\frac{\nu}{2} \frac{\partial \langle \delta \tilde{u}_i \delta \tilde{u}_j \rangle}{\partial X_k}}_{\text{Viscous transport}} \quad k = 1, 2, 3 \tag{2.11}$$

$$\psi_{ij,k} = \underbrace{\langle U_k^* \delta u_i'' \delta u_j'' \rangle}_{\text{Mean transport}} + \underbrace{\langle \tilde{u}_k^* \overline{\delta u_i'' \delta u_j''} \rangle}_{\text{Coherent transport}} + \underbrace{\langle u_k^* \delta u_i'' \delta u_j'' \rangle}_{\text{Turbulent transport}}$$
$$+ \underbrace{\frac{1}{\rho} \langle \delta p'' \delta u_i'' \rangle \delta_{kj}}_{\text{Pressure transport}} + \underbrace{\frac{1}{\rho} \langle \delta p'' \delta u_j'' \rangle \delta_{ki}}_{\text{Pressure transport}} \underbrace{-\frac{\nu}{2} \frac{\partial \langle \delta u_i'' \delta u_j'' \rangle}{\partial X_k}}_{\text{Viscous transport}} \quad k = 1, 2, 3 \tag{2.12}$$

and $\tilde{\xi}_{ij}$ and ξ_{ij} denote the source terms:

$$\tilde{\xi}_{ij} = \underbrace{-\langle\delta\tilde{u}_j\delta\tilde{u}_k\rangle\left(\frac{\partial U_i}{\partial x_k}\right)^* - \langle\delta\tilde{u}_i\delta\tilde{u}_k\rangle\left(\frac{\partial U_j}{\partial x_k}\right)^* - \langle\delta\tilde{u}_j\tilde{u}_k^*\rangle\delta\left(\frac{\partial U_i}{\partial x_k}\right) - \langle\delta\tilde{u}_i\tilde{u}_k^*\rangle\delta\left(\frac{\partial U_j}{\partial x_k}\right)}_{\text{Mean production } (\tilde{P}_{ij}^M)}$$
$$\underbrace{-\left[-\left\langle\overline{\delta u_i''\delta u_k''}\frac{\partial\delta\tilde{u}_j}{\partial r_k}\right\rangle - \left\langle\overline{\delta u_j''\delta u_k''}\frac{\partial\delta\tilde{u}_i}{\partial r_k}\right\rangle - \left\langle\overline{\delta u_i''u_k''^*}\frac{\partial\delta\tilde{u}_j}{\partial X_k}\right\rangle - \left\langle\overline{\delta u_j''u_k''^*}\frac{\partial\delta\tilde{u}_i}{\partial X_k}\right\rangle\right]}_{\text{Coherent production } (P_{ij}^C)}$$
$$\underbrace{+\frac{1}{\rho}\left\langle\delta\tilde{p}\frac{\partial\delta\tilde{u}_i}{\partial X_j}\right\rangle + \frac{1}{\rho}\left\langle\delta\tilde{p}\frac{\partial\delta\tilde{u}_j}{\partial X_i}\right\rangle}_{\text{Pressure strain } (\tilde{\Pi}_{ij})} \underbrace{-4\tilde{\epsilon}_{ij}^*}_{\text{Dissipation } (\tilde{D}_{ij})} \tag{2.13}$$

$$\xi_{ij} = \underbrace{-\left\langle\delta u_j''\delta u_k''\right\rangle\left(\frac{\partial U_i}{\partial x_k}\right)^* - \langle\delta u_i''\delta u_k''\rangle\left(\frac{\partial U_j}{\partial x_k}\right)^* - \left\langle\delta u_j''^* u_k''\right\rangle\delta\left(\frac{\partial U_i}{\partial x_k}\right) - \langle\delta u_i''u_k''^*\rangle\delta\left(\frac{\partial U_j}{\partial x_k}\right)}_{\text{Mean production } (P_{ij}^M)}$$
$$\underbrace{+\left[-\left\langle\overline{\delta u_i''\delta u_k''}\frac{\partial\delta\tilde{u}_j}{\partial r_k}\right\rangle - \left\langle\overline{\delta u_j''\delta u_k''}\frac{\partial\delta\tilde{u}_i}{\partial r_k}\right\rangle - \left\langle\overline{\delta u_i''u_k''^*}\frac{\partial\delta\tilde{u}_j}{\partial X_k}\right\rangle - \left\langle\overline{\delta u_j''u_k''^*}\frac{\partial\delta\tilde{u}_i}{\partial X_k}\right\rangle\right]}_{\text{Coherent production } (P_{ij}^C)}$$
$$\underbrace{+\frac{1}{\rho}\left\langle\delta p''\frac{\partial\delta u_i''}{\partial X_j}\right\rangle + \frac{1}{\rho}\left\langle\delta p''\frac{\partial\delta u_j''}{\partial X_i}\right\rangle}_{\text{Pressure strain } (\Pi_{ij})} \underbrace{-4\epsilon_{ij}^*}_{\text{Dissipation } (D_{ij})} \quad . \tag{2.14}$$

In these equations, ν is the kinematic viscosity, ρ is the density, δ_{ij} is the *Kronecker delta* and the $(\cdot)^*$ operator is the arithmetic mean of a given quantity between $\boldsymbol{X} \pm \boldsymbol{r_y}/2$; $\tilde{\epsilon}_{ij}$ and ϵ_{ij} are the pseudo-dissipation tensors associated with the coherent and fluctuating velocity fields, respectively.

Coherent and fluctuating AGKE describe production, transport, inter-component redistribution and dissipation of $\langle\delta\tilde{u}_i\delta\tilde{u}_j\rangle$ and $\left\langle\delta u_i''\delta u_j''\right\rangle$ considering simultaneously the space of scales and the physical space. The AGKE for $\langle\delta\tilde{u}_i\delta\tilde{u}_j\rangle$ concern the budget of stresses arising from a periodic fluctuation of the flow field, whereas the AGKE for $\left\langle\delta u_i''\delta u_j''\right\rangle$ describe the budget of the fluctuating velocity field, after the contribution of the coherent motion has been removed.

The six-dimensional vector fields of fluxes $\tilde{\boldsymbol{\Phi}}_{\boldsymbol{ij}} = [\tilde{\boldsymbol{\phi}}_{ij}; \tilde{\boldsymbol{\psi}}_{ij}]$ and $\boldsymbol{\Phi}_{ij} =$

$[\boldsymbol{\phi_{ij}}; \boldsymbol{\psi_{ij}}]$ represent the transport of $\langle \delta\tilde{u}_i \delta\tilde{u}_j \rangle$ and $\left\langle \delta u_i'' \delta u_j'' \right\rangle$ among scales and positions. Turbulent transport for $\tilde{\boldsymbol{\Phi}}_{\boldsymbol{ij}}$ and coherent transport for $\boldsymbol{\Phi_{ij}}$ are the only terms where stochastic and periodic velocity fluctuations communicate. Regarding $\tilde{\boldsymbol{\Phi}}_{\boldsymbol{ij}}$, turbulent transport in 2.9 and 2.11 describe how coherent stresses are transferred by the stochastic flow field. Concerning $\boldsymbol{\Phi_{ij}}$, the coherent transport in 2.10 and 2.12 denote the transfer of turbulent stresses due to the periodic motion.

The source terms $\tilde{\xi}_{ij}$ and ξ_{ij} denote the net production of $\langle \delta\tilde{u}_i \delta\tilde{u}_j \rangle$ and $\left\langle \delta u_i'' \delta u_j'' \right\rangle$ respectively. They can assume either positive or negative values depending on the relative weight of the terms appearing on the right hand side of equation 2.13 and 2.14. Among the terms involved in the production process, the mean production term provides information on the scales and position at which the mean flow feeds the fluctuating field; $\tilde{P}_{ij}^M$ deals with the coherent fields, while P_{ij}^M with the stochatic one. The coherent production P_{ij}^C indicates the interchange of stresses between the coherent and fluctuating fields and it is present in both the budgets of $\langle \delta\tilde{u}_i \delta\tilde{u}_j \rangle$ and $\left\langle \delta u_i'' \delta u_j'' \right\rangle$ with opposite sign. P_{ij}^C describes the process responsible for extracting energy from the coherent motion and transferring it to the fluctuations and highlights the characteristics scales and positions at which it takes place. Among the terms involved in the source, the coherent production is the only one connecting coherent and fluctuating budgets. $\tilde{D}_{ij}$ and D_{ij} denote the dissipation by viscous effect. Lastly, the pressure strain terms $\tilde{\Pi}_{ij}$ and Π_{ij} describe the interplay between the pressure and the velocity fields. These terms do not concern neither production nor dissipation of energy, but they describe the redistribution process among different components of the stress tensor.

Let $u_1 = u$, $u_2 = v$ and $u_3 = w$ be the velocity components in the streamwise (x), wall-normal (y) and spanwise (z) directions of an indefinite channel flow. In the most general case, the AGKE depend on seven independent variables, namely the three space separation (r_x, r_y, r_z), the three mid-point positions (X, Y, Z) and the time. When tailored to the channel flow the independent variables drop to four, namely (r_x, r_y, r_z, Y), as this flow is statistically stationary and both x and z are homogenoeus directions. Moreover, the finite size of the separation between the two walls of the channel enforces a physical constraint on two independent variables: $Y > r_y/2$. The mean wall-normal V and cross-stream W velocities are zero, as well as all mean velocity derivatives with respect to the two homogeneous directions x and z, namely $\partial U_i/\partial x = \partial U_i/\partial z = 0$. In the most general case of wall actuation, the

coherent velocity can depend on the three directions if no homogeneity in the forcing is present. In the specific case of spanwise time-oscillating walls, by homogeneity in both the streamwise and spanwise directions, phase-averaged velocities are also not function of neither x nor z, i.e. $\partial\tilde{u}_i/\partial x = \partial\tilde{u}_i/\partial z = 0$. Therefore, the combination of the incompressibility constraint applied to the coherent velocity vector which gives $\partial\tilde{v}/\partial y = 0$ and the no-penetration condition at the wall, i.e. $\tilde{v}(y=0,t) = 0$, yields $\tilde{v} = 0$. Albeit the streamwise coherent velocity $\tilde{u}$ does not vanish, in the spanwise wall oscillating case, its value is observed to be two order of magnitude smaller than spanwise coherent velocity $\tilde{w}$, therefore it can be neglected.

2.1.1 AGKE tailored to turbulent channel flow

In this subsection the AGKE tailored to the channel flow subjected to a spanwise wall-oscillation are presented.

Budget equation for $\langle \delta u'' \delta u'' \rangle$

$$\frac{\partial}{\partial r_x}\underbrace{\langle \delta U \delta u'' \delta u'' \rangle}_{\text{Mean transport}} + \frac{\partial}{\partial r_z}\underbrace{\left\langle \delta\tilde{w}\overline{\delta u'' \delta u''} \right\rangle}_{\text{Coherent transport}} + \frac{\partial}{\partial r_j}\underbrace{\left\langle \delta u_j'' \delta u'' \delta u'' \right\rangle}_{\text{Turbulent transport}} +$$

$$\frac{\partial}{\partial r_j}\underbrace{\frac{\partial}{\partial r_j}\left(-2\nu\langle \delta u'' \delta u'' \rangle\right)}_{\text{Viscous transport}} + \frac{\partial}{\partial Y}\underbrace{\left\langle \overline{v''^* \delta u''} \delta u'' \right\rangle}_{\text{Turbulent transport}} \frac{\partial}{\partial Y}\underbrace{\frac{\partial}{\partial Y}\left(-\frac{\nu}{2}\langle \delta u'' \delta u'' \rangle\right)}_{\text{Viscous transport}} =$$

$$\underbrace{-2\left\langle \delta v'' \delta u'' \left(\frac{\partial U}{\partial y}\right)^* \right\rangle - 2\left\langle \delta u'' v''^* \delta \left(\frac{\partial U}{\partial y}\right) \right\rangle}_{P_{11}^M} \underbrace{+\frac{2}{\rho}\left\langle \delta p'' \delta \left(\frac{\partial u''}{\partial x}\right) \right\rangle}_{\Pi_{11}} \underbrace{-2\left(\epsilon^+_{u''u''} + \epsilon_{u''u''}\right)}_{D_{11}} \tag{2.15}$$

Budget equation for $\langle \delta v'' \delta v'' \rangle$

$$\frac{\partial}{\partial r_x}\underbrace{\langle \delta U \delta u'' \delta u'' \rangle}_{\text{Mean transport}} + \frac{\partial}{\partial r_z}\underbrace{\left\langle \delta\tilde{w}\overline{\delta v'' \delta v''} \right\rangle}_{\text{Coherent transport}} + \frac{\partial}{\partial r_j}\underbrace{\left\langle \delta u_j'' \delta v'' \delta v'' \right\rangle}_{\text{Turbulent transport}} + \frac{\partial}{\partial r_j}\underbrace{\frac{\partial}{\partial r_j}\left(-2\nu\langle \delta v'' \delta v'' \rangle\right)}_{\text{Viscous diffusion}}$$
$$+\frac{\partial}{\partial Y}\underbrace{\langle v''^{*} \delta v'' \delta v'' \rangle}_{\text{Turbulent transport}} + \frac{\partial}{\partial Y}\underbrace{\frac{\partial}{\partial Y}\left(-\frac{\nu}{2}\langle \delta v'' \delta v'' \rangle\right)}_{\text{Viscous diffusion}} + \frac{\partial}{\partial Y}\underbrace{\left\langle \frac{2}{\rho}\delta p'' \delta v'' \right\rangle}_{\text{Pressure transport}} =$$
$$\underbrace{+\frac{2}{\rho}\left\langle \delta p'' \delta\left(\frac{\partial v''}{\partial y}\right)\right\rangle}_{\Pi_{22}} \underbrace{-2\left(\epsilon^{+}_{v''v''} + \epsilon_{v''v''}\right)}_{D_{22}} \tag{2.16}$$

Budget equation for $\langle \delta w'' \delta w'' \rangle$

$$\frac{\partial}{\partial r_x}\underbrace{\langle \delta U \delta w'' \delta w'' \rangle}_{\text{Mean transport}} + \frac{\partial}{\partial r_z}\underbrace{\left\langle \delta\tilde{w}\overline{\delta w'' \delta w''} \right\rangle}_{\text{Coherent transport}} + \frac{\partial}{\partial r_j}\underbrace{\left\langle \delta u_j'' \delta w'' \delta w'' \right\rangle}_{\text{Turbulent transport}} + \frac{\partial}{\partial r_j}\underbrace{\frac{\partial}{\partial r_j} - 2\nu\langle \delta w'' \delta w'' \rangle}_{\text{Viscous diffusion}}$$
$$+\frac{\partial}{\partial Y}\underbrace{\langle v''^{*} \delta w'' \delta w'' \rangle}_{\text{Turbulent transport}} + \frac{\partial}{\partial Y}\underbrace{\frac{\partial}{\partial Y}\left(-\frac{\nu}{2}\langle \delta w'' \delta w'' \rangle\right)}_{\text{Viscous diffusion}} =$$
$$\underbrace{-2\left\langle \overline{\delta v'' \delta w''}\left(\frac{\partial \tilde{w}}{\partial y}\right)^{*}\right\rangle - 2\left\langle \overline{\delta w'' v''^{*}}\delta\left(\frac{\partial \tilde{w}}{\partial y}\right)\right\rangle}_{P^{C}_{33}} \underbrace{+\frac{2}{\rho}\left\langle \delta p'' \delta\left(\frac{\partial w''}{\partial z}\right)\right\rangle}_{\Pi_{33}} \underbrace{-2\left(\epsilon^{+}_{w''w''} + \epsilon_{w''w''}\right)}_{D_{33}} \tag{2.17}$$

Budget equation for $\langle -\delta u''\delta v''\rangle$

$$\begin{aligned}
&\frac{\partial}{\partial r_x}\underbrace{\langle \delta U \delta u''\delta v''\rangle}_{\text{Mean transport}} + \frac{\partial}{\partial r_z}\underbrace{\langle \delta\tilde{w}\overline{\delta u''\delta v''}\rangle}_{\text{Coherent transport}} \\
&+\frac{\partial}{\partial r_j}\underbrace{\langle \delta u_j''\delta u''\delta v''\rangle}_{\text{Turbulent transport}} + \frac{\partial}{\partial r_j}\underbrace{\frac{\partial}{\partial r_j} - 2\nu\langle \delta u''\delta v''\rangle}_{\text{Viscous diffusion}} \\
+\frac{\partial}{\partial Y}&\underbrace{\langle v''^{*}\delta u''\delta v''\rangle}_{\text{Turbulent transport}} + \frac{\partial}{\partial Y}\underbrace{\frac{\partial}{\partial Y}\left(-\frac{\nu}{2}\langle \delta u''\delta v''\rangle\right)}_{\text{Viscous diffusion}} + \frac{\partial}{\partial Y}\underbrace{\left\langle \frac{1}{\rho}\delta p''\delta u''\right\rangle}_{\text{Pressure transport}} = \\
&\underbrace{-\left\langle \delta v''\delta v''\left(\frac{\partial \delta U}{\partial y}\right)^{*}\right\rangle - \left\langle \delta v'' v''^{*}\delta\left(\frac{\partial U}{\partial y}\right)\right\rangle}_{P_{12}^{M}} \\
&\underbrace{+\frac{1}{\rho}\left\langle \delta p''\delta\left(\frac{\partial u''}{\partial y}\right)\right\rangle + \frac{1}{\rho}\left\langle \delta p''\delta\left(\frac{\partial v''}{\partial x}\right)\right\rangle}_{\Pi_{12}}\underbrace{-2\left(\epsilon^{+}_{u''v''} + \epsilon_{u''v''}\right)}_{D_{12}}
\end{aligned} \tag{2.18}$$

Budget equation for $\langle \delta\tilde{w}\delta\tilde{w}\rangle$

$$\begin{aligned}
&\frac{\partial}{\partial r_x}\underbrace{\langle \delta U\delta\tilde{w}\delta\tilde{w}\rangle}_{\text{Mean transport}} + \frac{\partial}{\partial r_z}\underbrace{\langle \delta\tilde{w}\delta\tilde{w}\delta\tilde{w}\rangle}_{\text{Coherent transport}} + \frac{\partial}{\partial r_j}\underbrace{2\langle \overline{\delta u_j''\delta w''}\delta\tilde{w}\rangle}_{\text{Turbulent transport}} \\
&+\frac{\partial}{\partial r_y}\underbrace{\frac{\partial}{\partial r_y}\left(-2\nu\langle \delta\tilde{w}\delta\tilde{w}\rangle\right)}_{\text{Viscous diffusion}} + \frac{\partial}{\partial Y}\underbrace{2\langle \overline{v''^{*}\delta w''}\delta\tilde{w}\rangle}_{\text{Turbulent transport}} = \\
&\underbrace{-2\left\langle \delta w''\delta v''\left(\frac{\partial\delta\tilde{w}}{\partial y}\right)^{*}\right\rangle - 2\left\langle \delta w'' v''^{*}\delta\left(\frac{\partial\tilde{w}}{\partial y}\right)\right\rangle}_{P_{33}^{C}}\underbrace{-2\left(\tilde{\epsilon}^{+}_{\tilde{w}\tilde{w}} + \tilde{\epsilon}_{\tilde{w}\tilde{w}}\right)}_{\tilde{D}_{33}}
\end{aligned} \tag{2.19}$$

2.2 Simulation data

The analysis carried out by the present work stems from the post-processing of two Direct Numerical Simulation (DNS) of a fully-developed turbulent channel flow performed for the controlled and uncontrolled cases. The two databases have been produced under the CPI condition (Hasegawa *et al.*,

2014), i.e. fixing the value of $Re_\pi = U_\pi h/\nu$ (where U_π is the flow rate per unit width achieved by a given pumping power in the laminar regime and h is the channel semi-height) to enforce the controlled and uncotrolled flows to have the same power input.

The DNS code written in CPL programming language by Luchini & Quadrio (2006) exploits the $v - \eta$ formulation of the Navier Stokes equations proposed by Kim *et al.* (1987). A Fourier discretization is adopted in the homogeneous directions, and fourth-order compact explicit finite-differences schemes are used for the wall-normal derivatives. Temporal integration is partially implicit, with a third-order Runge–Kutta scheme for the explicit convective part and a second-order Crank–Nicolson scheme for the viscous terms treated implicitly. The size of the computational domain is $(L_x, L_y, L_z) = (4\pi h, 2h, 2\pi h)$ in the streamwise, wall-normal and spanwise direction. The number of Fourier modes is $N_x = 256$ in the streamwise direction and $N_z = 256$ in the spanwise direction (they are increased by a factor of 3/2 to remove the aliasing error). In the wall-normal direction a hyperbolic tangent distribution for the $N_y = 256$ points is used to obtain a more refined grid near the wall. For the controlled case the spanwise oscillation of the wall is enforced by imposing the wall boundary condition for the spanwise component of the velocity as:

$$w(t) = Asin\left(\frac{2\pi}{T}t\right) \tag{2.20}$$

where A and T are the prescribed amplitude and period of the sinusoidal oscillation. The control parameters are selected to make the oscillating work to work close to its optimum in CPI sense, corresponding to $T = 20.39$ and $A = 0.1375$, or $T^+ = 110$ and $A^+ = 4.77$ in actual viscous units; here and throughout the whole paper the superscript + indicates quantities non-dimensionalised by the kinematic viscosity ν and the friction velocity u_τ of the drag-reduced flow, i.e. actual viscous units.

The value of the Reynolds number is kept constant to the value of $Re_\pi = 6500$. For the reference case it corresponds to a friction Reynolds number of $Re_\tau = u_\tau h/\nu = 200$, where $u_\tau = \sqrt{\tau_w/\rho}$ is the friction velocity expressed in terms of the average wall shear stress τ_w and the density ρ, and to a bulk Reynolds number of $Re_b = U_b h/\nu = 3176$. For the controlled case, instead, this corresponds to a friction Reynolds number of $Re_\tau = 187$ and to a bulk Reynolds number of $Re_b = 3267$. Further details of the two simulations are reported in table 2.1.

	Re_π	Re_τ	Re_b	T^{+act}	T^{+nom}	A^{+act}	A^{+nom}
ref	6500	200	3176	-	-	-	-
ow	6500	187	3267	110	125.5	4.77	4.47

Table 2.1: Simulation parameters of the unactuated (ref) and actuated (ow) case. act: actual viscous units; nom: nominal viscous units.

The reference simulation has been advanced for a time interval of $4000h/U_\pi$ after that the statistical equilibrium has been reached, saving 200 uncorrelated velocity fields. In the controlled case, the simulation has been advanced in time for $\sim 610h/U_\pi$ after reaching the statistical equilibrium. In this time interval 240 velocity fields has been saved, so that 30 entire periods of wall oscillations has been performed, each of them divided in 8 phases equally spaced.

For the computation of the AGKE terms, a code in CPL language has been developed. The code is based on the code for the GKE terms described in Gatti *et al.* (2019) and it has been specialised for the case under study. The velocity and pressure fields are decomposed in their mean, periodic and purely fluctuating contributions. Then, in order to reduce the computational effort, each term of equations 2.9, 2.10, 2.11, 2.12, 2.13 and 2.14 is split in multiple but simpler correlations and computed in Fourier domain by means of Parseval theorem for the two homogeneous directions. In order to further reduce the computational cost, AGKE terms which only involve coherent velocity and pressure (i.e. all terms of the budget of $\langle \delta\tilde{u}_i \delta\tilde{u}_j \rangle$ but fluxes and P_{ij}^C) are computed only once per phase and averaged over the total number of phases. Some terms also need the computation of derivatives: those in the two homogeneous directions are performed in Fourier space, whereas those in wall-normal direction are computed by means of a finite-difference scheme with a five-points computational stencil. The outputs of the code are $\langle \delta\tilde{u}_i \delta\tilde{u}_j \rangle$ and $\langle \delta u_i'' \delta u_j'' \rangle$, the flux vectors $\tilde{\boldsymbol{\phi}}_{\boldsymbol{ij}}$, $\boldsymbol{\phi}_{\boldsymbol{ij}}$, $\tilde{\boldsymbol{\psi}}_{\boldsymbol{ij}}$ and $\boldsymbol{\psi}_{\boldsymbol{ij}}$ and every term involved in $\tilde{\xi_{ij}}$ and ξ_{ij}. For further details see appendix B.

Chapter 3

Results

The following considers a comparison between a natural channel flow and a channel flow subjected to a harmonic spanwise oscillation, in terms of structure functions of the coherent and fluctuating velocities and the terms involved in their budgets in the compound space of scales and positions. The analysis is mainly restricted to the subspace $r_x = 0$. This choice is motivated by the prevalent streamwise alignment of the turbulent vortical structures of the channel flow. Such structures typically induce the largest negative correlation of velocity components for $r_x = 0$. As a consequence, the maximum of each component of $\langle \delta u_i'' \delta u_j'' \rangle^+$ and ξ_{ij}^+ occur at $r_x \approx 0$. An exception is made by the coherent production term: within a period of oscillation, it assumes the largest value when the structures are more inclined in the (r_x, r_z)-plane, making its statistics relevant also at $r_x \neq 0$.

3.1 Diagonal components

3.1.1 Structure functions

In a channel flow, the position in the (r_z, r_y, Y)-space of the maxima of the diagonal components of $\langle \delta u_i'' \delta u_j'' \rangle^+$, hereinafter referred to with the subscript m, is consistent with the characteristic scales and wall-normal distance of the structures populating the near-wall region. Table 3.1 summarises the maximum values of the diagonal components of $\langle \delta u_i'' \delta u_j'' \rangle^+$ and their position in the (r_z^+, r_y^+, Y^+)-space for the uncontrolled and controlled flows. The same information are depicted in figure 3.1. In the uncontrolled flow, $\langle \delta u'' \delta u'' \rangle^+$

peaks at $Y^+ = 14$ and $r_y^+ = 0$, indicating the presence of alternating regions of low and high streamwise velocity separated by $r_z^+ = 59$, consistent with a couple of low- and high-speed streaks. The maximum of $\langle \delta v'' \delta v'' \rangle^+$, instead, occurs at $Y^+ = 52$, $r_z^+ = 59$ and $r_y^+ = 0$, whereas the maximum of $\langle \delta w'' \delta w'' \rangle^+$ at $Y^+ = 43$, $r_y^+ = 42$ and $r_z^+ = 0$. They are the statistical trace of the quasi-streamwise vortices, inducing large negative correlated regions of wall-normal velocity at $r_z^+ \neq 0$ and of spanwise velocity at $r_y^+ \neq 0$. The larger order of magnitude of $\langle \delta u \delta u \rangle$ compared to $\langle \delta v \delta v \rangle$ and $\langle \delta w \delta w \rangle$ clearly highlights the strong anisotropy of the flow and indicates that the turbulent kinetic energy is mainly contained in the streaks (Jiménez, 2013).

When the control is applied $\langle \delta u'' \delta u'' \rangle_m^+$, $\langle \delta v'' \delta v'' \rangle_m^+$ and $\langle \delta w'' \delta w'' \rangle_m^+$ decrease, indicating a weakening of the near-wall structures. We note that the drop in the structure function of streamwise fluctuation (-12%) is larger than the one of wall-normal (-7%) and spanwise (-0.3%) fluctuations. This indicates that the control leads to a slightly decrease of the flow anisotropy, consistently with the results of Touber & Leschziner (2012). The smaller drop of $\langle \delta w'' \delta w'' \rangle_m^+$ is explained by the additional source of $\langle \delta w'' \delta w'' \rangle$ that arises in the controlled case owing to the interaction of the turbulent fluctuations with the *Stokes layer*; this is investigated in detail in section § 3.1.4.

The different shift of the maxima of the three normal components of $\left\langle \delta u_i'' \delta u_j'' \right\rangle^+$ reveals the control affects differently the dynamics of the three normal stresses. The wall-normal distance of $\langle \delta u'' \delta u'' \rangle_m^+$ shifts outwards from $Y^+ = 14$ to 17, in agreement with the thickening of the viscous sublayer, firstly reported by Di Cicca *et al.* (2002). This does not hold true for $\langle \delta v'' \delta v'' \rangle^+$ and $\langle \delta w'' \delta w'' \rangle^+$ which maxima occur at the same wall-distance for both the controlled and uncontrolled cases. This suggests that the thickening of the viscous sublayer mainly affects the streaks as they are placed at lower Y.

In terms of scales, we note that in the controlled case both $\langle \delta v'' \delta v'' \rangle_m$ and $\langle \delta w'' \delta w'' \rangle_m$ shift towards lower r_z and r_y respectively; the former moves from $r_z^+ = 59$ to $r_z^+ = 55$, while the latter from $r_y^+ = 42$ to $r_y^+ = 39$. On the other hand, when the control is applied $\langle \delta u'' \delta u'' \rangle_m$ moves towards larger spanwise separation, from $r_z^+ = 59$ to $r_z^+ = 61$. Overall, this indicates that in the controlled flow the low- and high- velocity streaks are moved apart from the wall motion and that the cross section of the quasi-streamwise vortices in the (y, z)-plane slightly decreases.

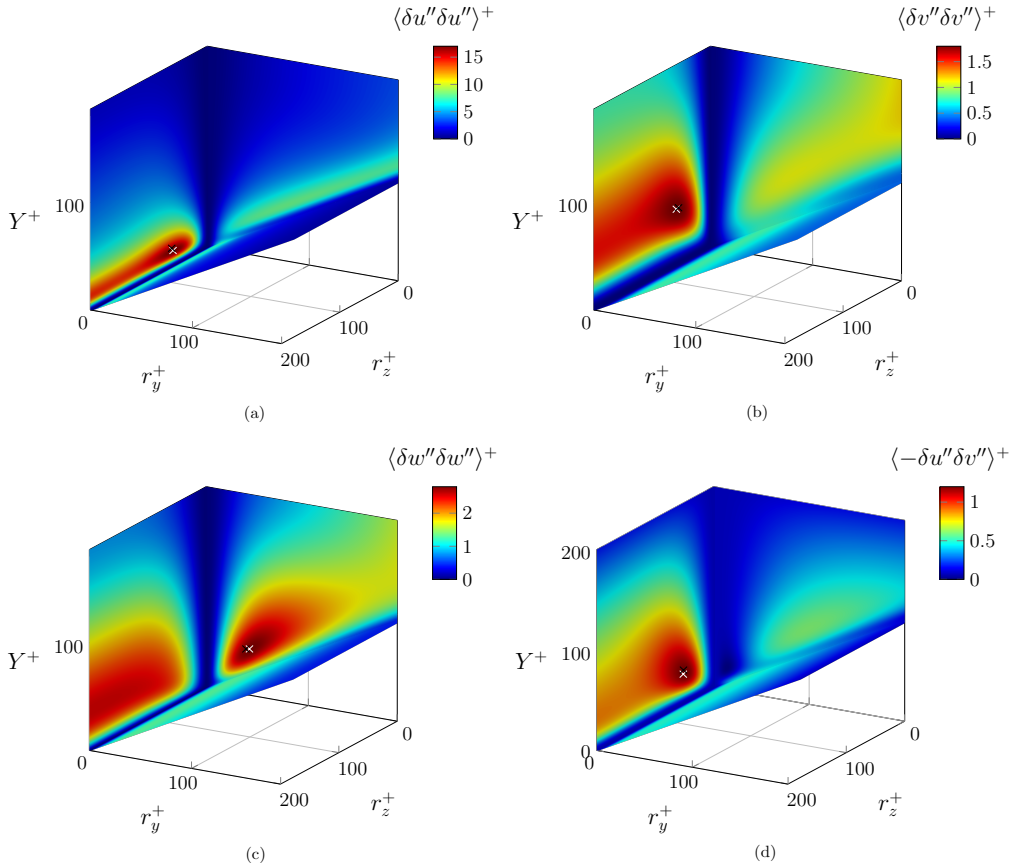

Figure 3.1: Second-order structure functions of the fluctuating velocity of the uncontrolled flow in the (r_z^+, r_y^+, Y^+)-space. *a*: $\langle \delta u'' \delta u'' \rangle^+$, *b*: $\langle \delta v'' \delta v'' \rangle^+$, *c*: $\langle \delta w'' \delta w'' \rangle^+$, *d*: $\langle -\delta u'' \delta v'' \rangle^+$. White $\times$: maximum value in the uncontrolled flow; black $\times$: maximum value in the controlled flow.

		$\langle \delta u_i \delta u_j \rangle^+_m$		$\xi^+_{ij,m}$		$P^+_{ij,m}$	
		Value	Position	Value	Position	Value	Position
i=j=1	ref	17.15	(59,0,14)	0.74	(39,0,12)	1.24	(43,0,12)
	ow	15.06	(61,0,17)	0.58	(37,0,14)	1.18	(37,0,13)
i=j=2	ref	1.76	(59,0,53)	0.037	(0,27,36)	-	-
	ow	1.64	(55,0,53)	0.039	(0,23,32)	-	-
i=j=3	ref	2.84	(0,42,43)	0.053	(43,0,9)	-	-
	ow	2.83	(0,39,43)	0.069	(40,0,12)	0.019	(11,0,31)
		$\lvert \Pi^+_{ij} \rvert_m$		$\lvert D^+_{ij} \rvert_m$			
		Value	Position	Value	Position		
i=j=1	ref	0.14	(24,0,24)	0.55	(-,-,0)		
	ow	0.17	(46,0,20)	0.47	(-,-,8.8)		
i=j=2	ref	0.068	(0,25,35)	0.034	(-,-,32)		
	ow	0.072	(0,22,33)	0.037	(-,-,31)		
i=j=3	ref	0.12	(46,0,12)	0.17	(-,-,0)		
	ow	0.15	(43,0,14)	0.17	(-,-,0)		

Table 3.1: Maximum values for the diagonal terms of $\langle \delta u_i \delta u_j \rangle^+$, its source ξ^+_{ij}, production P^{M+}_{ij} for i=j=1 and P^{C+}_{ij} for i=j=3, absolute pressure strain $|\Pi^+_{ij}|$ and dissipation $|D^+_{ij}|$ in the (r^+_z, r^+_y, Y^+)-space.

3.1.2 Production, redistribution and dissipation

Table 3.1 summarises the intensity and the position of the diagonal components of $\xi^+_{ij,m}$ and the terms they involve.

We start considering the source term for $\langle \delta u'' \delta u'' \rangle$. In the uncontrolled flow two well-separated regions of $\xi_{11} > 0$ can be detected at $r_y \approx 0$ (Gatti *et al.*, 2020). The first occurs in the buffer layer with $\xi^+_{11,m}$ placed at $(r_z^+, Y^+) = (39, 12)$ and it is linked to the near-wall cycle (Gatti *et al.*, 2020); see figure 3.2*a*. A second tiny region of positive ξ_{11} is detected in the overlap layer, at $Y^+ \approx r_z^+ \approx 95$. This is the statistical trace of the so-called outer cycle (Cossu & Hwang, 2017), as observed in Gatti *et al.* (2020). These regions perfectly agree with the two areas of positive source of scale energy (half the trace of $\langle \delta u_i'' \delta u_j'' \rangle$) reported by Cimarelli *et al.* (2013, 2016) and called driving scale range (DSR) and outer driving scale range (ODSR), respectively. In the controlled case, however, the control affects ξ_{11} in a way that these two regions of positive ξ_{11} are not more separated, but a region of slightly positive ξ_{11} arises connecting them; see figure 3.2*b*. This indicates that, at least at this low Reynolds number, the wall motion connects the near-wall and outer cycles. However, Cimarelli *et al.* (2013) found the separation between DSR and ODSR to be Re-dependent with the value of the source in this region becoming more negative as Re increases. Therefore, this effect seems to depend on the low Reynolds number considered in the present work. Further investigations are required to assess whether this effect is robust to a change of the control strategy and an increase of the Reynolds number.

To better elucidate the effect of the control on ξ_{11}, it is worth investigating separately its effect on the production (P^M_{11}) and pressure strain (Π_{11}) terms, shown in figures 3.2*c*-*d*. When the control is active the maximum of the streamwise production decreases by 5% and it moves at larger wall distance (from $Y^+ = 12$ to 13). P^+_{11} depends on two terms, namely $\langle -\delta u'' \delta v'' \rangle^+$ and dU/dy (see equation 2.14). The former shows that its local positive maximum in the (r_z^+, Y^+)-plane increases by 14% (see table 3.2) and moves from $Y^+ = 13$ to 18, proving an outward shift of the near-wall cycle; the latter moves its profile upwards due to the thickening of the viscous sublayer. For this reasons, albeit its maximum intensity is reduced, P^+_{11} increases for $Y^+ > 15$ in the whole range of r_z^+. Conversely, the negative maximum of the pressure strain becomes more negative and shifts closer to the wall (from $Y^+ \approx 24$ to 20). To complete the picture, $\epsilon^+_{11,m}$ decreases by 12.4% and moves away from the wall, up to $Y^+ = 8.8$. The relative shift among $P^+_{11,m}$, $\Pi^+_{11,m}$ and $\epsilon^+_{11,m}$

leads to the decrease of $\xi_{11.m}$ by 21% and explains the arise of the positive ξ_{11} connecting the near- and outer-cycle.

The source terms of $\langle \delta v'' \delta v'' \rangle^+$ and $\langle \delta w'' \delta w'' \rangle^+$ are much less affected by the oscillation of the wall than the one of $\langle \delta u'' \delta u'' \rangle^+$. However, the budget of $\langle \delta w'' \delta w'' \rangle^+$ features an additional term when the control is applied. It is the coherent production, arising from the interaction of $\langle \delta w'' \delta w'' \rangle^+$ with the dynamics of the *Stokes layer* (see § 3.1.4). The small changes in the intensity and positions of $\xi^+_{22,m}$, $\xi^+_{33,m}$ and the terms they involve are summarised in table 3.1.

3.1.3 Redistribution via pressure strain term

The pressure strain term denotes the redistribution of energy among the diagonal components of $\langle \delta u_i'' \delta u_j'' \rangle^+$ via velocity-pressure interaction. Π^+_{11} is negative in almost the whole space of scales and wall-normal distance, meaning that the interaction between the pressure and the turbulent field redistributes energy from the streamwise to the spanwise and the wall-normal fluctuations. Due to the incompressibily constraint, $\Pi^+_{33}/\Pi^+_{11} + \Pi^+_{22}/\Pi^+_{11} = -1$, hence energy redistribution is isotropic when $\Pi^+_{33}/\Pi^+_{11} = \Pi^+_{22}/\Pi^+_{11} = -0.5$. The thick line of figure 3.3 represents $\Pi^+_{33}/\Pi^+_{11} = -0.5$ and it distinguishes between the preferential redistribution towards $\langle \delta v'' \delta v'' \rangle^+$ at small scales and towards $\langle \delta w'' \delta w'' \rangle^+$ at large scales (Gatti *et al.*, 2020).

This property still holds when the control is applied, as can be evinced comparing the two panels of figure 3.3. However, the region of preferential redistribution towards $\langle \delta w'' \delta w'' \rangle^+$ slighly increases, meaning that the control redistributes energy to the spanwise fluctuations for a greater range of separations compared to the natural flow. The largest increase of Π^+_{33}/Π^+_{11} is visible in the $r_y^+ = 0$ plane along a line described by $Y^+ \approx r_z^+$ for $Y^+ < 100$. As reported in table 3.1, $\Pi^+_{11,m}$ becomes more negative, increasing its intensity by 23%. As a consequence, more energy is transferred towards both $\langle \delta v'' \delta v'' \rangle^+$ and $\langle \delta w'' \delta w'' \rangle^+$, such that both $\Pi^+_{22,m}$ and $\Pi^+_{33,m}$ increase compared to reference case. However, the former increases by 6%, the latter by 25%, suggesting that the wall motion enhances the transfer of energy at larger scales, namely from $\langle \delta u'' \delta u'' \rangle$ towards $\langle \delta w'' \delta w'' \rangle$ rather then towards $\langle \delta v'' \delta v'' \rangle$. This result agrees with the idea that the tilting of the near-wall structures, here enhanced by the wall motion, is the main driver of the transport of energy between streamwise and spanwise fluctuations via pressure-velocity interaction, as stated by Jeong *et al.* (1997).

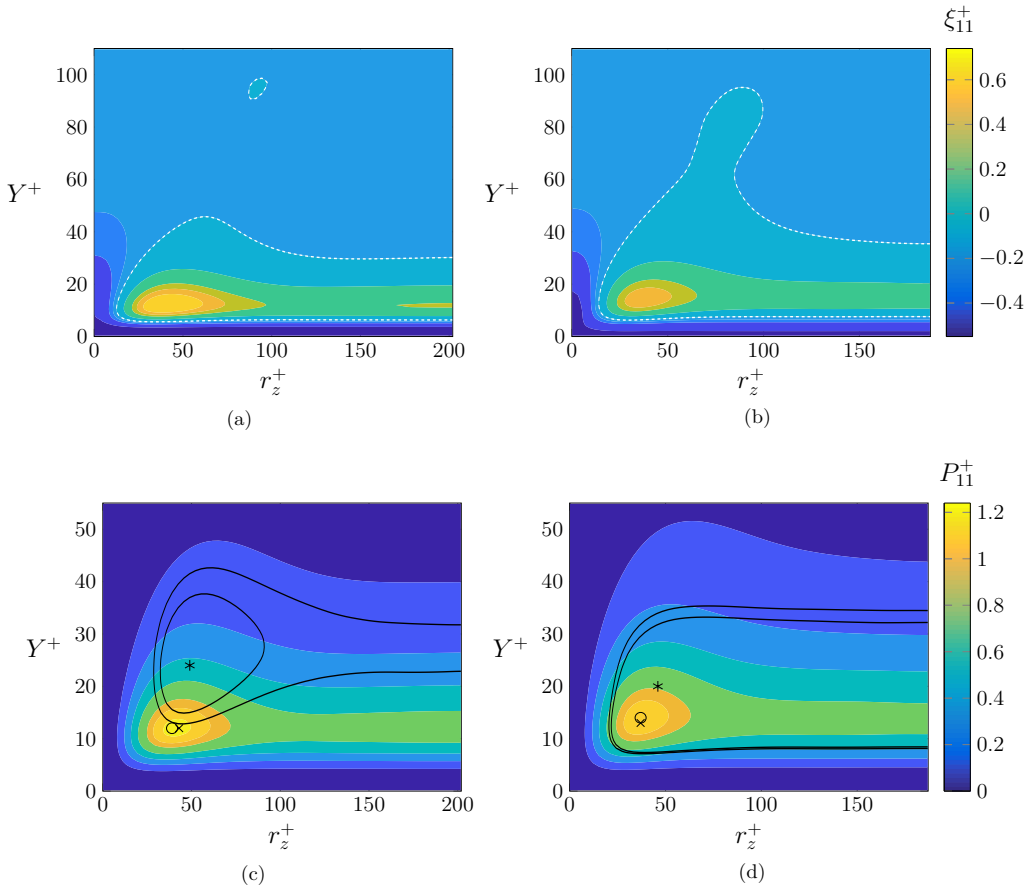

Figure 3.2: Contour plot of the budget terms for $\langle \delta u'' \delta u'' \rangle^+$ in (r_z^+, Y^+)-plane. *a-b*: filled contour of ξ_{11}^+ (-0.6:0.2:0.2,0.1,0:0.2:0.6) of (a) uncontrolled and (b) controlled flow, with zero line indicated by a white dashed line. *c-d*: filled contour of P_{11}^+ (0:0.2:1.2), contour lines of Π_{11}^+ (-0.125,-0.115,0), $\times : P_{11,m}^+, * : \Pi_{11,m}^+, \circ : \xi_{11,m}^+$ of (c) uncontrolled and (d) controlled flow.

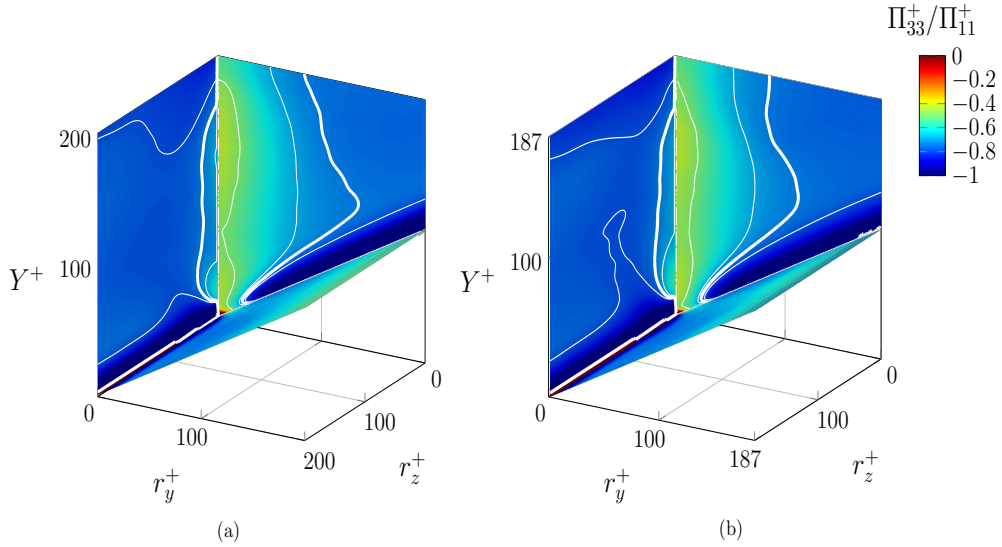

Figure 3.3: Π_{33}^+/Π_{11}^+. Contour lines (0,-0.4,-0.5,-0.6) with -0.5 line indicated by thick line in (a) uncontrolled and (b) controlled case

The larger increase of $\Pi_{33,m}^+$ compared to $\Pi_{11,m}^+$ is consistent with the decrease of the anisotropy in the controlled flow, as reported by Touber & Leschziner (2012).

3.1.4 Coherent and stochastic fluctuations interaction via coherent production term

The decomposion of the AGKE in their coherent and fluctuating contributions reveals the interaction between the dynamics of the *Stokes layer*, imposed by the wall motion and the turbulent fluctuations. The coherent production P_{ij}^C of equations 2.13 and 2.14 is the term of the AGKE which account for this cross-talk. In case of the spanwise wall motion, the term of the coherent production is present only in the budgets for $\langle \delta\tilde{w}\delta\tilde{w} \rangle$ and $\langle \delta w''\delta w'' \rangle$ so that the *Stokes layer* transfers its energy to the stochastic turbulent fluctuations directly interacting with the spanwise fluctuations only. This interaction occurs at precise wall distances and scales: its statistical trace in the complete four-dimensional space identifies the three characteristic scales of this process. Two well-defined peaks of P_{33}^{C+} are detected at

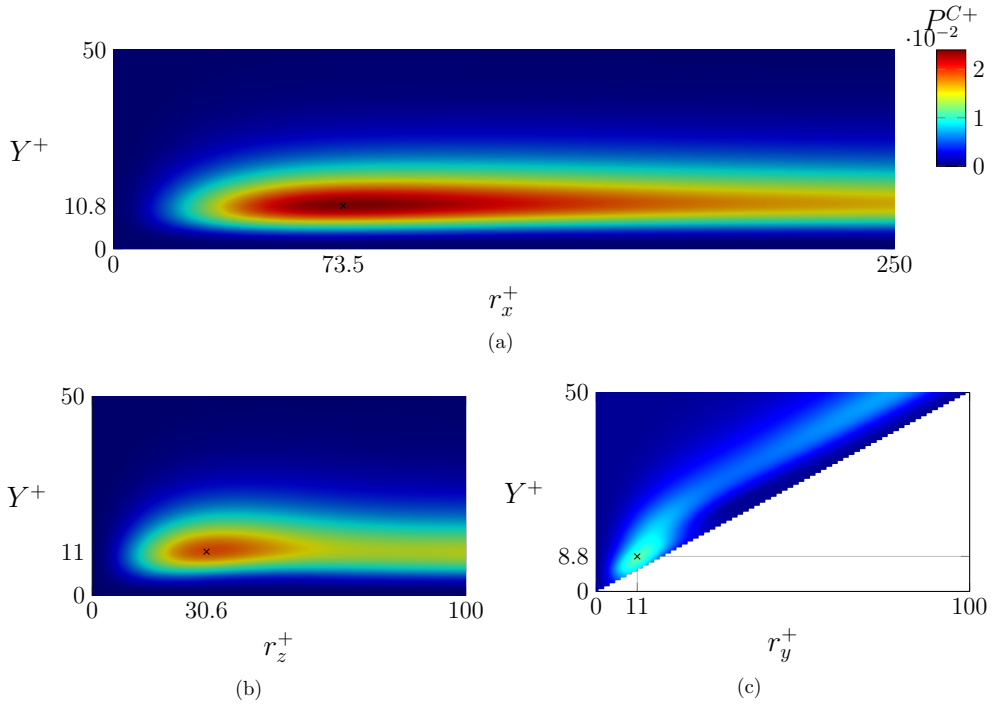

Figure 3.4: Coherent production peaks in (a) (r_x^+, Y^+)-plane, (b) (r_z^+, Y^+)-plane, (c) (r_y^+, Y^+)-plane

$r_y = 0$ and either $r_x \neq 0$ nor $r_z \neq 0$. The global maximum occurs at $(r_x^+, r_y^+, r_z^+, Y^+) = (73.5, 0, 0, 10.8)$ (figure 3.4*a*), whereas a second peak at $(0, 0, 30.6, 11)$ (figure 3.4*b*). It is worth highlighting that the wall distance of these peaks is about where the low- and high- speed streaks of the wall-cycle are, meaning that this produciton process is the result of the interaction of such structures with the *Stokes layer*.

Since this analysis is performed at $r_y = 0$, the second term of P_{33}^C in equation 2.17 vanishes. Thus, in the $r_y = 0$ space the coherent production reduces to:

$$P_{33}^C = -2\left\langle \overline{\delta v'' \delta w''} \left(\frac{d\tilde{w}}{dy} \right) \right\rangle. \tag{3.1}$$

The structures of the near wall-cycle, normally almost aligned to the direction of the mean flow, tend to re-orientate in the (x, z)-plane along the

direction of the new shear vector $[dU/dy, d\tilde{w}/dy]$, when a harmonic spanwise velocity $\tilde{w}$ is applied to the wall. $d\tilde{w}/dy$ changes continually during a period of oscillation, forcing the structures to re-orientate accordingly. If the wall oscillates at a frequency close to the optimum value for drag reduction, the structures do not have sufficient time to realign properly with the strain vector before it changes direction, and they show no well-defined behaviour. However, when the structures are more tilted, the spanwise shear changes relatively slowly in time, allowing the structures to become more vigorous and well-established. This condition is known as lingering (Touber & Leschziner, 2012) and it occurs at those phases for which $d\tilde{w}/dy$ is at its maximum intensity, either positive or negative, at $y^+ \approx 10$, corresponding to the typical wall-distace of the near-wall structure. Yakeno *et al.* (2014) provides a mathematical relation, which links the tilting angle to the ratio between the streamwise and the spanwise shear at $y^+ = 15$. Depending on the sign of $d\tilde{w}/dy$ at this wall-distance two different scenarios are possible.

First, we consider the phase corresponding to the largest positive tilting angle and a negative maximum of $d\tilde{w}/dy < 0$. In the leftmost panel of figure 3.5*b*, the projection of a positive rotating quasi-streamwise vortex (QSV) on the (x, y)-plane is considered. At its left side relative high-speed spanwise flow ($w'' > 0$) is advected upwards ($v'' > 0$) by its rotational motion. On the contrary, at its right side, relative low-speed spanwise flow ($w'' < 0$) is swept towards the wall ($v'' < 0$). Recalling that the structure function $\langle \delta u_i'' \delta u_j'' \rangle$ can be interpreted as the difference between the covariance $\langle u_i'' u_j'' \rangle$ and the cross-correlation function $R_{ij}(\boldsymbol{r})$ (Gatti *et al.*, 2020), the separation in the streamwise direction r_x, at which the anti-correlation is maximum, leads to highest value of $\overline{\delta v'' \delta w''}$ at that phase.

$$\overline{\delta v'' \delta w''} = \underbrace{\overline{v'' w''}}_{>0} - \underbrace{R_{23}(r_x)}_{<0} - \underbrace{R_{32}(r_x)}_{<0}, \tag{3.2}$$

Thus, the statistical trace of the contribution of the coherent production at this phase is positive and, at the separation $r_x = \delta x$, it has the maximum possible value.

$$P^C_{33,\theta_m>0} = -2 \underbrace{\overline{\delta v'' \delta w''}}_{>0} \underbrace{\left(\frac{d\tilde{w}}{dy} \right)}_{<0} > 0. \tag{3.3}$$

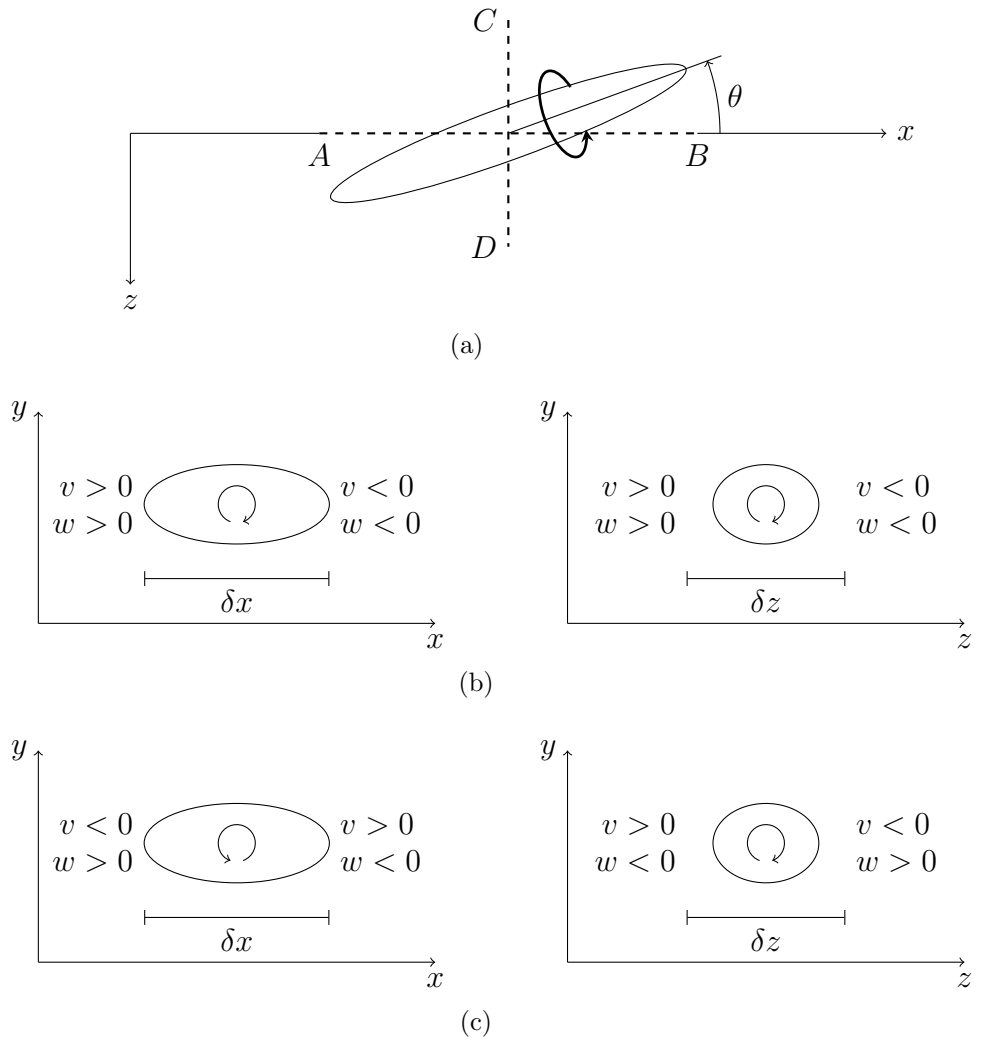

Figure 3.5: (a): Sketch of a SP tilted of an angle θ in the (x, z)-plane. (b): QSV at the phase when θ reaches its maximum positive value. Left: cross-section AB —projection in (x, y)-plane. Right: cross-section CD —projection in (z, y)-plane. (c): QSV at the phase when θ reaches its maximum negative value. Left: cross-section AB —projection in (x, y)-plane. Right: cross-section CD —projection in (z, y)-plane

The same line of reasoning is applied to the projection of a QSV on the (y, z)-plane (rightmost panel of figure 3.5b). The spanwise separation $r_z = \delta z$, at which the anti-correlation functions $R_{23}(r_z)$ and $R_{32}(r_z)$ peak, leads to the highest intensity of $\overline{\delta v'' \delta w''}$. Again, the contribution of the coherent production at this phase and this separation has positive sign and, under this conditions, it reaches its maximum value.

Conversely, at the phase at which the QSV reaches its maximum negative tilting, the value of the correspondent spanwise shear at $y^+ \approx 10$ has its positive peak. Looking at the projection of the QSV in the (x, y)-plane (leftmost panel of figure 3.5c), on the right side of the structure, relative low-speed spanwise flow ($w'' < 0$) is carried upwards ($v'' > 0$), whereas at its left side, relative high-speed spanwise flow ($w'' > 0$) is dragged towards the wall ($v'' < 0$). When the cross-correlation between wall-normal and spanwise fluctuations at the two sides of the vortical structure is maximum, the structure function $\overline{\delta v'' \delta w''}$ has a peak.

$$\overline{\delta v'' \delta w''} = \underbrace{\overline{v'' w''}}_{<0} - \underbrace{R_{23}(r_x)}_{>0} - \underbrace{R_{32}(r_x)}_{>0}, \tag{3.4}$$

so that the coherent production has a positive peak as well:

$$P^C_{33,\theta_m<0} = -2 \underbrace{\overline{\delta v'' \delta w''}}_{<0} \underbrace{\left(\frac{d\tilde{w}}{dy} \right)}_{>0} > 0. \tag{3.5}$$

As seen before, with the same line of reasoning, a spanwise characteristic length $r_z = \delta z$ can be found (rightmost panel of figure 3.5c).

Therefore, the coherent production term assumes large positive values when the structures are tilted the most in the (x, z)-plane either by a positive or negative angle. In this condition, the energy injected in the flow by the actuation is transferred from the coherent to the random fluctuations at precise scales and wall distance. Overall, this leads to a positive contribution of the coherent production to the budget of $\langle \delta w'' \delta w'' \rangle$ and to the definition of two characteristic scales (at $r_x \neq 0$ and $r_z \neq 0$) of this process.

Although the whole discussion has been based on the interplay between the coherent motion and a positive rotating QSV (SP), the same exact argument applies to a negative rotating QSV (SN), assuring coherent production to always assume positive value when the structures are inclined the most.

A third less intense peak of the coherent production term is detected at $(r_x^+, r_y^+, r_z^+, Y_c^+) = (0, 11, 0, 8.8)$ (figure 3.4*c*). This peak occurring at $r_y \neq 0$ does not allow the expression of P_{33}^C to reduce to the one of equation 3.1. Therefore, this local maximum can not be explained using the same reasoning used above and it needs to be further investigated to understand its physical meaning.

3.1.5 Fluxes

The flux vector $[\phi_y, \phi_z, \psi]$ describes how $\langle \delta u_i'' \delta u_j'' \rangle$ is transported among scales and along the wall-normal direction and it is visualised via its field lines. Both in the uncontrolled and controlled cases field lines of $\langle \delta u'' \delta u'' \rangle^+$ start in the buffer layer at $r_y = 0$, close to the locus of the maximum value of the source term. In the first part of their path, the field lines lay on a plane described by $Y^+ = r_y^+/2 + K_{11}^+$ — hereafter referred to as streamwise attached plane — transferring $\langle \delta u'' \delta u'' \rangle^+$ towards larger spanwise and wall-normal separations and away from the wall. Finally, they divert either towards the attached plane ($Y^+ = r_y^+/2$) or towards small separations, where they are dissipated. The wall motion affects the path of these field lines shifting the streamwise attached plane towards a larger wall-normal distance. The characteristic constant K_{11}^+ changes from the value of ~ 13 to the value of ~ 17 (figure 3.6*a*).

Conversely, there is no evidence of such shift in the field lines of $\langle \delta v'' \delta v'' \rangle^+$; in the first part of their path, they follow a line described by $Y^+ = r_y^+/2 + 40$ in both uncontrolled and controlled case.

Lastly, field lines of $\langle \delta w'' \delta w'' \rangle^+$ originate at $r_y \approx 0$ and they align along a line described by $Y_c^+ = r_y^+/2 + K_{33}^+$. Interestingly, in contrast to the streamwise fluxes, the spanwise attached plane shifts sligthly closer to the wall: K_{33}^+ decreases from 14.5 to 13.5 (figure 3.6*b*).

The upward shift of the flux of the streamwise stresses agrees with the thickening of the viscous sublayer, already highlighted by the change in the wall-normal position of $\langle \delta u'' \delta u'' \rangle_m^+$. The smaller modification affecting the fluxes of the other two normal stresses supports the idea that the thickening of the viscous sublayer mainly affects the streaks.

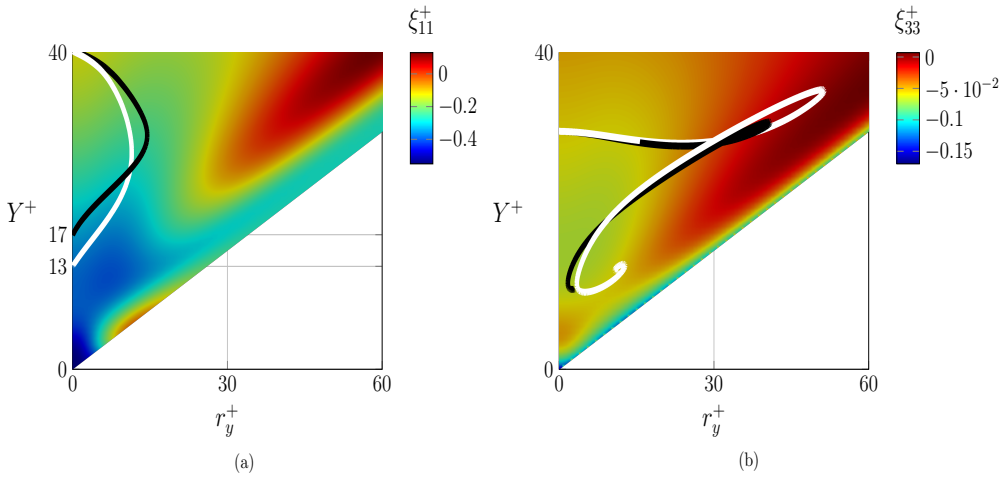

Figure 3.6: Field lines of the vector of fluxes of (a) $\langle \delta u'' \delta u'' \rangle^+$ and (b) $\langle \delta w'' \delta w'' \rangle^+$. White line describes a field line of uncontrolled case, black line of controlled case. Colour plot describes the source term ξ^+ of (a) $\langle \delta u'' \delta u'' \rangle$ and (b) $\langle \delta w'' \delta w'' \rangle$.

3.2 Off-diagonal component

3.2.1 Structure function

Among off-diagonal terms, the only one associated with a non-zero component of the Reynolds stress tensor is $\langle -\delta u'' \delta v'' \rangle$. Unlike diagonal terms, it can not be associated with the energy content of certain scales at a certain distance from the wall, since it is not defined in sign. The behaviour of $\langle -\delta u \delta v \rangle$ is considered as a proxy of the turbulent structures inducing a correlation between streamwise and vertical fluctuations. Table 3.2 summarises the changes of $\langle -\delta u'' \delta v'' \rangle_m^+$ between uncontrolled and controlled flow and figure 3.1 depicts them. $\langle -\delta u'' \delta v'' \rangle_m^+$ occurs at $r_y^+ = 0$. When the spanwise forcing is applied, it decreases by 6.9% and it shifts farther from the wall (from $Y^+ \approx 30$ to 34) with a negligible change in the spanwise separation. Similarly to the streamwise structure function, the shift in the vertical direction (by ~ 4 viscous units) is a trace of the thickening of the viscous sublayer.

3.2.2 Production, redistribution and dissipation

Both in uncontrolled and controlled cases the production and pressure strain terms are the main contributors to the source term. Indeed, the viscous dissipation D_{12} is negligible compared to P_{12} and Π_{12} (Gatti *et al.*, 2020). Table 3.2 summarises the maximum values of ξ_{12}^+ and the terms it involves, together with their positions.

Both positive and negative maxima of ξ_{12}^+ occur at $r_y = 0$. The former peak occurs at smaller spanwise separation in the buffer layer ($Y^+ = 13$), whereas the latter at larger spanwise separation at the wall. A second large region of negative ξ_{12}^+ occurs at $r_z \approx 0$, as depicted in figure 3.7*a-b*. When the control is applied, this peak becomes more negative and it shifts from the plane $Y^+ = r_y^+/2 + K^+$ described by $K^+ = 7$ to the plane described by $K^+ = 8.8$. This result is again compatible with the thickening of the viscous sublayer and the consequent upward shift of the near-wall cycle. At $r_y = 0$, the oscillation of the wall enhances the dependence of ξ_{12}^+ on the spanwise separation. Indeed, both maxima of $\xi_{12}^+ > 0$ and $\xi_{12}^+ < 0$ increase their intensities, creating two well-defined regions of opposite sign. This behaviour can be explained by the relative shift between peaks of production and pressure strain terms.

The negative maximum of the pressure strain term increases its value (+39%) and shift towards the wall (from $Y^+ = 16.5$ to 14), whereas the maximum production also increases (+21%) but shifts slightly farther from the wall (from $Y^+ = 13$ to 13.3). They both shift towards smaller spanwise separation: the former from $r_z^+ = 65$ to $r_z^+ = 55$, the latter from $r_z^+ = 36$ to $r_z^+ = 31$ (figure 3.7*e-f*). The combination of these changes leads to an increase of both the positive (+14%) and negative (+7%) peaks of the source term (figure 3.7*c-d*).

A last interesting difference between the uncontrolled and controlled case is the creation of a thin region of net production in the viscous sublayer (figure 3.7*d*). It extends down to the wall for $r_z^+ \in (0, 37)$, whereas for larger r_z^+ it is separated from the wall by a sink region. The rise of this area of $\xi_{12} > 0$ is associated with the pressure strain term. In the uncontrolled case, Π_{12}^+ is negative in the whole plane but a small region at $Y^+ \approx 5$ and $r_z^+ < 10$ (see figure 3.7*e*). When the spanwise forcing is active, this positive region shifts closer to the wall and at larger spanwise separation (see figure 3.7*f*). Its maximum increases by an order of magnitude, leading to the creation of this strip of net production.

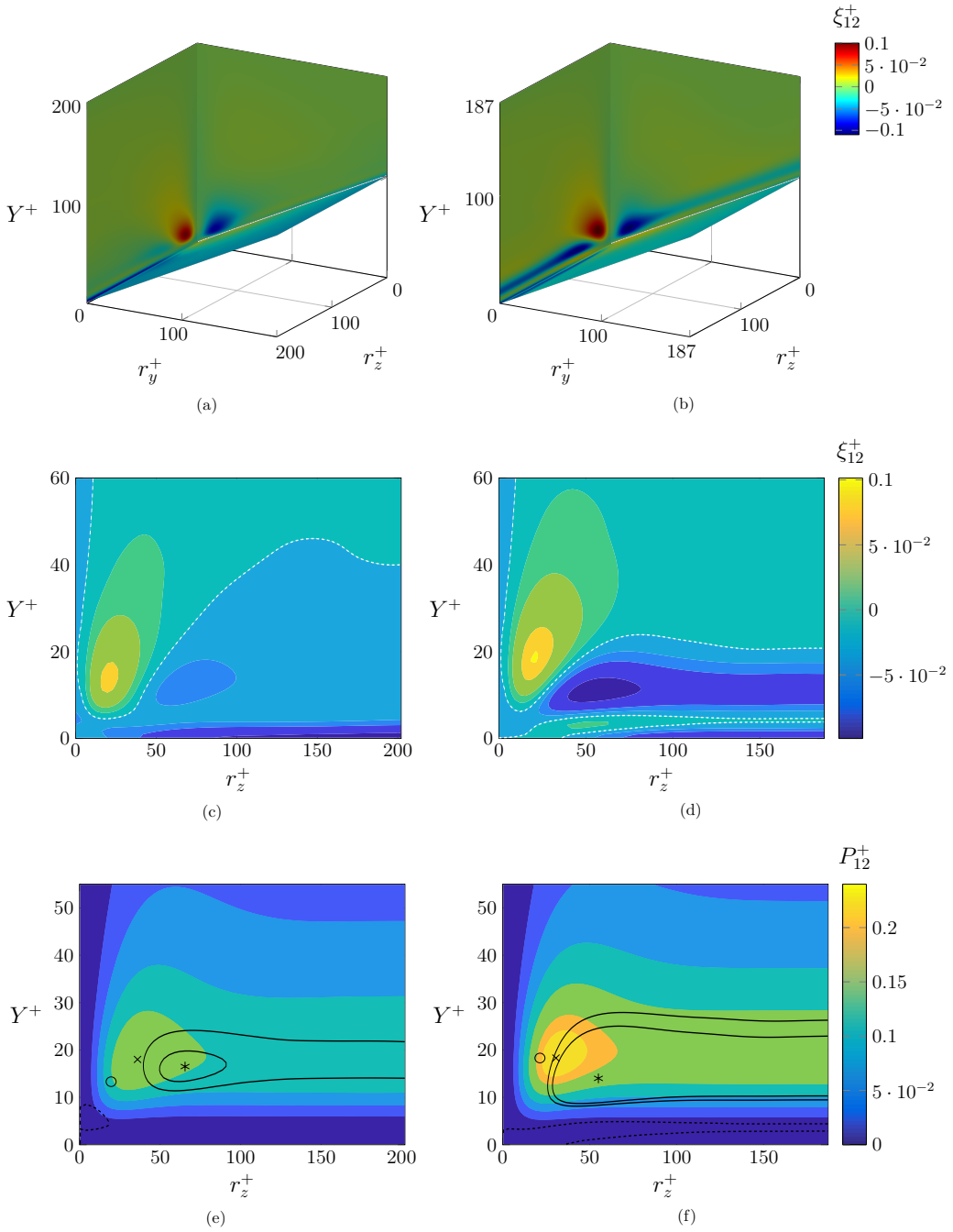

Figure 3.7: a-b: Source of $\langle -\delta u'' \delta v'' \rangle$ in (a) uncontrolled and (b) controlled flow in the (r_z^+, r_y^+, Y^+)-space. c-f: contour plot of the budget terms of $\langle -\delta u'' \delta v'' \rangle$ in (r_z^+, Y_c^+)-plane; filled contour of ξ_{12}^+ (-0.1:0.02:0.12), with zero line indicated by a white dashed line in uncontrolled (c) and controlled (d) flow; filled contour of P_{11}^+ (0:0.04:0.24), contour lines of $\Pi_{11,m}^+$ (-0.175,-0.155,0), $\times : P_{12,m}^+, * : \Pi_{12,m}^+, \circ : \xi_{12,m}^+$ of uncontrolled (e) and controlled (f) flow.

	$\langle -\delta u \delta v \rangle_m^+$		$\xi_{12,max}^+$		$\xi_{12,min}^+$	
	Value	Position	Value	Position	Value	Position
ref	2.06	(52,0,30)	0.089	(20,0,13)	-0.092	(202,0,0)
ow	1.92	(52,0,34)	0.102	(21,0,18)	-0.099	(55,0,11)
	$P_{ij,m}^+$		$\lvert\Pi_{ij}^+\rvert_m$			
	Value	Position	Value	Position		
ref	0.20	(36,0,18)	0.18	(65,0,16)		
ow	0.24	(31,0,18)	0.25	(55,0,14)		

Table 3.2: Maximum values of $\langle -\delta u'' \delta v'' \rangle^+$, its positive $\xi_{12,max}^+$ and negative $\xi_{12,min}^+$ source terms, production P_{12}^+, absolute pressure strain $|\Pi_{12}^+|$ in the (r_z^+, r_y^+, Y^+)-space.

Chapter 4

Conclusions

The present work studies a channel flow controlled by spanwise wall-oscillation with a focus on the interaction between the coherent motion imposed by the control, i.e. the *Stokes layer* and the near-wall cycle. The aim is to contribute to the understanding of the fundamental mechanism responsible for the reduction of the friction drag resulting from the wall motion. Two Direct Numerical Simulations for the controlled and uncontrolled flows have been performed and compared to highlight the changes the turbulent field undergoes when subjected to a spanwise forcing. The amplitude and period of the oscillation have been chosen close to the optimum value to achieve the maximum net saving. The analysis has been carried out using the Anisotropic Generalised Kolmogorov Equations (AGKE), the budget equation for the second-order structure function tensor $\langle \delta u_i \delta u_j \rangle$ (Gatti *et al.*, 2020). The AGKE describe the production, transport, redistribution and dissipation processes of each component of the Reynolds stress tensor, considering together the space of scales and the physical space. In the present work, the AGKE have been written for the first time for the triple decomposition of the velocity into the mean, coherent and stochastic contributions; they perfectly fit with our aim of highlighting the interaction between the coherent motions imposed by the spanwise forcing and the turbulent field.

The three diagonal components $\langle \delta u'' \delta u'' \rangle$, $\langle \delta v'' \delta v'' \rangle$ and $\langle \delta w'' \delta w'' \rangle$ are weaken when the control is applied, consistently with a slight decrease of the turbulent intensity. However, the spanwise wall-oscillation affects the diagonal components differently, leading to a decrease in the flow anisotropy. Indeed, the decrease of the intensity of $\langle \delta u'' \delta u'' \rangle$ is larger compared to the decrease of the cross-stream components. This indicates that the streaks of streamwise

velocity are affected by the *Stokes layer* more than the quasi-streamwise vortices. This observation is further confirmed by the shift faced by the maxima of the three diagonal components and by their fluxes. Indeed, the maximum of $\langle \delta u'' \delta u'' \rangle$ and its fluxes — that indicate the main transport processes — are shifted towards larger wall distances of about 3 wall units in the controlled case, indicating that the thickening of the viscous sublayer affects the position of the streaks. On the contrary, the positions of the largest values of $\langle \delta v'' \delta v'' \rangle$, $\langle \delta w'' \delta w'' \rangle$ and of their fluxes are almost unaffected by the control, indicating that the thickening of the viscous sublayer does not affect the average wall distance at which the QSV are placed. The decrease of the flow anisotropy is partially explained by the changes of the pressure strain in the controlled case. When the control is applied, the negative peak of Π_{11} at the scales and position typical of the near-wall cycle increases, indicating that the redistribution of $\langle \delta u'' \delta u'' \rangle$ towards the cross-stream components is enhanced. Consistently, this is accompanied by a tiny increase of the positive peak of Π_{22} and by a larger increase of Π_{33}. Therefore, the picture is that when the control is active, the interaction of the *Stokes layer* with the near-wall cycle enhances the redistribution via pressure strain of $\langle \delta u'' \delta u'' \rangle$ towards the cross-stream components, with $\langle \delta w'' \delta w'' \rangle$ being the main receiver. This explains the decrease of the flow anisotropy shown by the intensity of $\left\langle \delta u_i'' \delta u_j'' \right\rangle$.

The spanwise wall motion also slightly affects the typical scales of the near-wall cycle. In the controlled case the peak of $\langle \delta u'' \delta u'' \rangle$ moves towards larger spanwise separations of about 3 wall units, while those of $\langle \delta v'' \delta v'' \rangle$ and $\langle \delta w'' \delta w'' \rangle$ towards lower r_z. This is consistent with the picture of low- and high- velocity streaks moving apart when the control is applied and of a slight decrease of the average cross-section of the quasi-streamwise vortices in the (y, z)-plane.

In writing the AGKE for the triple decomposition, a new production term, namely P^C arises in the budget equation for $\langle \delta w'' \delta w'' \rangle$ that highlights the cross-talk between the coherent motion of the *Stokes layer* and the stochastic turbulent fluctuations. This term describes at which scales and position the spanwise energy is transferred from the *Stokes layer* to the stochastic turbulent field and vice-versa due to the interaction of the quasi-streamwise vortices with the spanwise velocity shear. P^C is found to be positive at all scales and positions, indicating that on average, the *Stokes layer* acts like a donor and the spanwise fluctuating field like a receiver. Three localised peaks of P^C have been detected to highlight the scales at which such energy exchange occurs. The harmonic wall oscillation enforced by the control im-

poses a spanwise velocity shear, which forces the quasi-streamwise vortices to continually re-orientate in wall-parallel planes. When the QSV are tilted the most in the (x, z)-plane, the energy injected in the flow by the actuation is transferred from the coherent to the random fluctuations, leading to large values of the coherent production at two well-defined scales and wall distances at alternatively $r_x \neq 0$ and $r_z \neq 0$. However, further investigation is needed to assess the dependence of such a process on the different phases of the wall-oscillation. Indeed, although on average P^C is a positive source of the fluctuating field and a sink for the *Stokes layer*, the opposite may occur during the phases of the oscillation.

Further investigation can also be performed to assess the dependence of the processes studied in the present work upon the amplitude and the period of the oscillation of the spanwise forcing. On one hand, the increased amplitude of the oscillation allows to enhance the variations between the uncontrolled and the controlled case in terms of intensity, scales and positions and to increase the drag-reduction rate; on the other hand, moving away from the near-optimum oscillation period reduces the drag-reduction margin but allows to enhance the effect of the direct interaction between coherent motion and stochastic fluctuations via coherent production term. A further extension of the present work is to exploit the AGKE written for the triple decomposition also to study the case of a turbulent channel controlled via travelling waves (Quadrio *et al.*, 2009) to describe the interaction between the *generalised Stokes layer* (Quadrio & Ricco, 2011) and the turbulent field. This may further elucidate the differences in the mechanism leading to drag reduction in the two cases.

Finally, it is worth stressing that the AGKE written for the triple decomposition have great potential in general. Indeed, they perfectly fit for more complex problems where both inhomogeneity and anisotropy are important, such as flows presenting a coherent motion superimposed of the turbulent fluctuations. An example is the turbulent flow past bluff bodies that features the coexistence of large-scale motions typical of the Kàrmàn vortices and small-scale motions typical of the turbulent fluctuations.

Appendix A

Budget equations for $\left\langle \delta u_i \delta u_j \right\rangle$ and $\left\langle \delta \tilde{u}_i \delta \tilde{u}_j \right\rangle$

In this appendix coherent and fluctuating anisotropic generalised Kolmogorov equations are derived from Navier-Stokes equations for an indefinite plane channel flow. For this purpose it is considered a Cartesian coordinate system in which x and z denote the homogeneous streamwise and spanwise directions respectively, whereas y is the wall-normal direction. Index notation is used throughout this section.
Using a triple decomposition the velocity vector $\boldsymbol{v}$ can be decomposed in the mean velocity $\boldsymbol{U}$, the coherent/periodic part of the flow $\tilde{\boldsymbol{u}}$ and the random/cahotic part of the flow $\boldsymbol{u}$:

$$\boldsymbol{v} = \boldsymbol{U} + \tilde{\boldsymbol{u}} + \boldsymbol{u}. \tag{A.1}$$

We define $\boldsymbol{u}'$ as the sum of $\tilde{\boldsymbol{u}}$ and $\boldsymbol{u}$, i.e. the fluctuating field with respect to the mean flow:

$$\boldsymbol{u}' = \tilde{\boldsymbol{u}} + \boldsymbol{u}. \tag{A.2}$$

In the following $\langle \cdot \rangle$ denotes averaging in time and in homogeneous directions if present, whereas $\tilde{\cdot}$ phase averaging. One may observe that for the second order structure function:

$$\left\langle \delta u_i' \delta u_j' \right\rangle = \langle \delta \tilde{u}_i \delta \tilde{u}_j \rangle + \langle \delta u_i \delta u_j \rangle \tag{A.3}$$

as a result the AGKE for $\left\langle \delta u_j' \delta u_j' \right\rangle$ comes from the sum of the AGKE for $\langle \delta \tilde{u}_i \delta \tilde{u}_j \rangle$ and for $\langle \delta u_i \delta u_j \rangle$.

A.1 Budget equation for U_i, $\tilde{u}_i$ and u_i'

We start from the Navier–Stokes equations, i.e.

$$\frac{\partial v_i}{\partial t} + v_j \frac{\partial v_i}{\partial x_j} = -\frac{1}{\rho}\frac{\partial p}{\partial x_i} + \nu \frac{\partial^2 v_i}{\partial x_j \partial x_j}. \tag{A.4}$$

We introduce the triple decomposition for v_i and obtain:

$$\frac{\partial \tilde{u}_i}{\partial t} + \frac{\partial u_i}{\partial t} + (U_j + \tilde{u}_j + u_j)\frac{\partial}{\partial x_j}(U_i + \tilde{u}_i + u_i) = -\frac{1}{\rho}\frac{\partial}{\partial x_i}(P + \tilde{p} + p) + \nu \frac{\partial^2}{\partial x_j \partial x_j}(U_i + \tilde{u}_i + u_i) \tag{A.5}$$

which can be written as

$$\frac{\partial \tilde{u}_i}{\partial t} + \frac{\partial u_i}{\partial t} + U_j\frac{\partial U_i}{\partial x_j} + U_j\frac{\partial \tilde{u}_i}{\partial x_j} + U_j\frac{\partial u_i}{\partial x_j} + \tilde{u}_j\frac{\partial U_i}{\partial x_j} + \tilde{u}_j\frac{\partial \tilde{u}_i}{\partial x_j} + \tilde{u}_j\frac{\partial u_i}{\partial x_j} +$$
$$u_j\frac{\partial U_i}{\partial x_j} + u_j\frac{\partial \tilde{u}_i}{\partial x_j} + u_j\frac{\partial u_i}{\partial x_j} = -\frac{1}{\rho}\frac{\partial P}{\partial x_i} - \frac{1}{\rho}\frac{\partial \tilde{p}}{\partial x_i} - \frac{1}{\rho}\frac{\partial p}{\partial x_i} + \nu\frac{\partial^2 U_i}{\partial x_j \partial x_j} + \nu\frac{\partial^2 \tilde{u}_i}{\partial x_j \partial x_j} + \nu\frac{\partial^2 u_i}{\partial x_j \partial x_j} \tag{A.6}$$

Now we use the $\langle\cdot\rangle$ operator and we get the budget equation for U_i, i.e.

$$U_j\frac{\partial U_i}{\partial x_j} + \left\langle \tilde{u}_j\frac{\partial \tilde{u}_i}{\partial x_j}\right\rangle + \left\langle u_j\frac{\partial u_i}{\partial x_j}\right\rangle = -\frac{1}{\rho}\frac{\partial P}{\partial x_i} + \nu\frac{\partial^2 U_i}{\partial x_j \partial x_j} \tag{A.7}$$

If, instead, we use the phase-average operator $\overline{\cdot}$, we get:

$$\frac{\partial \tilde{u}_i}{\partial t} + U_j\frac{\partial U_i}{\partial x_j} + \tilde{u}_j\frac{\partial U_i}{\partial x_j} + U_j\frac{\partial \tilde{u}_i}{\partial x_j} + \tilde{u}_i\frac{\partial \tilde{u}_i}{\partial x_j} + \overline{u_j\frac{\partial u_i}{\partial x_j}} = -\frac{1}{\rho}\frac{\partial P}{\partial x_i} - \frac{1}{\rho}\frac{\partial \tilde{p}}{x_i} + \nu\frac{\partial^2 U_i}{\partial x_j \partial x_j} + \nu\frac{\partial^2 \tilde{u}_i}{\partial x_j \partial x_j} \tag{A.8}$$

which can be written differently using the budget equation for U_i, i.e.:

$$\frac{\partial \tilde{u}_i}{\partial t} + \tilde{u}_j\frac{\partial U_i}{\partial x_j} + U_j\frac{\partial \tilde{u}_i}{\partial x_j} + \tilde{u}_j\frac{\partial \tilde{u}_i}{\partial x_j} + \overline{u_j\frac{\partial u_i}{\partial x_j}} - \left\langle \tilde{u}_j\frac{\partial \tilde{u}_i}{\partial x_j}\right\rangle - \left\langle u_j\frac{\partial u_i}{\partial x_j}\right\rangle = -\frac{1}{\rho}\frac{\tilde{p}}{\partial x_i} + \nu\frac{\partial^2 \tilde{u}_i}{\partial x_j \partial x_j} \tag{A.9}$$

which turns to be the budget equation for $\tilde{u}_i$, i.e.

$$\frac{\partial \tilde{u}_i}{\partial t} + U_j\frac{\partial \tilde{u}_i}{\partial x_j} + \tilde{u}_j\frac{\partial U_i}{\partial x_j} + \frac{\partial}{\partial x_j}(\tilde{u}_i\tilde{u}_j - \langle \tilde{u}_i\tilde{u}_j\rangle) + \frac{\partial}{\partial x_j}(\overline{u_i u_j} - \langle u_i u_j\rangle) = -\frac{1}{\rho}\frac{\partial \tilde{p}}{\partial x_i} + \nu\frac{\partial^2 \tilde{u}_i}{\partial x_j \partial x_j} \tag{A.10}$$

The budget equation for u_i, instead, is obtained subtracting from equation A.6 the budget equations for U_i (equation A.7) and $\tilde{u}_i$ (equation A.10), i.e.:

$$\frac{\partial u_i}{\partial t}+U_j\frac{\partial u_i}{\partial x_j}+\tilde{u}_j\frac{\partial u_i}{\partial x_j}+u_j\frac{\partial U_i}{\partial x_j}+u_j\frac{\partial \tilde{u}_i}{\partial x_j}+\frac{\partial}{\partial x_j}\left(u_iu_j-\overline{u_iu_j}\right)=-\frac{1}{\rho}\frac{\partial p}{\partial x_i}+\nu\frac{\partial^2 u_i}{\partial x_j\partial x_j} \tag{A.11}$$

A.2 AGKE for $\langle \delta\tilde{u}_i\delta\tilde{u}_j\rangle$

First we write the budget equation for $\tilde{u}_i$ in $\boldsymbol{x}$ and $\boldsymbol{x}^+=\boldsymbol{x}+\boldsymbol{r}$ and we subtract the first to the second one:

$$\begin{gathered}\Delta\left(\frac{\partial\tilde{u}_i}{\partial t}\right)+\Delta\left(U_j\frac{\partial\tilde{u}_i}{\partial x_j}\right)+\Delta\left(\tilde{u}_j\frac{\partial U_i}{\partial x_j}\right)+\\ \Delta\left(\frac{\partial}{\partial x_j}\left(\tilde{u}_i\tilde{u}_j-\langle\tilde{u}_i\tilde{u}_j\rangle\right)\right)+\Delta\left(\frac{\partial}{\partial x_j}\left(\overline{u_iu_j}-\langle u_iu_j\rangle\right)\right)=\\ -\Delta\left(\frac{1}{\rho}\frac{\partial\tilde{p}}{\partial x_i}\right)+\Delta\left(\nu\frac{\partial^2\tilde{u}_i}{\partial x_j\partial x_j}\right).\end{gathered} \tag{A.12}$$

by recalling that the two reference systems are independent one may write for example:

$$\Delta\left(U_j\frac{\partial\tilde{u}_i}{\partial x_j}\right)=U_j^+\frac{\partial\delta\tilde{u}_i}{\partial x_j^+}+U_j\frac{\partial\delta\tilde{u}_i}{\partial x_j}; \tag{A.13}$$

using the same line of reasoning for all the other terms one obtains

$$\begin{gathered}\frac{\partial\delta\tilde{u}_i}{\partial t}+U_j^+\frac{\partial\delta\tilde{u}_i}{\partial x_j^+}+U_j\frac{\partial\delta\tilde{u}_i}{\partial x_j}+\\ +\tilde{u}_j^+\frac{\partial\delta U_i}{\partial x_j^+}+\tilde{u}_j\frac{\partial\delta U_i}{\partial x_j}+\tilde{u}_j^+\frac{\partial\delta\tilde{u}_i}{\partial x_j^+}+\tilde{u}_j\frac{\partial\delta\tilde{u}_i}{\partial x_j}-\\ \left\langle\tilde{u}_j^+\frac{\partial\delta\tilde{u}_i}{\partial x_j^+}\right\rangle-\left\langle\tilde{u}_j\frac{\partial\delta\tilde{u}_i}{\partial x_j}\right\rangle+\overline{u_j^+\frac{\partial\delta u_i}{\partial x_j^+}}+\overline{u_j\frac{\partial\delta u_i}{\partial x_j}}-\\ \left\langle u_j^+\frac{\partial\delta u_i}{\partial x_j^+}\right\rangle-\left\langle u_j\frac{\partial\delta u_i}{\partial x_j}\right\rangle=-\frac{1}{\rho}\frac{\partial\delta\tilde{p}}{\partial x_i^+}-\frac{1}{\rho}\frac{\partial\delta\tilde{p}}{\partial x_i}+\\ \nu\left(\frac{\partial^2}{\partial x_j^+\partial x_j^+}+\frac{\partial^2}{\partial x_j\partial x_j}\right)\delta\tilde{u}_i.\end{gathered} \tag{A.14}$$

Then one may write for example

$$\tilde{u}_j^+ \frac{\partial \delta\tilde{u}_i}{\partial x_j^+} = \delta\tilde{u}_j \frac{\partial \delta\tilde{u}_i}{\partial x_j^+} + \tilde{u}_j \frac{\partial \delta\tilde{u}_i}{\partial x_j^+} \tag{A.15}$$

and using this expression for all the terms we obtain the budget equation for $\delta\tilde{u}_i$:

$$\begin{aligned}
&\frac{\partial \delta\tilde{u}_i}{\partial t} + \delta U_j \frac{\partial \delta\tilde{u}_i}{\partial x_j^+} + U_j \left(\frac{\partial}{\partial x_j^+} + \frac{\partial}{\partial x_j} \right) \delta\tilde{u}_i + \\
&\delta\tilde{u}_j \frac{\partial \delta U_i}{\partial x_j^+} + \tilde{u}_j \left(\frac{\partial}{\partial x_j^+} + \frac{\partial}{\partial x_j} \right) \delta U_i + \\
&\delta\tilde{u}_j \frac{\partial \delta\tilde{u}_i}{\partial x_j^+} + \tilde{u}_j \left(\frac{\partial}{\partial x_j^+} + \frac{\partial}{\partial x_j} \right) \delta\tilde{u}_i - \\
&\left\langle \delta\tilde{u}_j \frac{\partial \delta\tilde{u}_i}{\partial x_j^+} \right\rangle - \left\langle \tilde{u}_j \left(\frac{\partial}{\partial x_j^+} + \frac{\partial}{\partial x_j} \right) \delta\tilde{u}_i \right\rangle + \\
&\overline{\delta u_j \frac{\partial \delta u_i}{\partial x_j^+}} + \overline{u_j \left(\frac{\partial}{\partial x_j^+} + \frac{\partial}{\partial x_j} \right) \delta u_i} = \\
&-\frac{1}{\rho} \frac{\partial \delta\tilde{p}}{\partial x_i^+} - \frac{1}{\rho} \frac{\partial \delta\tilde{p}}{\partial x_i} + \nu \left(\frac{\partial^2}{\partial x_j^+ \partial x_j^+} + \frac{\partial^2}{\partial x_j \partial x_j} \right) \delta\tilde{u}_i.
\end{aligned} \tag{A.16}$$

Then we multiply this equation for $\delta\tilde{u}_k$ and we obtain:

$$\begin{aligned}
&\delta\tilde{u}_k\frac{\partial\delta\tilde{u}_i}{\partial t}+\delta\tilde{u}_k\delta U_j\frac{\partial\delta\tilde{u}_i}{\partial x_j^+}+\delta\tilde{u}_k U_j\left(\frac{\partial}{\partial x_j^+}+\frac{\partial}{\partial x_j}\right)\delta\tilde{u}_i+\\
&\delta\tilde{u}_k\delta\tilde{u}_j\frac{\partial\delta U_i}{\partial x_j^+}+\delta\tilde{u}_k\tilde{u}_j\left(\frac{\partial}{\partial x_j^+}+\frac{\partial}{\partial x_j}\right)\delta U_i+\\
&\delta\tilde{u}_k\delta\tilde{u}_j\frac{\partial\delta\tilde{u}_i}{\partial x_j^+}+\delta\tilde{u}_k\tilde{u}_j\left(\frac{\partial}{\partial x_j^+}+\frac{\partial}{\partial x_j}\right)\delta\tilde{u}_i-\\
&\delta\tilde{u}_k\left\langle\delta\tilde{u}_j\frac{\partial\delta\tilde{u}_i}{\partial x_j^+}\right\rangle-\delta\tilde{u}_k\left\langle\tilde{u}_j\left(\frac{\partial}{\partial x_j^+}+\frac{\partial}{\partial x_j}\right)\delta\tilde{u}_i\right\rangle+\\
&\overline{\delta\tilde{u}_k\delta u_j\frac{\partial\delta u_i}{\partial x_j^+}}+\overline{\delta\tilde{u}_k u_j\left(\frac{\partial}{\partial x_j^+}+\frac{\partial}{\partial x_j}\right)\delta u_i}=\\
&-\delta\tilde{u}_k\frac{1}{\rho}\left(\frac{\partial}{\partial x_i^+}+\frac{\partial}{\partial x_i}\right)\delta\tilde{p}+\nu\delta\tilde{u}_k\left(\frac{\partial^2}{\partial x_j^+\partial x_j^+}+\frac{\partial^2}{\partial x_j\partial x_j}\right)\delta\tilde{u}_i.
\end{aligned}\tag{A.17}$$

Then we write the same equation inverting the i index and the k index and we sum them together.

$$
\begin{aligned}
&\frac{\partial}{\partial t}\delta\tilde{u}_i\delta\tilde{u}_k + \delta\tilde{u}_k\delta U_j\frac{\partial\delta\tilde{u}_i}{\partial x_j^+} + \delta\tilde{u}_i\delta U_j\frac{\partial\delta\tilde{u}_k}{\partial x_j^+} + \\
&\delta\tilde{u}_k U_j\left(\frac{\partial}{\partial x_j^+}+\frac{\partial}{\partial x_j}\right)\delta\tilde{u}_i + \delta\tilde{u}_i U_j\left(\frac{\partial}{\partial x_j^+}+\frac{\partial}{\partial x_j}\right)\delta\tilde{u}_k + \\
&\delta\tilde{u}_k\delta\tilde{u}_j\frac{\partial\delta U_i}{\partial x_j^+} + \delta\tilde{u}_i\delta\tilde{u}_j\frac{\partial\delta U_k}{\partial x_j^+} + \\
&\delta\tilde{u}_k\tilde{u}_j\left(\frac{\partial}{\partial x_j^+}+\frac{\partial}{\partial x_j}\right)\delta U_i + \delta\tilde{u}_i\tilde{u}_j\left(\frac{\partial}{\partial x_j^+}+\frac{\partial}{\partial x_j}\right)\delta U_k + \\
&\delta\tilde{u}_k\delta\tilde{u}_j\frac{\partial\delta\tilde{u}_i}{\partial x_j^+} + \delta\tilde{u}_i\delta\tilde{u}_j\frac{\partial\delta\tilde{u}_k}{\partial x_j^+} + \\
&\delta\tilde{u}_k\tilde{u}_j\left(\frac{\partial}{\partial x_j^+}+\frac{\partial}{\partial x_j}\right)\delta\tilde{u}_i + \delta\tilde{u}_i\tilde{u}_j\left(\frac{\partial}{\partial x_j^+}+\frac{\partial}{\partial x_j}\right)\delta\tilde{u}_k - \\
&\delta\tilde{u}_k\left\langle\delta\tilde{u}_j\frac{\partial\delta\tilde{u}_i}{\partial x_j^+}\right\rangle - \delta\tilde{u}_i\left\langle\delta\tilde{u}_j\frac{\partial\delta\tilde{u}_k}{\partial x_j^+}\right\rangle - \\
&\delta\tilde{u}_k\left\langle\tilde{u}_j\left(\frac{\partial}{\partial x_j^+}+\frac{\partial}{\partial x_j}\right)\delta\tilde{u}_i\right\rangle - \delta\tilde{u}_i\left\langle\tilde{u}_j\left(\frac{\partial}{\partial x_j^+}+\frac{\partial}{\partial x_j}\right)\delta\tilde{u}_k\right\rangle + \\
&\overline{\delta\tilde{u}_k\delta u_j\frac{\partial\delta u_i}{\partial x_j^+}} + \overline{\delta\tilde{u}_i\delta u_j\frac{\partial\delta u_k}{\partial x_j^+}} + \\
&\overline{\delta\tilde{u}_k u_j\left(\frac{\partial}{\partial x_j^+}+\frac{\partial}{\partial x_j}\right)\delta u_i} + \overline{\delta\tilde{u}_i u_j\left(\frac{\partial}{\partial x_j^+}+\frac{\partial}{\partial x_j}\right)\delta u_k} = \\
&-\delta\tilde{u}_k\frac{1}{\rho}\left(\frac{\partial}{\partial x_i^+}+\frac{\partial}{\partial x_i}\right)\delta\tilde{p} - \delta\tilde{u}_i\frac{1}{\rho}\left(\frac{\partial}{\partial x_k^+}+\frac{\partial}{\partial x_k}\right)\delta\tilde{p} + \\
&\nu\delta\tilde{u}_k\left(\frac{\partial^2}{\partial x_j^+\partial x_j^+}+\frac{\partial^2}{\partial x_j\partial x_j}\right)\delta\tilde{u}_i + \nu\delta\tilde{u}_i\left(\frac{\partial^2}{\partial x_j^+\partial x_j^+}+\frac{\partial^2}{\partial x_j\partial x_j}\right)\delta\tilde{u}_k.
\end{aligned}
\tag{A.18}
$$

At this point we use the phase-average operator $\bar{\cdot}$ and then the time-average operator $\langle\cdot\rangle$ and we obtain:

$$\begin{gathered}
\frac{\partial}{\partial x_j^+}\langle\delta U_j\delta\tilde{u}_i\delta\tilde{u}_k\rangle+\left(\frac{\partial}{\partial x_j^+}+\frac{\partial}{\partial x_j}\right)\langle U_j\delta\tilde{u}_i\tilde{u}_k\rangle+\\
\langle\delta\tilde{u}_k\delta\tilde{u}_j\rangle\frac{\partial\delta U_i}{\partial x_j^+}+\langle\delta\tilde{u}_i\delta\tilde{u}_j\rangle\frac{\partial\delta U_k}{\partial x_j^+}+\\
\langle\delta\tilde{u}_k\tilde{u}_j\rangle\left(\frac{\partial}{\partial x_j^+}+\frac{\partial}{\partial x_j}\right)\delta U_i+\langle\delta\tilde{u}_i\tilde{u}_j\rangle\left(\frac{\partial}{\partial x_j^+}+\frac{\partial}{\partial x_j}\right)\delta U_k+\\
\frac{\partial}{\partial x_j^+}\langle\delta\tilde{u}_j\delta\tilde{u}_i\delta\tilde{u}_k\rangle+\left(\frac{\partial}{\partial x_j^+}+\frac{\partial}{\partial x_j}\right)\langle\tilde{u}_j\delta\tilde{u}_i\delta\tilde{u}_k\rangle+\\
\left\langle\delta\tilde{u}_k\frac{\partial}{\partial x_j^+}\overline{\delta u_i\delta u_j}\right\rangle+\left\langle\delta\tilde{u}_i\frac{\partial}{\partial x_j^+}\overline{\delta u_k\delta u_j}\right\rangle+\\
\left\langle\delta\tilde{u}_k\overline{u_j\left(\frac{\partial}{\partial x_j^+}+\frac{\partial}{\partial x_j}\right)\delta u_i}\right\rangle+\left\langle\delta\tilde{u}_i\overline{u_j\left(\frac{\partial}{\partial x_j^+}+\frac{\partial}{\partial x_j}\right)\delta u_k}\right\rangle=\\
-\left\langle\delta\tilde{u}_k\frac{1}{\rho}\left(\frac{\partial}{\partial x_i^+}+\frac{\partial}{\partial x_i}\right)\delta\tilde{p}\right\rangle-\left\langle\delta\tilde{u}_i\frac{1}{\rho}\left(\frac{\partial}{\partial x_k^+}+\frac{\partial}{\partial x_k}\right)\delta\tilde{p}\right\rangle+\\
\nu\left\langle\delta\tilde{u}_k\left(\frac{\partial^2}{\partial x_j^+\partial x_j^+}+\frac{\partial^2}{\partial x_j\partial x_j}\right)\delta\tilde{u}_i\right\rangle+\\
\nu\left\langle\delta\tilde{u}_i\left(\frac{\partial^2}{\partial x_j^+\partial x_j^+}+\frac{\partial^2}{\partial x_j\partial x_j}\right)\delta\tilde{u}_k\right\rangle.
\end{gathered}\tag{A.19}$$

We now introduce the new independent variables $\boldsymbol{X}$ and $\boldsymbol{r}$ such that

$$X_i=\frac{x_i+x_i^+}{2}\qquad r_i=x_i^+-x_i.$$

As a result the x_i- and x_i^+-derivatives are related to the X_i- and r_i-derivatives by:

$$\frac{\partial}{\partial x_i}=\frac{1}{2}\frac{\partial}{\partial X_i}-\frac{\partial}{\partial r_i};\quad \frac{\partial}{\partial x_i^+}=\frac{1}{2}\frac{\partial}{\partial X_i}+\frac{\partial}{\partial r_i};\quad \frac{\partial^2}{\partial x_j^+\partial x_j^+}+\frac{\partial^2}{\partial x_j\partial x_j}=\frac{1}{2}\frac{\partial^2}{\partial X_j\partial X_j}+2\frac{\partial^2}{\partial r_j\partial r_j}$$

As a result the previous equation becomes:

$$\left(\frac{1}{2}\frac{\partial}{\partial X_j}+\frac{\partial}{\partial r_j}\right)\langle\delta U_j\delta\tilde{u}_i\delta\tilde{u}_k\rangle+\frac{\partial}{\partial X_j}\langle U_j\delta\tilde{u}_i\delta\tilde{u}_k\rangle+$$
$$\langle\delta\tilde{u}_k\delta\tilde{u}_j\rangle\left(\frac{1}{2}\frac{\partial}{\partial X_j}+\frac{\partial}{\partial r_j}\right)\delta U_i+\langle\delta\tilde{u}_i\delta\tilde{u}_j\rangle\left(\frac{1}{2}\frac{\partial}{\partial X_j}+\frac{\partial}{\partial r_j}\right)\delta U_k+$$
$$\langle\delta\tilde{u}_k\tilde{u}_j\rangle\frac{\partial}{\partial X_j}\delta U_i+\langle\delta\tilde{u}_i\tilde{u}_j\rangle\frac{\partial}{\partial X_j}\delta U_k+$$
$$\left(\frac{1}{2}\frac{\partial}{\partial X_j}+\frac{\partial}{\partial r_j}\right)\langle\delta\tilde{u}_j\delta\tilde{u}_i\delta\tilde{u}_k\rangle+\frac{\partial}{\partial X_j}\langle\tilde{u}_j\delta\tilde{u}_i\delta\tilde{u}_k\rangle+$$
$$\left\langle\delta\tilde{u}_k\left(\frac{1}{2}\frac{\partial}{\partial X_j}+\frac{\partial}{\partial r_j}\right)\overline{\delta u_i\delta u_j}\right\rangle+\left\langle\delta\tilde{u}_i\left(\frac{1}{2}\frac{\partial}{\partial X_j}+\frac{\partial}{\partial r_j}\right)\overline{\delta u_k\delta u_j}\right\rangle+ \tag{A.20}$$
$$\left\langle\delta\tilde{u}_k\overline{u_j\frac{\partial}{\partial X_j}\delta u_i}\right\rangle+\left\langle\delta\tilde{u}_i\overline{u_j\frac{\partial}{\partial X_j}\delta u_k}\right\rangle=$$
$$-\left\langle\delta\tilde{u}_k\frac{1}{\rho}\left(\frac{\partial}{\partial X_i}\right)\delta\tilde{p}\right\rangle-\left\langle\delta\tilde{u}_i\frac{1}{\rho}\left(\frac{\partial}{\partial X_k}\right)\delta\tilde{p}\right\rangle+$$
$$\nu\left\langle\delta\tilde{u}_k\left(\frac{1}{2}\frac{\partial^2}{\partial X_j\partial X_j}+2\frac{\partial^2}{\partial r_j\partial r_j}\right)\delta\tilde{u}_i\right\rangle+$$
$$\nu\left\langle\delta\tilde{u}_i\left(\frac{1}{2}\frac{\partial^2}{\partial X_j\partial X_j}+2\frac{\partial^2}{\partial r_j\partial r_j}\right)\delta\tilde{u}_k\right\rangle.$$

We may observe that

$$\left\langle\delta\tilde{u}_k\left(\frac{1}{2}\frac{\partial}{\partial X_j}+\frac{\partial}{\partial r_j}\right)\overline{\delta u_i\delta u_j}\right\rangle+\left\langle\delta\tilde{u}_k\overline{u_j\frac{\partial}{\partial X_j}\delta u_i}\right\rangle=$$
$$\left\langle\delta\tilde{u}_k\left(\frac{1}{2}\frac{\partial}{\partial X_j}+\frac{\partial}{\partial r_j}\right)\overline{\delta u_i\delta u_j}\right\rangle+\left\langle\delta\tilde{u}_k\frac{\partial}{\partial X_j}\overline{u_j\delta u_i}\right\rangle=$$
$$\left\langle\delta\tilde{u}_k\frac{\partial}{\partial r_j}\overline{\delta u_i\delta u_j}\right\rangle+\left\langle\delta\tilde{u}_k\frac{\partial}{\partial X_j}\overline{\frac{1}{2}\left(u_j+u_j^+\right)\delta u_i}\right\rangle= \tag{A.21}$$
$$\frac{\partial}{\partial r_j}\langle\overline{\delta u_i\delta u_j}\delta\tilde{u}_k\rangle-\left\langle\overline{\delta u_i\delta u_j}\frac{\partial\delta\tilde{u}_k}{\partial r_j}\right\rangle+$$
$$\frac{\partial}{\partial X_j}\langle\overline{u_j^*\delta u_i}\delta\tilde{u}_k\rangle-\left\langle\overline{u_j^*\delta u_i}\frac{\partial}{\partial X_j}\delta\tilde{u}_k\right\rangle$$

The viscous term can be written in an easier form:

$$\left\langle \nu\delta\tilde{u}_k \left(\frac{1}{2}\frac{\partial^2}{\partial X_j \partial X_j} + 2\frac{\partial^2}{\partial r_j \partial r_j}\right)\delta\tilde{u}_i \right\rangle + \left\langle \nu\delta\tilde{u}_i \left(\frac{1}{2}\frac{\partial^2}{\partial X_j \partial X_j} + 2\frac{\partial^2}{\partial r_j \partial r_j}\right)\delta\tilde{u}_k \right\rangle =$$
$$\frac{\nu}{2}\frac{\partial^2}{\partial X_j \partial X_j}\langle\delta\tilde{u}_i\delta\tilde{u}_k\rangle + 2\nu\frac{\partial^2}{\partial r_j \partial r_j}\langle\delta\tilde{u}_i\delta\tilde{u}_k\rangle - \nu\left\langle \frac{\partial\delta\tilde{u}_i}{\partial X_j}\frac{\partial\delta\tilde{u}_k}{\partial X_j}\right\rangle - 4\nu\left\langle \frac{\partial\delta\tilde{u}_i}{\partial r_j}\frac{\partial\delta\tilde{u}_k}{\partial r_j}\right\rangle =$$
$$\frac{\nu}{2}\frac{\partial^2}{\partial X_j \partial X_j}\langle\delta\tilde{u}_i\delta\tilde{u}_k\rangle + 2\nu\frac{\partial^2}{\partial r_j \partial r_j}\langle\delta\tilde{u}_i\delta\tilde{u}_k\rangle - 2\left(\tilde{\epsilon}^{+}_{ik} + \tilde{\epsilon}_{ik}\right) \tag{A.22}$$

where $\tilde{\epsilon}_{ik}$ is the pseudo-dissipation tensor of the coherent part of the velocity, defined as:

$$\tilde{\epsilon}_{ik} = \nu\left\langle \frac{\partial\tilde{u}_i}{\partial x_j}\frac{\partial\tilde{u}_k}{\partial x_j}\right\rangle \tag{A.23}$$

Morover we can write:

$$\langle\delta\tilde{u}_k\delta\tilde{u}_j\rangle\frac{\partial\delta U_i}{\partial r_j} = \langle\delta\tilde{u}_k\delta\tilde{u}_j\rangle\left(\frac{\partial U_i}{\partial x_j}\right)^* \tag{A.24}$$

where the $(\cdot)^*$ operator denotes the average of a given quantity among $\boldsymbol{x}$ and $\boldsymbol{x}^*$. In the same way:

$$\left\langle\delta\tilde{u}_k\tilde{u}^*_j\right\rangle\frac{\partial}{\partial X_j}\delta U_i = \left\langle\delta\tilde{u}_k\tilde{u}^*_j\right\rangle\delta\left(\frac{\partial U_i}{\partial x_j}\right) \tag{A.25}$$

as a result we obtain the budget equation for $\langle\delta\tilde{u}_i\delta\tilde{u}_k\rangle$:

$$\frac{\partial}{\partial r_j}\langle\delta U_j\delta\tilde{u}_i\delta\tilde{u}_k\rangle + \frac{\partial}{\partial X_j}\left\langle U^*_j\delta\tilde{u}_i\delta\tilde{u}_k\right\rangle + \frac{\partial}{\partial r_j}\langle\delta\tilde{u}_j\delta\tilde{u}_i\delta\tilde{u}_k\rangle + \frac{\partial}{\partial X_j}\left\langle\tilde{u}^*_j\delta\tilde{u}_i\delta\tilde{u}_k\right\rangle +$$
$$\frac{\partial}{\partial r_j}\left\langle\overline{\delta u_j\delta u_i}\delta\tilde{u}_k\right\rangle + \frac{\partial}{\partial X_j}\left\langle\overline{u^*_j\delta u_i}\delta\tilde{u}_k\right\rangle + \frac{\partial}{\partial r_j}\left\langle\overline{\delta u_j\delta u_k}\delta\tilde{u}_i\right\rangle + \frac{\partial}{\partial X_j}\left\langle\overline{u^*_j\delta u_k}\delta\tilde{u}_i\right\rangle -$$
$$2\nu\frac{\partial^2}{\partial r_j\partial r_j}\langle\delta\tilde{u}_i\delta\tilde{u}_k\rangle - \frac{\nu}{2}\frac{\partial}{\partial X_j}\left(\frac{\partial}{\partial X_j}\langle\delta\tilde{u}_i\delta\tilde{u}_k\rangle\right) + \frac{\partial}{\partial X_i}\frac{1}{\rho}\langle\delta\tilde{p}\delta\tilde{u}_k\rangle + \frac{\partial}{\partial X_k}\frac{1}{\rho}\langle\delta\tilde{p}\delta\tilde{u}_i\rangle =$$
$$-\langle\delta\tilde{u}_k\delta\tilde{u}_j\rangle\left(\frac{\partial U_i}{\partial x_j}\right)^* - \langle\delta\tilde{u}_i\delta\tilde{u}_j\rangle\left(\frac{\partial U_k}{\partial x_j}\right)^* - \left\langle\delta\tilde{u}_k\tilde{u}^*_j\right\rangle\delta\left(\frac{\partial U_i}{\partial x_j}\right) - \left\langle\delta\tilde{u}_i\tilde{u}^*_j\right\rangle\delta\left(\frac{\partial U_k}{\partial x_j}\right) +$$
$$\left\langle\overline{\delta u_i\delta u_j}\frac{\partial\delta\tilde{u}_k}{\partial r_j}\right\rangle + \left\langle\overline{\delta u_i u^*_j}\frac{\partial\delta\tilde{u}_k}{\partial X_j}\right\rangle + \left\langle\overline{\delta u_k\delta u_j}\frac{\partial\delta\tilde{u}_i}{\partial r_j}\right\rangle + \left\langle\overline{\delta u_k u^*_j}\frac{\partial\delta\tilde{u}_i}{\partial X_j}\right\rangle +$$
$$\frac{1}{\rho}\left\langle\delta\tilde{p}\frac{\partial\delta\tilde{u}_k}{\partial X_i}\right\rangle + \frac{1}{\rho}\left\langle\delta\tilde{p}\frac{\partial\delta\tilde{u}_i}{\partial X_k}\right\rangle - 4\tilde{\epsilon}_{ik} \tag{A.26}$$

By exploiting the property of the avarage operator $\langle\overline{u_i u_j}\tilde{u_k}\rangle = \langle\overline{u_i u_j \tilde{u_k}}\rangle = \langle u_i u_j \tilde{u_k}\rangle$, the budget equation for $\langle\delta\tilde{u}_i\delta\tilde{u}_k\rangle$ may be written in an easier form:

$$\frac{\partial}{\partial r_j}\langle\delta U_j\delta\tilde{u}_i\delta\tilde{u}_k\rangle+\frac{\partial}{\partial X_j}\left\langle U_j^*\delta\tilde{u}_i\delta\tilde{u}_k\right\rangle+\frac{\partial}{\partial r_j}\langle\delta\tilde{u}_j\delta\tilde{u}_i\delta\tilde{u}_k\rangle+\frac{\partial}{\partial X_j}\left\langle\tilde{u}_j^*\delta\tilde{u}_i\delta\tilde{u}_k\right\rangle+$$
$$\frac{\partial}{\partial r_j}\langle\delta u_j\delta u_i\delta\tilde{u}_k\rangle+\frac{\partial}{\partial X_j}\left\langle u_j^*\delta u_i\delta\tilde{u}_k\right\rangle+\frac{\partial}{\partial r_j}\langle\delta u_j\delta u_k\delta\tilde{u}_i\rangle+\frac{\partial}{\partial X_j}\left\langle u_j^*\delta u_k\delta\tilde{u}_i\right\rangle-$$
$$2\nu\frac{\partial^2}{\partial r_j\partial r_j}\langle\delta\tilde{u}_i\delta\tilde{u}_k\rangle-\frac{\nu}{2}\frac{\partial}{\partial X_j}\left(\frac{\partial}{\partial X_j}\langle\delta\tilde{u}_i\delta\tilde{u}_k\rangle\right)+\frac{\partial}{\partial X_i}\frac{1}{\rho}\langle\delta\tilde{p}\delta\tilde{u}_k\rangle+\frac{\partial}{\partial X_k}\frac{1}{\rho}\langle\delta\tilde{p}\delta\tilde{u}_i\rangle=$$
$$-\langle\delta\tilde{u}_k\delta\tilde{u}_j\rangle\left(\frac{\partial U_i}{\partial x_j}\right)^*-\langle\delta\tilde{u}_i\delta\tilde{u}_j\rangle\left(\frac{\partial U_k}{\partial x_j}\right)^*-\left\langle\delta\tilde{u}_k\tilde{u}_j^*\right\rangle\delta\left(\frac{\partial U_i}{\partial x_j}\right)-\left\langle\delta\tilde{u}_i\tilde{u}_j^*\right\rangle\delta\left(\frac{\partial U_k}{\partial x_j}\right)+$$
$$\left\langle\delta u_i\delta u_j\frac{\partial\delta\tilde{u}_k}{\partial r_j}\right\rangle+\left\langle\delta u_i u_j^*\frac{\partial\delta\tilde{u}_k}{\partial X_j}\right\rangle+\left\langle\delta u_k\delta u_j\frac{\partial\delta\tilde{u}_i}{\partial r_j}\right\rangle+\left\langle\delta u_k u_j^*\frac{\partial\delta\tilde{u}_i}{\partial X_j}\right\rangle+$$
$$\frac{1}{\rho}\left\langle\delta\tilde{p}\frac{\partial\delta\tilde{u}_k}{\partial X_i}\right\rangle+\frac{1}{\rho}\left\langle\delta\tilde{p}\frac{\partial\delta\tilde{u}_i}{\partial X_k}\right\rangle-4\tilde{\epsilon}_{ik} \tag{A.27}$$

A.2.1 Compact expression

The AGKE for $\langle\delta\tilde{u}_i\delta\tilde{u}_j\rangle$ can be compactly written as:

$$\frac{\partial\tilde{\phi}_{ij,k}}{\partial r_k}+\frac{\partial\tilde{\psi}_{ij,k}}{\partial X_k}=\tilde{P}_{ij}^M-P_{ij}^C+\tilde{\Pi}_{ij}+\tilde{D}_{ij} \tag{A.28}$$

where $\tilde{\phi}_{ij,k}$ denotes the fluxes in the space of scales $\boldsymbol{r}$:

$$\tilde{\phi}_{ij,k}=\underbrace{\langle\delta U_k\delta\tilde{u}_i\delta\tilde{u}_j\rangle}_{\text{Mean Transport}}+\underbrace{\langle\delta\tilde{u}_k\delta\tilde{u}_i\delta\tilde{u}_j\rangle}_{\text{Coherent Transport}}+\underbrace{\left\langle\overline{\delta u_k\delta u_i}\delta\tilde{u}_j\right\rangle}_{\text{Turbulent transport}}$$
$$+\underbrace{\left\langle\overline{\delta u_k\delta u_j}\delta\tilde{u}_i\right\rangle}_{\text{Turbulent transport}}\underbrace{-2\nu\frac{\partial\langle\delta\tilde{u}_i\delta\tilde{u}_j\rangle}{\partial r_k}}_{\text{Viscous transport}}\quad k=1,2,3 \tag{A.29}$$

$\tilde{\psi}_{ij,k}$ denotes the fluxes in the physical space $\boldsymbol{X}$:

$$\tilde{\psi}_{ij,k} = \underbrace{\langle U_k^* \delta\tilde{u}_i \delta\tilde{u}_j \rangle}_{\text{Mean Transport}} + \underbrace{\langle \tilde{u}_k^* \delta\tilde{u}_i \delta\tilde{u}_j \rangle}_{\text{Coherent transport}} + \underbrace{\langle \overline{u_k^* \delta u_i} \delta\tilde{u}_j \rangle}_{\text{Turbulent transport}} + \underbrace{\langle \overline{u_k^* \delta u_j} \delta\tilde{u}_i \rangle}_{\text{Turbulent transport}}$$
$$+ \underbrace{\frac{1}{\rho}\langle \delta\tilde{p}\delta\tilde{u}_i \rangle \delta_{kj}}_{\text{Pressure transport}} + \underbrace{\frac{1}{\rho}\langle \delta\tilde{p}\delta\tilde{u}_j \rangle \delta_{ki}}_{\text{Pressure transport}} \underbrace{-\frac{\nu}{2}\frac{\partial \langle \delta\tilde{u}_i \delta\tilde{u}_j \rangle}{\partial X_k}}_{\text{Viscous transport}} \quad k = 1, 2, 3 \tag{A.30}$$

$\tilde{P}_{ij}^M$ denotes the transfer of the Reynolds stresses between the coherent and the mean field:

$$\begin{aligned} \tilde{P_{ij}}^M = &-\langle \delta\tilde{u}_j \delta\tilde{u}_k \rangle \left(\frac{\partial U_i}{\partial x_k} \right)^* - \langle \delta\tilde{u}_i \delta\tilde{u}_k \rangle \left(\frac{\partial U_j}{\partial x_k} \right)^* \\ &-\langle \delta\tilde{u}_j \tilde{u}_k^* \rangle \delta \left(\frac{\partial U_i}{\partial x_k} \right) - \langle \delta\tilde{u}_i \tilde{u}_k^* \rangle \delta \left(\frac{\partial U_j}{\partial x_k} \right) \end{aligned} \tag{A.31}$$

P_{ij}^c indicates the transfer of the Reynolds stresses between the coherent and fluctuating field:

$$P_{ij}^C = -\left\langle \overline{\delta u_i \delta u_k} \frac{\partial \delta\tilde{u}_j}{\partial r_k} \right\rangle - \left\langle \overline{\delta u_j \delta u_k} \frac{\partial \delta\tilde{u}_i}{\partial r_k} \right\rangle - \left\langle \overline{\delta u_i u_k^*} \frac{\partial \delta\tilde{u}_j}{\partial X_k} \right\rangle - \left\langle \overline{\delta u_j u_k^*} \frac{\partial \delta\tilde{u}_i}{\partial X_k} \right\rangle \tag{A.32}$$

$\tilde{\Pi}_{ij}$ denotes the pressure strain term:

$$\tilde{\Pi}_{ij} = \frac{1}{\rho}\left\langle \delta\tilde{p} \frac{\partial \delta\tilde{u}_i}{\partial X_j} \right\rangle + \frac{1}{\rho}\left\langle \delta\tilde{p} \frac{\partial \delta\tilde{u}_j}{\partial X_i} \right\rangle \tag{A.33}$$

and $\tilde{D}_{ij}$ denotes the dissipation term:

$$\tilde{D}_{ij} = -4\tilde{\epsilon}_{ij} = -4\nu\left\langle \frac{\partial \tilde{u}_i}{\partial x_k} \frac{\partial \tilde{u}_j}{\partial x_k} \right\rangle \tag{A.34}$$

A.3 AGKE for $\langle \delta u_i \delta u_j \rangle$

We write the budget equation for u_i in $\boldsymbol{x}$ and $\boldsymbol{x}^+ = \boldsymbol{x} + \boldsymbol{r}$ and we subtract the first to the second one:

$$\begin{gathered}\Delta\left(\frac{\partial u_i}{\partial t}\right) + \Delta\left(U_j \frac{\partial u_i}{\partial x_j}\right) + \Delta\left(\tilde{u}_j \frac{\partial u_i}{\partial x_j}\right) + \\ \Delta\left(u_j \frac{\partial U_i}{\partial x_j}\right) + \Delta\left(u_j \frac{\partial \tilde{u}_i}{\partial x_j}\right) + \Delta\left(\frac{\partial}{\partial x_j}\left(u_i u_j - \overline{u_i u_j}\right)\right) = \\ -\Delta\left(\frac{1}{\rho}\frac{\partial p}{\partial x_i}\right) + \Delta\left(\nu \frac{\partial^2 u_i}{\partial x_j^2}\right)\end{gathered} \tag{A.35}$$

Recalling again that the frameworks $\boldsymbol{x}$ and $\boldsymbol{x}^+$ are independent we can write:

$$\Delta\left(U_j \frac{\partial u_i}{\partial x_j}\right) = U_j^+ \frac{\partial \delta u_i}{\partial x_j^+} + U_j \frac{\partial \delta u_i}{\partial x_j} \tag{A.36}$$

and following the same line of reasoning for all the terms we obtain the equation for δu_i, i.e:

$$\begin{gathered}\frac{\partial}{\partial t}\delta u_i + U_j^+ \frac{\partial \delta u_i}{\partial x_j^+} + U_j \frac{\partial \delta u_i}{\partial x_j} + \tilde{u}_j^+ \frac{\partial \delta u_i}{\partial x_j^+} + \tilde{u}_j \frac{\partial \delta u_i}{\partial x_j} + \\ u_j^+ \frac{\partial \delta U_i}{\partial x_j^+} + u_j \frac{\partial \delta U_i}{\partial x_j} + u_j^+ \frac{\partial \delta \tilde{u}_i}{\partial x_j^+} + u_j \frac{\partial \delta \tilde{u}_i}{\partial x_j} + \\ u_j^+ \frac{\partial \delta u_i}{\partial x_j^+} + u_j \frac{\partial \delta u_i}{\partial x_j} - \overline{u_j^+ \frac{\partial \delta u_i}{\partial x_j^+}} - \overline{u_j \frac{\partial \delta u_i}{\partial x_j}} = \\ -\frac{1}{\rho}\frac{\partial \delta p}{\partial x_i^+} - \frac{1}{\rho}\frac{\partial \delta p}{\partial x_i} + \nu\left(\frac{\partial^2}{\partial x_j^+ \partial x_j^+} + \frac{\partial^2}{\partial x_j \partial x_j}\right)\delta u_i.\end{gathered} \tag{A.37}$$

Then we write for example

$$u_j^+ \frac{\partial \delta U_i}{\partial x_j^+} = \delta u_j \frac{\partial \delta U_i}{\partial x_j^+} + u_j \frac{\partial \delta U_i}{\partial x_j^+} \tag{A.38}$$

and the budget equation for δu_i can be written as

$$\begin{aligned}
&\frac{\partial \delta u_i}{\partial t} + \delta U_j \frac{\partial \delta u_i}{\partial x_j^+} + U_j \frac{\partial \delta u_i}{\partial x_j^+} + U_j \frac{\partial \delta u_i}{\partial x_j} + \\
&\delta \tilde{u}_j \frac{\partial \delta u_i}{\partial x_j^+} + \tilde{u}_j \frac{\partial \delta u_i}{\partial x_j^+} + \tilde{u}_j \frac{\partial \delta u_i}{\partial x_j} + \delta u_j \frac{\partial \delta U_i}{\partial x_j^+} + u_j \frac{\partial \delta U_i}{\partial x_j^+} + u_j \frac{\partial \delta U_i}{\partial x_j} + \\
&\delta u_j \frac{\partial \delta \tilde{u}_i}{\partial x_j^+} + u_j \frac{\partial \delta \tilde{u}_i}{\partial x_j^+} + u_j \frac{\partial \delta \tilde{u}_i}{\partial x_j} + \delta u_j \frac{\partial \delta u_i}{\partial x_j^+} + u_j \frac{\partial \delta u_i}{\partial x_j^+} + u_j \frac{\partial \delta u_i}{\partial x_j} - \\
&\overline{\delta u_j \frac{\partial \delta u_i}{\partial x_j^+} - u_j \left(\frac{\partial}{\partial x_j^+} + \frac{\partial}{\partial x_j} \right) \delta u_i} = \\
&-\frac{1}{\rho} \frac{\partial \delta p}{\partial x_i^+} - \frac{1}{\rho} \frac{\partial \delta p}{\partial x_i} + \nu \left(\frac{\partial^2}{\partial x_j^+ \partial x_j^+} + \frac{\partial^2}{\partial x_j \partial x_j} \right) \delta u_i.
\end{aligned} \tag{A.39}$$

We then compact the equation and multiply for δu_k:

$$\begin{aligned}
&\delta u_k \frac{\partial \delta u_i}{\partial t} + \delta u_k \delta U_j \frac{\partial \delta u_i}{\partial x_j^+} + \delta u_k U_j \left(\frac{\partial}{\partial x_j^+} + \frac{\partial}{\partial x_j} \right) \delta u_i + \\
&\delta u_k \delta \tilde{u}_j \frac{\partial \delta u_i}{\partial x_j^+} + \delta u_k \tilde{u}_j \left(\frac{\partial}{\partial x_j^+} + \frac{\partial}{\partial x_j} \right) \delta u_i + \\
&\delta u_k \delta u_j \frac{\partial \delta U_i}{\partial x_j^+} + \delta u_k u_j \left(\frac{\partial}{\partial x_j^+} + \frac{\partial}{\partial x_j} \right) \delta U_i + \\
&\delta u_k \delta u_j \frac{\partial \delta \tilde{u}_i}{\partial x_j^+} + \delta u_k u_j \left(\frac{\partial}{\partial x_j^+} + \frac{\partial}{\partial x_j} \right) \delta \tilde{u}_i + \\
&\delta u_k \delta u_j \frac{\partial \delta u_i}{\partial x_j^+} + \delta u_k u_j \left(\frac{\partial}{\partial x_j^+} + \frac{\partial}{\partial x_j} \right) \delta u_i - \\
&\overline{\delta u_k \delta u_j \frac{\partial \delta u_i}{\partial x_j^+} - \delta u_k u_j \left(\frac{\partial}{\partial x_j^+} + \frac{\partial}{\partial x_j} \right) \delta u_i} = \\
&-\delta u_k \frac{1}{\rho} \frac{\partial \delta p}{\partial x_i^+} - \delta u_k \frac{1}{\rho} \frac{\partial \delta p}{\partial x_i} + \nu \delta u_k \left(\frac{\partial^2}{\partial x_j^+ \partial x_j^+} + \frac{\partial^2}{\partial x_j \partial x_j} \right) \delta u_i.
\end{aligned} \tag{A.40}$$

Then we sum the same equation but inverting the i-index with the k-index. Using the incompressibility constraint and the independence of the $\boldsymbol{x}$ and $\boldsymbol{x}^+$

references we can write:

$$\frac{\partial}{\partial t}\delta u_i\delta u_k + \frac{\partial}{\partial x_j^+}\left(\delta U_j\delta u_i\delta u_k\right) + \left(\frac{\partial}{\partial x_j^+} + \frac{\partial}{\partial x_j}\right)\left(U_j\delta u_i\delta u_k\right) +$$
$$\delta u_k\delta\tilde{u}_j\frac{\partial\delta u_i}{\partial x_j^+} + \delta u_i\delta\tilde{u}_j\frac{\partial\delta u_k}{\partial x_j^+} +$$
$$\delta u_k\tilde{u}_j\left(\frac{\partial}{\partial x_j^+} + \frac{\partial}{\partial x_j}\right)\delta u_i + \delta u_i\tilde{u}_j\left(\frac{\partial}{\partial x_j^+} + \frac{\partial}{\partial x_j}\right)\delta u_k +$$
$$\delta u_k\delta u_j\frac{\partial\delta U_i}{\partial x_j^+} + \delta u_i\delta u_j\frac{\partial\delta U_k}{\partial x_j^+} +$$
$$\delta u_k u_j\left(\frac{\partial}{\partial x_j^+} + \frac{\partial}{\partial x_j}\right)\delta U_i + \delta u_i u_j\left(\frac{\partial}{\partial x_j^+} + \frac{\partial}{\partial x_j}\right)\delta U_k +$$
$$\delta u_k\delta u_j\frac{\partial\delta\tilde{u}_i}{\partial x_j^+} + \delta u_i\delta u_j\frac{\partial\delta\tilde{u}_k}{\partial x_j^+} + \delta u_k u_j\left(\frac{\partial}{\partial x_j^+} + \frac{\partial}{\partial x_j}\right)\delta\tilde{u}_i + \delta u_i u_j\left(\frac{\partial}{\partial x_j^+} + \frac{\partial}{\partial x_j}\right)\delta\tilde{u}_k +$$
$$\frac{\partial}{\partial x_j^+}\delta u_j\delta u_i\delta u_k + \left(\frac{\partial}{\partial x_j^+} + \frac{\partial}{\partial x_j}\right)u_j\delta u_i\delta u_k -$$
$$\overline{\delta u_k\frac{\partial}{\partial x_j^+}\delta u_i\delta u_j} - \overline{\delta u_i\frac{\partial}{\partial x_j^+}\delta u_j\delta u_k} -$$
$$\overline{\delta u_k\left(\frac{\partial}{\partial x_j^+} + \frac{\partial}{\partial x_j}\right)\delta u_i\delta u_j} - \overline{\delta u_i\left(\frac{\partial}{\partial x_j^+} + \frac{\partial}{\partial x_j}\right)\delta u_k\delta u_j} =$$
$$-\delta u_k\frac{1}{\rho}\left(\frac{\partial}{\partial x_i^+} + \frac{\partial}{\partial x_i}\right)\delta p - \delta u_i\frac{1}{\rho}\left(\frac{\partial}{\partial x_k^+} + \frac{\partial}{\partial x_k}\right)\delta p +$$
$$\nu\delta u_k\left(\frac{\partial^2}{\partial x_j^+\partial x_j^+} + \frac{\partial^2}{\partial x_j\partial x_j}\right)\delta u_i + \nu\delta u_i\left(\frac{\partial^2}{\partial x_j^+\partial x_j^+} + \frac{\partial^2}{\partial x_j\partial x_j}\right)\delta u_k \tag{A.41}$$

At this point we use the phase-average operator $\bar{\cdot}$ and the the time-average operator $\langle\cdot\rangle$ and we obtain:

$$\frac{\partial}{\partial x_j^+}\langle\delta U_j\delta u_i\delta u_k\rangle+\left(\frac{\partial}{\partial x_j^+}+\frac{\partial}{\partial x_j}\right)\langle U_j\delta u_i\delta u_k\rangle+$$
$$\langle\delta u_k\delta u_j\rangle\frac{\partial\delta U_i}{\partial x_j^+}+\langle\delta u_i\delta u_j\rangle\frac{\partial\delta U_k}{\partial x_j^+}+$$
$$\langle\delta u_k u_j\rangle\left(\frac{\partial}{\partial x_j^+}+\frac{\partial}{\partial x_j}\right)\delta U_i+\langle\delta u_i u_j\rangle\left(\frac{\partial}{\partial x_j^+}+\frac{\partial}{\partial x_j}\right)\delta U_k+$$
$$\frac{\partial}{\partial x_j^+}\langle\delta u_k\delta\tilde{u}_j\delta u_i\rangle+\left(\frac{\partial}{\partial x_j^+}+\frac{\partial}{\partial x_j}\right)\langle\delta u_k\tilde{u}_j\delta u_i\rangle+$$
$$\left\langle\overline{\delta u_k\delta u_j}\frac{\partial\delta\tilde{u}_i}{\partial x_j^+}\right\rangle+\left\langle\overline{\delta u_i\delta u_j}\frac{\partial\delta\tilde{u}_k}{\partial x_j^+}\right\rangle+$$
$$\left\langle\overline{\delta u_k u_j}\left(\frac{\partial}{\partial x_j^+}+\frac{\partial}{\partial x_j}\right)\delta\tilde{u}_i\right\rangle+\left\langle\overline{\delta u_i u_j}\left(\frac{\partial}{\partial x_j^+}+\frac{\partial}{\partial x_j}\right)\delta\tilde{u}_k\right\rangle+$$
$$\frac{\partial}{\partial x_j}+\langle\delta u_j\delta u_i\delta u_k\rangle+\left(\frac{\partial}{\partial x_j^+}+\frac{\partial}{\partial x_j}\right)\langle u_j\delta u_i\delta u_j\rangle=$$
$$-\frac{1}{\rho}\left(\frac{\partial}{\partial x_i^+}+\frac{\partial}{\partial x_i}\right)\langle\delta p\delta u_k\rangle-\frac{1}{\rho}\left(\frac{\partial}{\partial x_k^+}+\frac{\partial}{\partial x_k}\right)\langle\delta p\delta u_i\rangle+$$
$$\left\langle\frac{1}{\rho}\delta p\left(\frac{\partial}{\partial x_i^+}+\frac{\partial}{\partial x_i}\right)\delta u_k\right\rangle+\left\langle\frac{1}{\rho}\delta p\left(\frac{\partial}{\partial x_k^+}+\frac{\partial}{\partial x_k}\right)\delta u_i\right\rangle+$$
$$\nu\left\langle\delta u_k\left(\frac{\partial^2}{\partial x_j^+\partial x_j^+}+\frac{\partial^2}{\partial x_j\partial x_j}\right)\delta u_i\right\rangle+\nu\left\langle\delta u_i\left(\frac{\partial^2}{\partial x_j^+\partial x_j^+}+\frac{\partial^2}{\partial x_j\partial x_j}\right)\delta u_k\right\rangle. \tag{A.42}$$

We introduce again $\boldsymbol{X}$ and $\boldsymbol{r}$ and we obtain

$$\begin{gathered}
\frac{\partial}{\partial r_j}\langle \delta U_j \delta u_i \delta u_k \rangle + \frac{\partial}{\partial X_j}\left\langle U_j^* \delta u_i \delta u_k \right\rangle + \\
\langle \delta u_k \delta u_j \rangle \frac{\partial \delta U_i}{\partial r_j} + \langle \delta u_i \delta u_j \rangle \frac{\partial \delta U_k}{\partial r_j} + \left\langle \delta u_k u_j^* \right\rangle \frac{\partial \delta U_i}{\partial X_j} + \left\langle \delta u_i u_j^* \right\rangle \frac{\partial \delta U_k}{\partial X_j} + \\
\left\langle \overline{\delta u_k \delta u_j} \frac{\partial \delta \tilde{u}_i}{\partial r_j} \right\rangle + \left\langle \overline{\delta u_k u_j^*} \frac{\partial \delta \tilde{u}_i}{\partial X_j} \right\rangle + \left\langle \overline{\delta u_i \delta u_j} \frac{\partial \delta \tilde{u}_k}{\partial r_j} \right\rangle + \left\langle \overline{\delta u_k u_j^*} \frac{\partial \delta \tilde{u}_k}{\partial X_j} \right\rangle + \\
\frac{\partial}{\partial r_j}\langle \delta u_j \delta u_i \delta u_k \rangle + \frac{\partial}{\partial X_j}\left\langle u_j^* \delta u_i \delta u_k \right\rangle + \frac{\partial}{\partial r_j}\langle \delta \tilde{u}_j \delta u_i \delta u_k \rangle + \frac{\partial}{\partial X_j}\left\langle \tilde{u}_j^* \delta u_i \delta u_k \right\rangle + \\
\frac{\partial}{\partial X_i}\frac{1}{\rho}\langle \delta p \delta u_k \rangle + \frac{\partial}{\partial X_k}\frac{1}{\rho}\langle \delta p \delta u_i \rangle = \\
\left\langle \frac{1}{\rho}\delta p \frac{\partial \delta u_k}{\partial X_i} \right\rangle + \left\langle \frac{1}{\rho}\delta p \frac{\partial \delta u_i}{\partial X_k} \right\rangle + \\
\frac{\nu}{2}\frac{\partial^2}{\partial X_j^2}\langle \delta u_i \delta u_k \rangle + 2\nu \frac{\partial^2}{\partial r_j^2}\langle \delta u_i \delta u_k \rangle - 2\left(\epsilon_{ik}^+ + \epsilon_{ik}\right)
\end{gathered} \tag{A.43}$$

where

$$\epsilon_{ik} = \nu \left\langle \frac{\partial u_i}{\partial x_j}\frac{\partial u_k}{\partial x_j} \right\rangle \tag{A.44}$$

we can write

$$\langle \delta u_k \delta u_j \rangle \frac{\partial \delta U_i}{\partial r_j} = \langle \delta u_k \delta u_j \rangle \left(\frac{\partial U_i}{\partial x_j}\right)^* \tag{A.45}$$

and

$$\left\langle \delta u_k u_j^* \right\rangle \frac{\partial \delta U_i}{\partial X_j} = \left\langle \delta u_k u_j^* \right\rangle \delta \left(\frac{\partial U_i}{\partial x_j}\right) \tag{A.46}$$

and we finally obtain the budget equation for $\langle \delta u_i \delta u_k \rangle$:

$$\begin{gathered}
\frac{\partial}{\partial r_j}\langle \delta U_j \delta u_i \delta u_k \rangle + \frac{\partial}{\partial X_j}\left\langle U_j^* \delta u_i \delta u_k \right\rangle + \frac{\partial}{\partial r_j}\langle \delta u_j \delta u_i \delta u_k \rangle + \frac{\partial}{\partial X_j}\left\langle u_j^* \delta u_i \delta u_k \right\rangle + \\
\frac{\partial}{\partial r_j}\left(-2\nu \frac{\partial}{\partial r_j}\langle \delta u_i \delta u_k \rangle \right) + \frac{\partial}{\partial X_j}\left(-\frac{\nu}{2}\frac{\partial}{\partial X_j}\langle \delta u_i \delta u_k \rangle \right) + \\
\frac{\partial}{\partial r_j}\left\langle \delta \tilde{u}_j \overline{\delta u_i \delta u_k} \right\rangle + \frac{\partial}{\partial X_j}\left\langle \tilde{u}_j^* \overline{\delta u_i \delta u_k} \right\rangle + \\
\frac{\partial}{\partial X_i}\frac{1}{\rho}\langle \delta p \delta u_k \rangle + \frac{\partial}{\partial X_k}\frac{1}{\rho}\langle \delta p \delta u_i \rangle = \\
-\langle \delta u_k \delta u_j \rangle \left(\frac{\partial U_i}{\partial x_j} \right)^* - \langle \delta u_i \delta u_j \rangle \left(\frac{\partial U_k}{\partial X_j} \right)^* - \\
\left\langle \delta u_k u_j^* \right\rangle \delta \left(\frac{\partial U_i}{\partial x_j} \right) - \left\langle \delta u_i u_j^* \right\rangle \delta \left(\frac{\partial U_k}{\partial x_j} \right) - \\
\left\langle \overline{\delta u_k \delta u_j} \left(\frac{\partial \tilde{u}_i}{\partial x_j} \right)^* \right\rangle - \left\langle \overline{\delta u_i \delta u_j} \left(\frac{\partial \tilde{u}_k}{\partial x_j} \right)^* \right\rangle - \\
\left\langle \overline{\delta u_k u_j^*} \delta \left(\frac{\partial \tilde{u}_i}{\partial x_j} \right) \right\rangle - \left\langle \overline{\delta u_i u_j^*} \delta \left(\frac{\partial \tilde{u}_k}{\partial x_j} \right) \right\rangle + \\
\left\langle \frac{1}{\rho} \delta p \frac{\partial \delta u_k}{\partial X_i} \right\rangle + \left\langle \frac{1}{\rho} \delta p \frac{\partial \delta u_i}{\partial X_k} \right\rangle - 4\epsilon_{ik}^*
\end{gathered} \tag{A.47}$$

By exploiting the property of the avarage operator $\langle\overline{u_i u_j}\tilde{u_k}\rangle = \langle\overline{u_i u_j \tilde{u_k}}\rangle = \langle u_i u_j \tilde{u_k}\rangle$, the budget equation for $\langle\delta u_i \delta u_k\rangle$ may be written in a easier form:

$$\begin{gathered}
\frac{\partial}{\partial r_j}\langle\delta U_j \delta u_i \delta u_k\rangle + \frac{\partial}{\partial X_j}\left\langle U_j^* \delta u_i \delta u_k\right\rangle + \frac{\partial}{\partial r_j}\langle\delta u_j \delta u_i \delta u_k\rangle + \frac{\partial}{\partial X_j}\left\langle u_j^* \delta u_i \delta u_k\right\rangle + \\
\frac{\partial}{\partial r_j}\left(-2\nu\frac{\partial}{\partial r_j}\langle\delta u_i \delta u_k\rangle\right) + \frac{\partial}{\partial X_j}\left(-\frac{\nu}{2}\frac{\partial}{\partial X_j}\langle\delta u_i \delta u_k\rangle\right) + \\
\frac{\partial}{\partial r_j}\langle\delta\tilde{u}_j \delta u_i \delta u_k\rangle + \frac{\partial}{\partial X_j}\left\langle\tilde{u}_j^* \delta u_i \delta u_k\right\rangle + \\
\frac{\partial}{\partial X_i}\frac{1}{\rho}\langle\delta p \delta u_k\rangle + \frac{\partial}{\partial X_k}\frac{1}{\rho}\langle\delta p \delta u_i\rangle = \\
-\langle\delta u_k \delta u_j\rangle\left(\frac{\partial U_i}{\partial x_j}\right)^* - \langle\delta u_i \delta u_j\rangle\left(\frac{\partial U_k}{\partial X_j}\right)^* - \\
\left\langle\delta u_k u_j^*\right\rangle\delta\left(\frac{\partial U_i}{\partial x_j}\right) - \left\langle\delta u_i u_j^*\right\rangle\delta\left(\frac{\partial U_k}{\partial x_j}\right) - \\
\left\langle\delta u_k \delta u_j\left(\frac{\partial\tilde{u}_i}{\partial x_j}\right)^*\right\rangle - \left\langle\delta u_i \delta u_j\left(\frac{\partial\tilde{u}_k}{\partial x_j}\right)^*\right\rangle - \\
\left\langle\delta u_k u_j^*\delta\left(\frac{\partial\tilde{u}_i}{\partial x_j}\right)\right\rangle - \left\langle\delta u_i u_j^*\delta\left(\frac{\partial\tilde{u}_k}{\partial x_j}\right)\right\rangle + \\
\left\langle\frac{1}{\rho}\delta p\frac{\partial\delta u_k}{\partial X_i}\right\rangle + \left\langle\frac{1}{\rho}\delta p\frac{\partial\delta u_i}{\partial X_k}\right\rangle - 4\epsilon_{ik}^*
\end{gathered} \tag{A.48}$$

A.3.1 Compact expression

Again the AGKE for $\langle\delta u_i \delta u_j\rangle$ can be compactly written as

$$\frac{\partial\phi_{ij,k}}{\partial r_k} + \frac{\partial\psi_{ij,k}}{\partial X_k} = P_{ij}^M + P_{ij}^C + \Pi_{ij} + D_{ij} \tag{A.49}$$

where $\phi_{ij,k}$ denotes the flux of $\langle\delta u_i \delta u_j\rangle$ in the space of scales $\boldsymbol{r}$:

$$\begin{aligned}
\phi_{ij,k} = &\underbrace{\langle\delta U_k \delta u_i \delta u_j\rangle}_{\text{Mean transport}} + \underbrace{\langle\delta u_k \delta u_i \delta u_j\rangle}_{\text{Turbulent transport}} \\
&+ \underbrace{\left\langle\delta\tilde{u}_k\overline{\delta u_i \delta u_j}\right\rangle}_{\text{Coherent transport}} \underbrace{-2\nu\frac{\partial\langle\delta u_i \delta u_j\rangle}{\partial r_k}}_{\text{Viscous transport}} \quad k = 1, 2, 3
\end{aligned} \tag{A.50}$$

$\psi_{ij,k}$ denotes the flux of $\langle \delta u_i \delta u_j \rangle$ in the physical space $\boldsymbol{X}$:

$$\begin{aligned}\psi_{ij,k} = &\underbrace{\langle U_k^* \delta u_i \delta u_j \rangle}_{\text{Mean transport}} + \underbrace{\langle u_k^* \delta u_i \delta u_j \rangle}_{\text{Turbulent transport}} + \underbrace{\langle \tilde{u}_k^* \overline{\delta u_i \delta u_j} \rangle}_{\text{Coherent transport}} \\ &\underbrace{-\frac{\nu}{2} \frac{\partial \langle \delta u_i \delta u_j \rangle}{\partial X_k}}_{\text{Viscous transport}} + \underbrace{\frac{1}{\rho} \langle \delta p \delta u_i \rangle \delta_{kj}}_{\text{Pressure transport}} + \underbrace{\frac{1}{\rho} \langle \delta p \delta u_j \rangle \delta_{ki}}_{\text{Pressure transport}} \qquad k = 1, 2, 3\end{aligned} \tag{A.51}$$

P_{ij}^M denotes the transfer of the Reynolds stresses from the mean flow to the fluctuating field

$$\begin{aligned}P_{ij}^M = &-\langle \delta u_j \delta u_k \rangle \left(\frac{\partial U_i}{\partial x_k} \right)^* - \langle \delta u_i \delta u_k \rangle \left(\frac{\partial U_j}{\partial x_k} \right)^* \\ &-\langle \delta u_j u_k^* \rangle \delta \left(\frac{\partial U_i}{\partial x_k} \right) - \langle \delta u_i u_k^* \rangle \delta \left(\frac{\partial U_j}{\partial x_k} \right)\end{aligned} \tag{A.52}$$

P_{ij}^C, as said before, is the transfer of the Reynolds stresses between the fluctuating field and the coherent field:

$$P_{ij}^C = -\left\langle \overline{\delta u_i \delta u_k} \frac{\partial \delta \tilde{u}_j}{\partial r_k} \right\rangle - \left\langle \overline{\delta u_j \delta u_k} \frac{\partial \delta \tilde{u}_i}{\partial r_k} \right\rangle - \left\langle \overline{\delta u_i u_k^*} \frac{\partial \delta \tilde{u}_j}{\partial X_k} \right\rangle - \left\langle \overline{\delta u_j u_k^*} \frac{\partial \delta \tilde{u}_i}{\partial X_k} \right\rangle \tag{A.53}$$

Π_{ij} is the pressure strain term

$$\Pi_{ij} = \frac{1}{\rho} \left\langle \delta p \frac{\partial \delta u_i}{\partial X_j} \right\rangle + \frac{1}{\rho} \left\langle \delta p \frac{\partial \delta u_j}{\partial X_i} \right\rangle \tag{A.54}$$

and D_{ij} the dissipation term:

$$D_{ij} = -4\epsilon_{ij} = -4\nu \left\langle \frac{\partial u_i}{\partial x_k} \frac{\partial u_j}{\partial x_k} \right\rangle \tag{A.55}$$

Appendix B

Numerical method

B.1 Solver description

In the present work, a solver for the computation of the AGKE terms written in CPL language has been developed. The code is based on Gatti *et al.* (2019) and it has been specialised for the case under study. The novelty of the present code is the computation of the AGKE terms of both the second-order structure functions $\langle \delta u_i \delta u_j \rangle$ and $\langle \delta \tilde{u}_i \delta \tilde{u}_j \rangle$ where the velocity component v_i has been decomposed in the mean velocity U_i, the periodic part of the flow $\tilde{u}_i$ and the chaotic part of the flow u_i:

$$v_i = U_i + \tilde{u}_i + u_i. \tag{B.1}$$

It finds application in those problems where the flow exhibits a well-defined non-stochastic (e.g. periodic) flow feature and thus velocity and pressure can be decomposed as shown above. Here it is applied to the case of spanwise oscillating walls but it can be easily used for different periodic flows (e.g. streamwise travelling waves) with minimal changes. The main characteristics of the present code, which allows it to be highly computationally efficient are now briefly summarised. AGKE terms are split in multiple but simpler correlations and, exploiting the geometric features of the indefinite plane channel flow, computed in Fourier domain by means of Parseval theorem for the two homogenous directions. Furthermore, in order to easily take advantage of their symmetries, AGKE terms are not computeted in the (r_x, r_z, r_y, Y_c) four-dimensional domain, but in the analogous (r_x, r_z, Y_1, Y_2) domain where $Y_1 = Y_c - r_y/2$ and $Y_2 = Y_c + r_y/2$. The structure of the

code is composed of three main steps, here briefly described and illustrated in the flowchart of figure B.1. First of all, mean and periodic velocity and pressure, as well as velocity gradients, are computed, together with instantaneous and coherent pseudo-dissipation. These quantities are computed outside the main code and they feed it as inputs. The main solver consists of four nested loops. First, a loop on phases and a loop on periods are performed in order to scan the velocity and pressure fields and to assign them to the phase they belong. Here *Step 1* takes place and fluctuating velocity and pressure are computed subtracting to the whole quantities, mean and periodic ones, previously computed. *Step 2* represents the core of the algorithm where most of AGKE terms are actually computed. It is made by two main nested loops. At the outer level, the code loops on Y_1 while at the inner level on Y_2, where Y_1 and Y_2 represent the distance from the wall in the above-mentioned four-dimensional space. For each Y_1, the AGKE terms are computed for Y_2 ranging from Y_1 to $2h - Y_1$, where h represents the mid-channel height. Since all the AGKE terms are either symmetric or anti-symmetric with respect to an inversion of the wall-normal axis, one half of the channel is used to increase the size of the statistical sample. Hence, Y_1 scans through half the grid points in the wall-normal direction (as shown in Figure B.2, i.e. loops from y_{-1} to $y_{n_y/2}$. For each (Y_1, Y_2) also the terms from the pair $(2h - Y_1, 2h - Y_2)$ are computed to contribute to the statistics, with the sign of each term properly set according to the relevant symmetry. Here, Y_1 and Y_2 represent the wall-normal position where AGKE terms are actually evaluated whereas y_1 and y_2 the position where they are actually used, with y_1 ranging from -1 to $n_y + 1$, i.e. from the lower to the upper wall. Strategies used in order to take advantage of the existing symmetries are described below. Inside the four nested loops of *Step 2* the AGKE terms are computed. First, in-plane Fourier convolution terms at y_1 are computed in physical space. Then, in the inner loop, in-plane Fourier convolutions at y_2 are evaluated in physical space; finally the required cross-plane correlations, for example $\langle uv \rangle (r_x, r_z; y_{i_1}, y_{i_2})$ are computed in Fourier space. Lastly, each AGKE terms, rewritten in terms of the sum of two or three-point correlations is assembled. When the last temporal snapshot is reached, the actual time average of each term is obtained by dividing for the total number of samples. In order to further reduce the computational effort, terms which only involve coherent velocity and pressure (i.e. all terms of $\langle \delta\tilde{u}_i \delta\tilde{u}_j \rangle$ equation but fluxes and P_{ij}^C) are computed only once per phase and averaged over the total number of phases. Outside the loops, *Step 3* is the last part of the algorithm

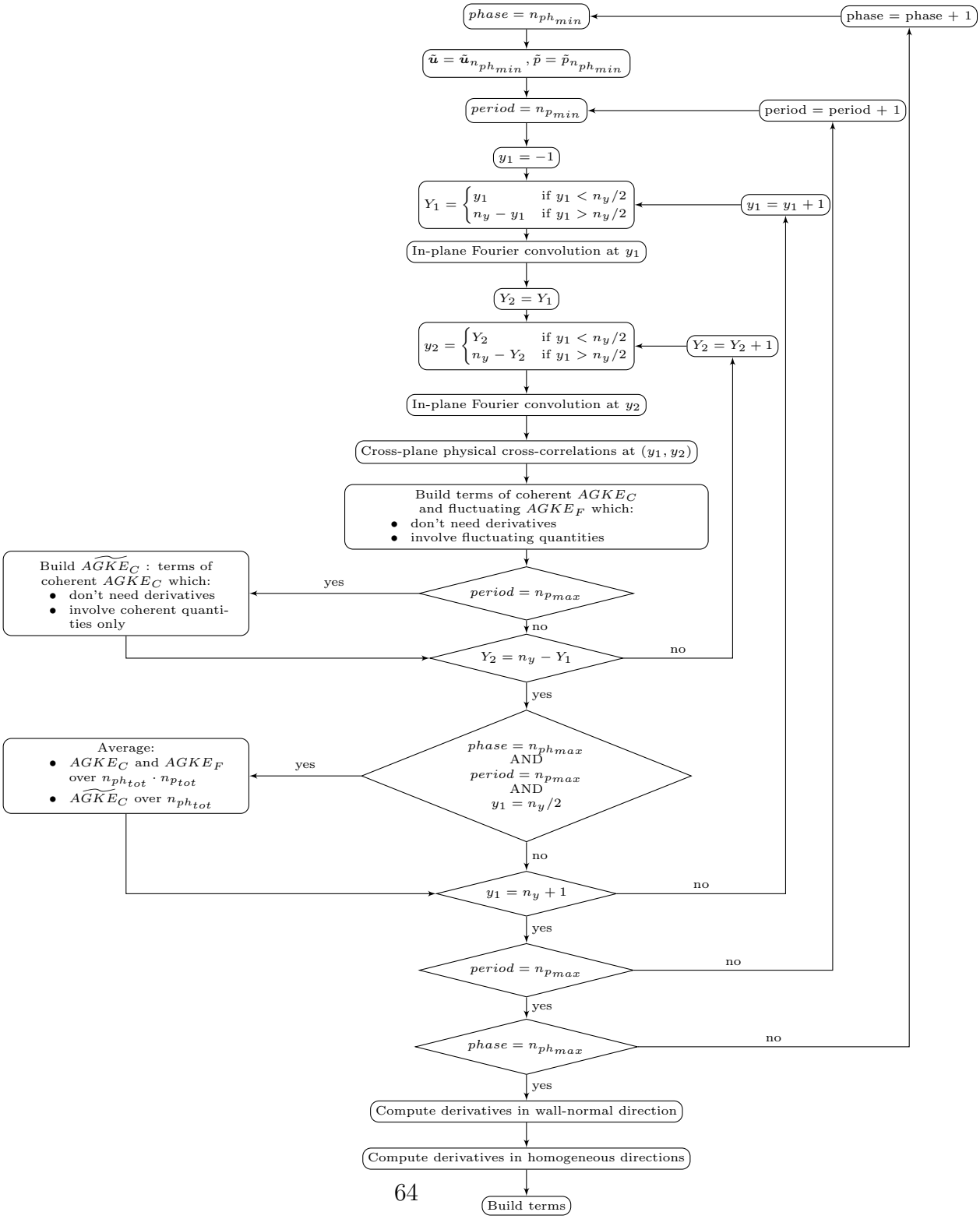
$phase = n_{ph_{min}}$
phase = phase + 1
$\tilde{\boldsymbol{u}} = \tilde{\boldsymbol{u}}_{n_{ph_{min}}}, \tilde{p} = \tilde{p}_{n_{ph_{min}}}$
$period = n_{p_{min}}$
period = period + 1
$y_1 = -1$
$Y_1 = \begin{cases} y_1 & \text{if } y_1 < n_y/2 \\ n_y - y_1 & \text{if } y_1 > n_y/2 \end{cases}$
$y_1 = y_1 + 1$
In-plane Fourier convolution at y_1
$Y_2 = Y_1$
$y_2 = \begin{cases} Y_2 & \text{if } y_1 < n_y/2 \\ n_y - Y_2 & \text{if } y_1 > n_y/2 \end{cases}$
$Y_2 = Y_2 + 1$
In-plane Fourier convolution at y_2
Cross-plane physical cross-correlations at (y_1, y_2)
Build terms of coherent $AGKE_C$ and fluctuating $AGKE_F$ which:
• don't need derivatives
• involve fluctuating quantities
Build $\widetilde{AGKE_C}$: terms of coherent $AGKE_C$ which:
• don't need derivatives
• involve coherent quantities only
yes
$period = n_{p_{max}}$
no
$Y_2 = n_y - Y_1$
no
yes
Average:
• $AGKE_C$ and $AGKE_F$ over $n_{ph_{tot}} \cdot n_{p_{tot}}$
• $\widetilde{AGKE_C}$ over $n_{ph_{tot}}$
yes
$phase = n_{ph_{max}}$ AND $period = n_{p_{max}}$ AND $y_1 = n_y/2$
no
$y_1 = n_y + 1$
no
yes
$period = n_{p_{max}}$
no
yes
$phase = n_{ph_{max}}$
no
yes
Compute derivatives in wall-normal direction
Compute derivatives in homogeneous directions
Build terms

Figure B.1: Flow chart of the code implemented to compute the terms of the evolution equations of the second-order structure functions of the generic component of the Reynolds stresses tensor.

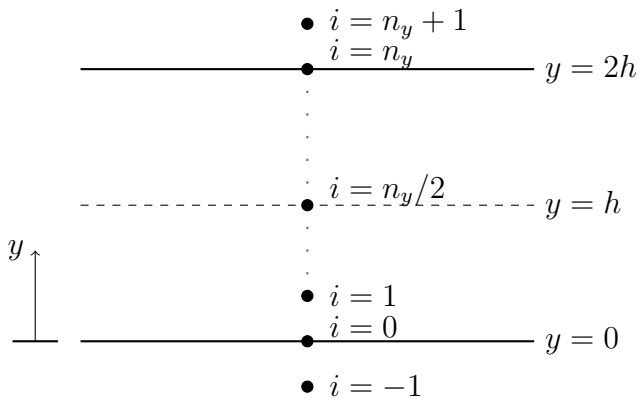

Figure B.2: Sketch of the grid points in the wall-normal direction: the indices $i = 0$ and $i = n_y$ identify the grid points at the two walls, $y = 0$ and $y = 2h$. The grid possesses two ghost nodes for $i = -1$ and $i = n_{y+1}$.

and it concerns derivatives. Those in the two homogeneous directions are performed in Fourier space; those in wall-normal direction are computed by means of a finite-difference scheme with a five-points computational stencil. Symmetries are invoked also within this step when values to fill the stencil are needed in correspondence of non-available wall-normal positions (y_1, y_2).

The validation of the code has been performed by checking that the sum of the coherent and fluctuating AGKE is equal to the total AGKE, and the statistical convergence is verified by ensuring that the residuals of equations 2.8 and 2.7 are negligible compared to the values of the production, pressure strain and dissipation terms (see appendix C).

B.2 Symmetries

As already stated, in order to reduce the computational cost and the amount of memory required by the code, all available symmetries are exploited, with respect to an inversion of both the wall-normal direction y and separation vector $\boldsymbol{r}$. AGKE terms are not directly computed by looping on Y_1 and Y_2,

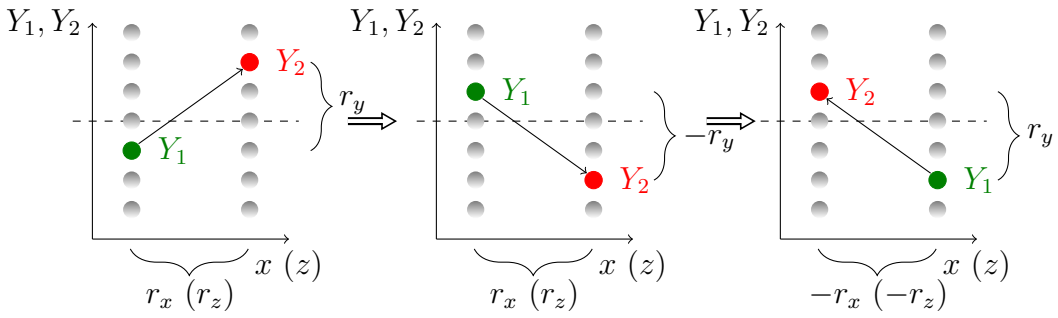

Figure B.3: Graphical representation of the symmetries used to recover the AGKE terms in the planes of the four-dimensional domain $(r_x, r_z, Y_1, Y2)$ with $Y_1 < h$ and $Y_2 > 2h - Y_1$. The dashed line denotes the centerline of the channel, i.e. $Y_i = h$. From the left panel to the central one it has been used the inversion of y, whereas from the central one to the right one the inversion of $\boldsymbol{r}$.

and thus symmetry exploitation is needed, when $Y_2 < Y_1$, $Y_2 > 2h - Y_1$, or $Y_1 > h$.

- $Y_2 < Y_1$ and $Y_1 < h$
  In this case the exploitation of the symmetry is performed by an inversion of the separation vector $\boldsymbol{r}$, i.e. going from (r_x, r_z, Y_1, Y_2) to $(-r_x, -r_z, Y_2, Y_1)$ domain, as shown in the two rightmost panels of figure B.3. The sign of each specific AGKE term has to be determined according to its symmetric or anti-symmetric behaviour with respect to an inversion of $\boldsymbol{r}$ (a complete list is available in Gatti *et al.* (2020)).

- $Y_2 > 2h - Y_1$ and $Y_1 < h$
  In this case, two consecutive inversions are needed. First an inversion of y is performed, as shown in the two leftmost panels of figure B.3, going from (r_x, r_z, Y_1, Y_2) to $(r_x, r_z, 2h - Y_1, 2h - Y_2)$. Here not every AGKE term can be computed yet and a further symmetry exploitation is needed. This intermediate point falls under the case considered above, thus an inversion of the separation vector is applied. Again the sign of each specific term has to be determined taking into account both the performed steps.

Appendix C

Residuals

In this appendix, the residuals of the budget equations for $\langle \delta u \delta u \rangle$, $\langle \delta v \delta v \rangle$, $\langle \delta w \delta w \rangle$ and $\langle -\delta u \delta v \rangle$ in the controlled case are shown in the $r_x^+ = 6$ and $r_y^+ = 0$ plane. The value of the residuals of equation 2.8 are compared to the maxima of the source (ξ^+), mean production (P^{M+}), coherent production (P^{C+}), pressure strain (P^+_{strain}) and dissipation (D^+) in order to ensure the statistical convergence of the data used to perform the analysis.

C.1 $\langle \delta u \delta u \rangle$

$\xi^+_{max} = 0.53$, $\xi^+_{min} = -0.43$, $P^{M+} = 1.1$, $P^+_{strain} = -0.15$, $D^+ = -0.49$.

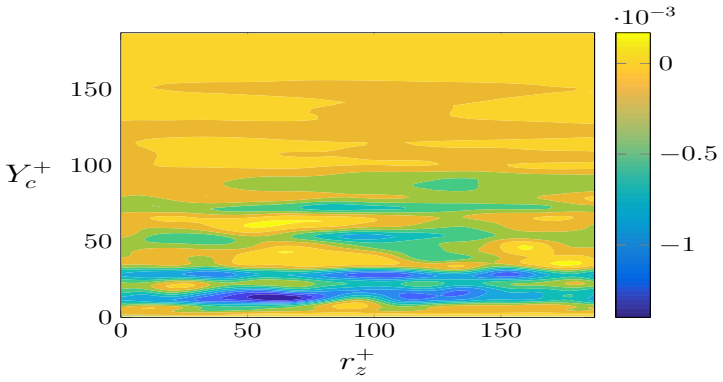

Figure C.1: Residual of the budget equation for $\langle \delta u \delta u \rangle$ in the plane $r_x^+ = 6$ and $r_y^+ = 0$.

C.2 $\langle \delta v \delta v \rangle$

$\xi^+_{max} = 0.026$, $\xi^+_{min} = -0.060$, $P^+_{strain,max} = 0.063$, $P^+_{strain,min} = -0.055$, $D^+ = -0.037$.

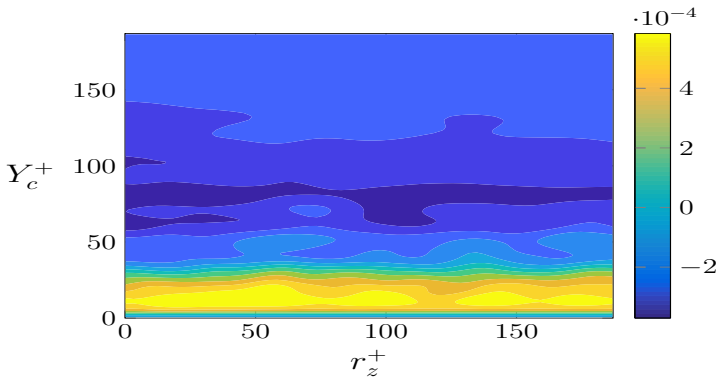

Figure C.2: Residual of the budget equation for $\langle \delta v \delta v \rangle$ in the plane $r_x^+ = 6$ and $r_y^+ = 0$.

C.3 $\langle \delta w \delta w \rangle$

$\xi^+_{max} = 0.042$, $\xi^+_{min} = -0.17$, $P^{C+} = 0.016$, $P^+_{strain} = -0.13$, $D^+ = -0.17$.

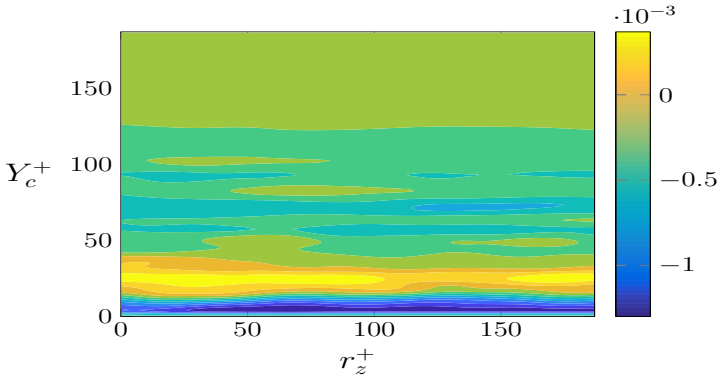

Figure C.3: Residual of the budget equation for $\langle \delta w \delta w \rangle$ in the plane $r_x^+ = 6$ and $r_y^+ = 0$.

C.4 $\langle -\delta u \delta v \rangle$

$\xi^+_{max} = 0.071$, $\xi^+_{min} = -0.10$, $P^{M+} = 0.22$, $P^+_{strain} = -0.24$, $D^+ = -0.019$.

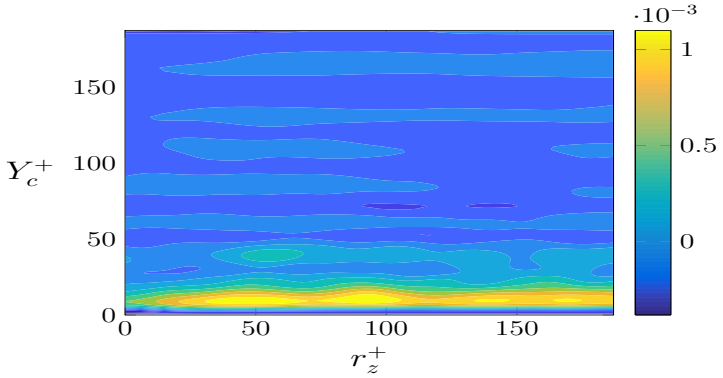

Figure C.4: Residual of the budget equation for $\langle -\delta u \delta v \rangle$ in the plane $r_x^+ = 6$ and $r_y^+ = 0$.

Appendix D

Single point statistics

In this appendix, the behaviour of $\langle uu \rangle$, $\langle vv \rangle$, $\langle ww \rangle$, $\langle -uv \rangle$ and $\langle \tilde{w}\tilde{w} \rangle$ and the terms involved in their budgets are plotted as a function of y^+ in the case of a channel flow under an harmonic oscillation walls control.

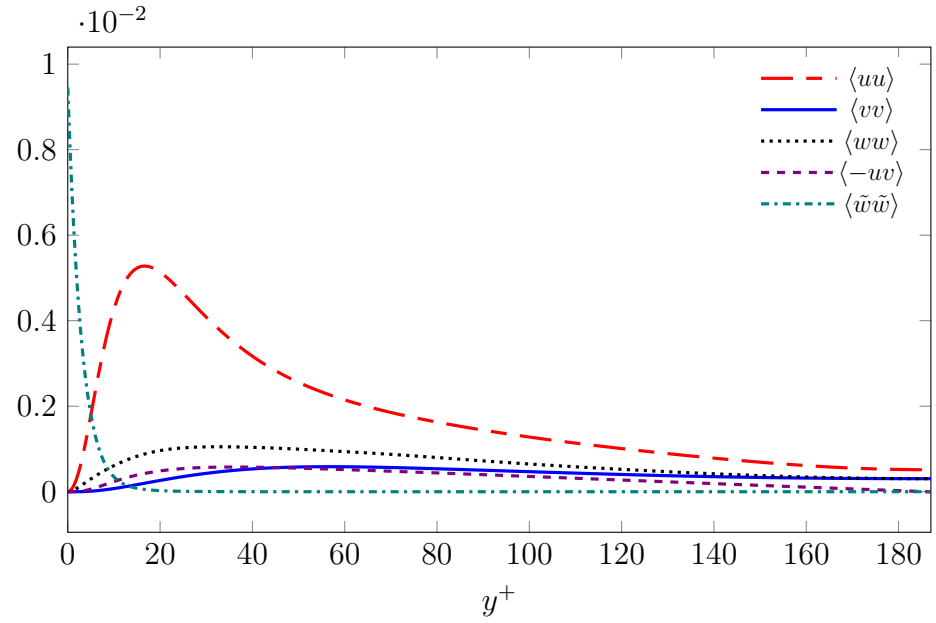

Figure D.1: Plot of $\langle uu \rangle$, $\langle vv \rangle$, $\langle ww \rangle$, $\langle -uv \rangle$ and $\langle \tilde{w}\tilde{w} \rangle$ as a function of y^+

D.1 $\langle uu \rangle$

$$\underbrace{\frac{d}{dy}\left[\rho\langle uuv\rangle\right]}_{T_{trsp}} \underbrace{-\frac{d}{dy}\left[\mu\frac{d}{dy}\langle uu\rangle\right]}_{V_{diff}} = \underbrace{-2\rho\langle uv\rangle\frac{dU}{dy}}_{P^M} \underbrace{+2\left\langle p\frac{\partial u}{\partial x}\right\rangle}_{P_{strain}} \underbrace{-2\mu\left\langle \frac{\partial u}{\partial x_j}\frac{\partial u}{\partial x_j}\right\rangle}_{\epsilon} \tag{D.1}$$

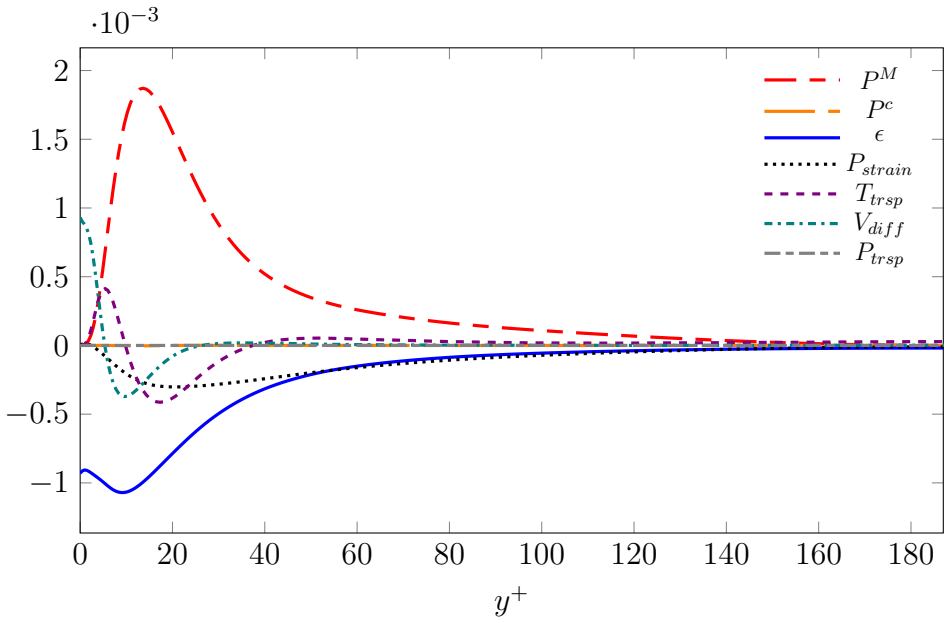

Figure D.2: Budget for $\langle uu \rangle$ as a function of y^+

D.2 $\langle vv \rangle$

$$\underbrace{\frac{d}{dy}\left[\rho\langle vvv\rangle\right]}_{T_{trsp}} \underbrace{+2\frac{d}{dy}\langle pv\rangle}_{P_{trsp}} \underbrace{-\frac{d}{dy}\left[\mu\frac{d}{dy}\langle vv\rangle\right]}_{V_{diff}} = \underbrace{+2\left\langle p\frac{\partial v}{\partial y}\right\rangle}_{P_{strain}} \underbrace{-2\mu\left\langle \frac{\partial v}{\partial x_j}\frac{\partial v}{\partial x_j}\right\rangle}_{\epsilon} \tag{D.2}$$

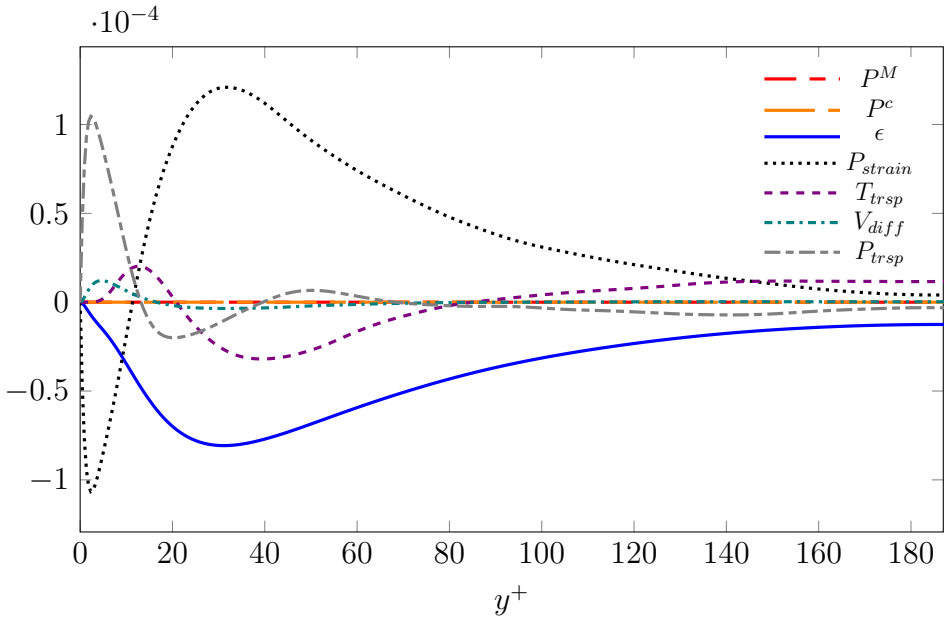

Figure D.3: Budget for $\langle vv \rangle$ as a function of y^+

D.3 $\langle ww \rangle$

$$\underbrace{\frac{d}{dy}\left[\rho\langle wwv\rangle\right]}_{T_{trsp}} \underbrace{-\frac{d}{dy}\left[\mu\frac{d}{dy}\langle ww\rangle\right]}_{V_{diff}} = \underbrace{-2\rho\langle vw\rangle\frac{d\tilde{w}}{dy}}_{P^C} \underbrace{+2\left\langle p\frac{\partial w}{\partial z}\right\rangle}_{P_{strain}} \underbrace{-2\mu\left\langle \frac{\partial w}{\partial x_j}\frac{\partial w}{\partial x_j}\right\rangle}_{\epsilon} \tag{D.3}$$

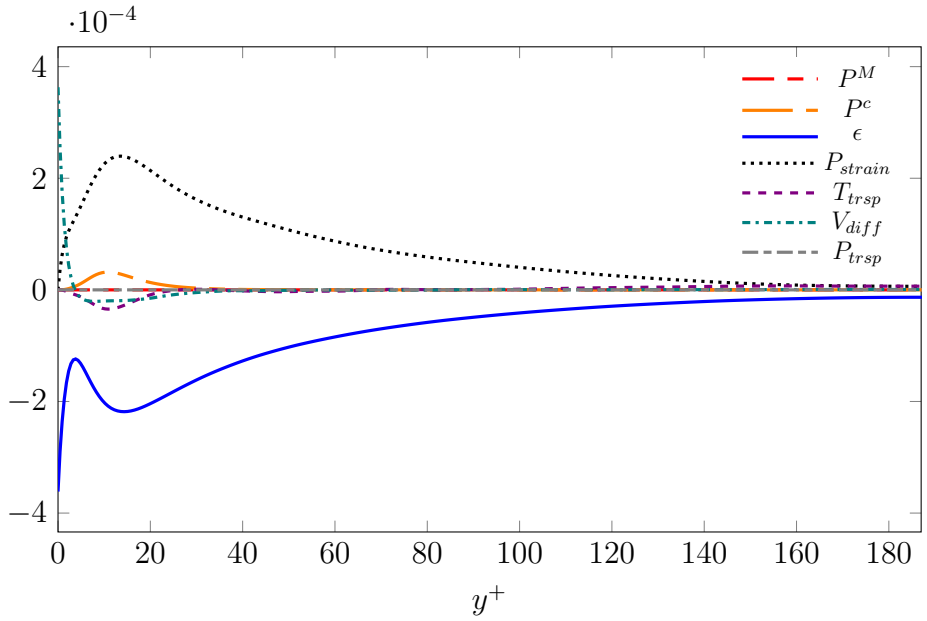

Figure D.4: Budget for $\langle ww \rangle$ as a function of y^+

D.4 $\langle -uv \rangle$

$$\underbrace{\frac{d}{dy}\left[\rho\langle uvv\rangle\right]}_{T_{trsp}} + \underbrace{\frac{d}{dy}\langle pu\rangle}_{P_{trsp}} - \underbrace{\frac{d}{dy}\left[\mu\frac{d}{dy}\langle uu\rangle\right]}_{V_{diff}} = \underbrace{-\rho\langle vv\rangle\frac{dU}{dy}}_{P^M} + \underbrace{\left\langle p\frac{\partial u}{\partial y}\right\rangle + \left\langle p\frac{\partial v}{\partial x}\right\rangle}_{P_{strain}} \underbrace{-2\mu\left\langle \frac{\partial u}{\partial x_j}\frac{\partial v}{\partial x_j}\right\rangle}_{\epsilon} \tag{D.4}$$

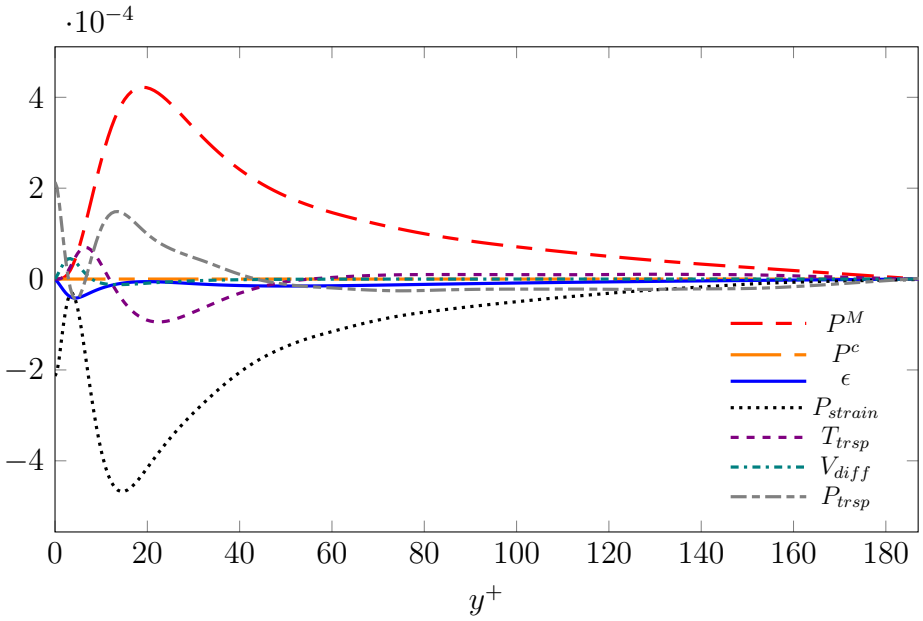

Figure D.5: Budget for $\langle -uv \rangle$ as a function of y^+

D.5 $\langle \tilde{w}\tilde{w} \rangle$

$$\underbrace{\frac{d}{dy}\left[2\rho\langle w\tilde{w}v\rangle\right]}_{T_{trsp}} \underbrace{-\frac{d}{dy}\left[\mu\frac{d}{dy}\langle\tilde{w}\tilde{w}\rangle\right]}_{V_{diff}} = \underbrace{2\rho\langle vw\rangle\frac{d\tilde{w}}{dy}}_{P^C} \underbrace{-2\mu\left\langle\frac{\partial\tilde{w}}{\partial x_j}\frac{\partial\tilde{w}}{\partial x_j}\right\rangle}_{\epsilon} \tag{D.5}$$

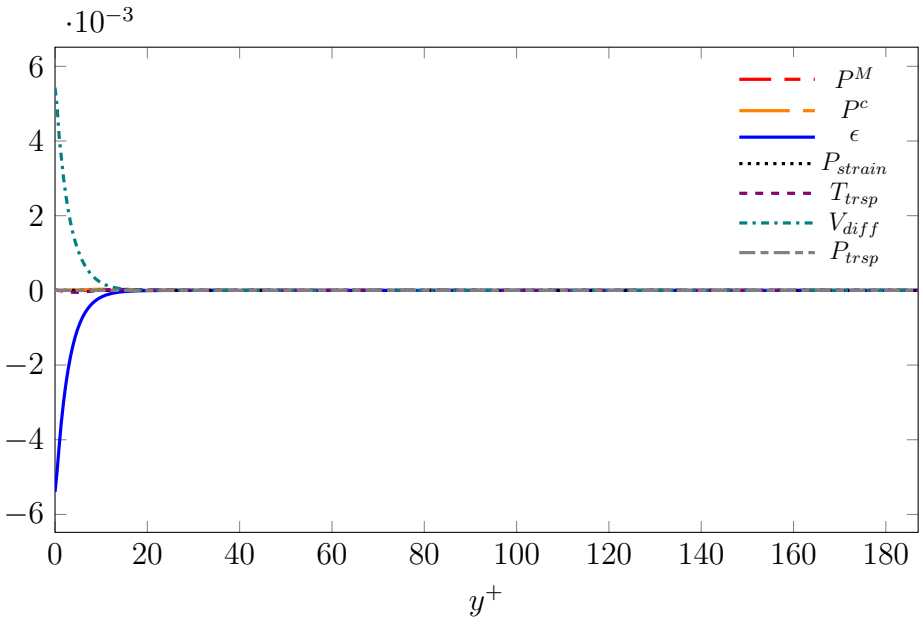

Figure D.6: Budget for $\langle \tilde{w}\tilde{w} \rangle$ as a function of y^+

List of Figures

List of Tables

Bibliography

Agostini, L. & Leschziner, M. 2017 Spectral analysis of near-wall turbulence in channel flow at Re_τ=4200 with emphasis on the attached-eddy hypothesis. *Physical Review Fluids* **2** (1), 014603.

Agostini, Lionel & Leschziner, Michael 2018 The Impact of Footprints of Large-Scale Outer Structures on the Near-Wall Layer in the Presence of Drag-Reducing Spanwise Wall Motion. *Flow, Turbulence and Combustion* **100** (4), 1037–1061.

Agostini, L., Touber, E. & Leschziner, M.A. 2014 Spanwise oscillatory wall motion in channel flow: Drag-reduction mechanisms inferred from DNS-predicted phase-wise property variations at Reτ=1000. *Journal of Fluid Mechanics* **743**, 606–635.

Baron, A. & Quadrio, M. 1996 Turbulent drag reduction by spanwise wall oscillations. *Applied Scientific Research* **55**, 311–326.

Bechert, D.W., Bruse, M., Hage, W., van der Hoeven, J.G.T. & Hoppe, G. 1997 Experiments on drag-reducing surfaces and their optimization with an adjustable geometry. *Journal of Fluid Mechanics* **338**, 59–87.

Blesbois, Olivier, Chernyshenko, Sergei I., Touber, Emile & Leschziner, Michael A. 2013 Pattern prediction by linear analysis of turbulent flow with drag reduction by wall oscillation. *Journal of Fluid Mechanics* **724**, 607–641.

Chiarini, A., Quadrio, M. & Gatti, D. 2019 Skin-friction drag reduction described via the Anisotropic Generalized Kolmogorov Equations. In *European Drag Reduction and Flow Control Meeting – EDRFCM 2019*.

European Drag Reduction and Flow Control Meeting, Bad Herrenhalb, Germany, March 23–26 2019, Bad Herrenalb, Germany.

Choi, H., Moin, P. & Kim, J. 1994 Active turbulence control for drag reduction in wall-bounded flows. *Journal of Fluid Mechanics* **262**, 75–110.

Choi, J.-I., Xu, C.-X. & Sung, H. J. 2002 Drag reduction by spanwise wall oscillation in wall-bounded turbulent flows. *AIAA Journal* **40** (5), 842–850.

Choi, K.-S. 2002 Near-wall structure of turbulent boundary layer with spanwise-wall oscillation. *Physics of Fluids* **14** (7), 2530–2542.

Choi, K.-S. & Clayton, B.R. 2001 The mechanism of turbulent drag reduction with wall oscillation. *International Journal of Heat and Fluid Flow* **22**, 1–9.

Cimarelli, A., De Angelis, E. & Casciola, C.M. 2013 Paths of energy in turbulent channel flows. *Journal of Fluid Mechanics* **715**, 436–451.

Cimarelli, A., De Angelis, E., Jimenez, J. & Casciola, C.M. 2016 Cascades and wall-normal fluxes in turbulent channel flows. *Journal of Fluid Mechanics* **796**, 417–436.

Cossu, C. & Hwang, Y. 2017 Self-sustaining processes at all scales in wall-bounded turbulent shear flows. *Phil. Trans. Roy. Soc. A* **375** (2089), 20160088.

Di Cicca, G.M., Iuso, G., Spazzini, P.G. & Onorato, M. 2002 PIV investigation of turbulent boundary layer manipulated by spanwise wall oscillations. *Journal of Fluid Mechanics* **467**, 41–56.

Du, Y. & Karniadakis, G. E. 2000 Suppressing wall turbulence by means of a transverse traveling wave. *Science* **288**, 1230–1234.

Du, Y., Symeonidis, V. & Karniadakis, G. E. 2002 Drag reduction in wall-bounded turbulence via a transverse travelling wave. *Journal of Fluid Mechanics* **457**, 1–34.

Fukagata, K., Iwamoto, K. & Kasagi, N. 2002 Contribution of Reynolds stress distribution to the skin friction in wall-bounded flows. *Physics of Fluids* **14** (11), L73–L76.

Gatti, D., Chiarini, A., Cimarelli, A. & Quadrio, M. 2020 Structure function tensor equations in inhomogeneous turbulence. *Journal of Fluid Mechanics* **898**.

Gatti, D. & Quadrio, M. 2013 Performance losses of drag-reducing spanwise forcing at moderate values of the Reynolds number. *Physics of Fluids* **25**, 125109(17).

Gatti, D., Remigi, A., Chiarini, A., Cimarelli, A. & Quadrio, M. 2019 An efficient numerical method for the Generalized Kolmogorov Equation. *J. Turbulence* **20** (8), 457–480.

Gatti, D., Remigi, A., Frohnapfel, B., Hasegawa, Y., Cimarelli, A. & Quadrio, M. 2017 Scale energy fluxes in turbulent channels with drag reduction at a constant power input. In *16th European Turbulence Conference*. Stockholm, Sweden.

Hasegawa, Y., Quadrio, M. & Frohnapfel, B. 2014 Numerical simulation of turbulent duct flows at constant power input. *Journal of Fluid Mechanics* **750**, 191–209.

Hill, R.J. 2001 Equations relating structure functions of all orders. *Journal of Fluid Mechanics* **434**, 379–388.

Howard, R.J.A. & Sandham, N.D. 2000 Simulation and modelling of a skewed turbulent channel flow. *Flow, Turb. Comb.* **65**, 83–109.

Hussain, A.K.M.F. & Reynolds, W.C. 1970 The mechanics of an organized wave in turbulent shear flow. *Journal of Fluid Mechanics* **41** (2), 241–258.

Jeong, J., Hussain, F., Schoppa, W. & Kim, J. 1997 Coherent structures near the wall in a turbulent channel flow. *Journal of Fluid Mechanics* **332**, 185–214.

Jiménez, J. 2013 Near-wall turbulence. *Physics of Fluids* **25** (10), 101302.

Jung, W.J., Mangiavacchi, N. & Akhavan, R. 1992 Suppression of turbulence in wall-bounded flows by high-frequency spanwise oscillations. *Physics of Fluids A* **4 (8)**, 1605–1607.

Karniadakis, G.E. & Choi, K.-S. 2003 Mechanisms on transverse motions in turbulent wall flows. *Ann. Rev. Fluid Mech.* **35**, 45–62.

Kim, J., Moin, P. & Moser, R. 1987 Turbulence statistics in fully developed channel flow at low Reynolds number. *Journal of Fluid Mechanics* **177**, 133–166.

Laadhari, F., Skandaji, L. & Morel, R. 1994 Turbulence reduction in a boundary layer by a local spanwise oscillating surface. *Physics of Fluids* **6 (10)**, 3218–3220.

Luchini, P. & Quadrio, M. 2006 A low-cost parallel implementation of direct numerical simulation of wall turbulence. *J. Comp. Phys.* **211** (2), 551–571.

Marati, N., Casciola, C.M. & Piva, R. 2004 Energy cascade and spatial fluxes in wall turbulence. *Journal of Fluid Mechanics* **521**, 191–215.

Nakanishi, R., Mamori, H. & Fukagata, K. 2012 Relaminarization of turbulent channel flow using traveling wave-like wall deformation. *Int J Heat Fluid Flow* **35**, 152–159.

Portela, F. Alves, Papadakis, G. & Vassilicos, J.C. 2017 The turbulence cascade in the near wake of a square prism. *Journal of Fluid Mechanics* **825**, 315–352.

Portela, F. Alves, Papadakis, G. & Vassilicos, J. C. 2020 The role of coherent structures and inhomogeneity in near-field interscale turbulent energy transfers. *Journal of Fluid Mechanics* **896**.

Quadrio, M. & Ricco, P. 2004 Critical assessment of turbulent drag reduction through spanwise wall oscillation. *Journal of Fluid Mechanics* **521**, 251–271.

Quadrio, M. & Ricco, P. 2011 The laminar generalized Stokes layer and turbulent drag reduction. *Journal of Fluid Mechanics* **667**, 135–157.

Quadrio, M., Ricco, P. & Viotti, C. 2009 Streamwise-traveling waves of spanwise wall velocity for turbulent drag reduction. *Journal of Fluid Mechanics* **627**, 161–178.

Quadrio, M. & Sibilla, S. 2000 Numerical simulation of turbulent flow in a pipe oscillating around its axis. *Journal of Fluid Mechanics* **424**, 217–241.

Rincon, F. 2006 Anisotropy, inhomogeneity and inertial-range scalings in turbulent convection. *Journal of Fluid Mechanics* **563**, 43–69.

Schoppa, W. & Hussain, F. 2002 Coherent structure generation in near-wall turbulence. *Journal of Fluid Mechanics* **453**, 57–108.

Touber, E. & Leschziner, M.A. 2012 Near-wall streak modification by spanwise oscillatory wall motion and drag-reduction mechanisms. *Journal of Fluid Mechanics* **693**, 150–200.

Wallace, J. M., Eckelmann, H. & Brodkey, R. S. 1972 The wall region in turbulent shear flow. *Journal of Fluid Mechanics* **54** (1), 39â–48.

Yakeno, A., Hasegawa, Y. & Kasagi, N. 2014 Modification of quasi-streamwise vortical structure in a drag-reduced turbulent channel flow with spanwise wall oscillation. *Physics of Fluids* **26**, 085109.